Università degli Studi di Cagliari

PhD program in Life, Environmental and Drug Sciences

Curriculum Drug Sciences

XXXIII° Cycle

Lipid nanocarriers and 3D printed hollow microneedles as strategies to promote drug delivery via the skin

SSD: CHIM/09

PhD Student: Giulia Pitzanti

Supervisor: Prof. Chiara Sinico

Academic Year 2019 – 2020

Thesis defence: March 2021

REGIONE AUTONOMA DELLA SARDEGNA

Giulia Pitzanti gratefully acknowledges Sardinian Regional Government for the financial support of her PhD scholarship (P.O.R. Sardegna F.S.E.- Operational Programme of the Autonomous Region of Sardinia, European Social Fund 2014-2020 - Axis III Education and training, Thematic goal 10, Investment Priority 10ii), Specific goal 10.5

Index of contents

Abstract

The skin represents an interesting site for the administration of active pharmaceutical ingredients. It offers several advantages over the most conventionally used routes of administration such as the oral and the parental route. Indeed, it bypass the 1st pass metabolism, avoids variables that affect drug absorption in the gastrointestinal tract (i.e. pH, enzymatic activity and drug-food interactions), it is a convenient and non-invasive means of drug delivery and does not require specialized healthcare staff for drug administration. However, due to the structural properties of the skin, only drugs with selected physicochemical features are suitable to be delivered via this administration route.

In order to facilitate skin drug delivery various strategies have been studied over the years such as the use of chemical enhancers, external energy or nanodelivery systems.

In this thesis lipid nanocarriers combined with the penetration enhancer Transcutol® P (Part 1) and 3D printed hollow microneedles (Part 2) are employed as strategies to promote drug delivery via the skin.

Part 1 of this thesis investigates the combination of the penetration enhancer Transcutol® P with two different lipid nanocarriers, solid lipid nanoparticles and phospholipid vesicles, as tools to promote the skin accumulation of 8-methoxypsoralen (8-MOP).

More in detail, *Chapter 1* focuses on solid lipid nanoparticles (SLNs). Empty and drug loaded SLNs including the penetration enhancer Transcutol® (TRC) at different concentrations (2% or 4%) were obtained by hot homogenization followed by ultrasonication. The respective loaded and unloaded formulation without the penetration enhancer were also prepared as control. SLNs were characterized with respect to size, polydispersity index, zeta potential and entrapment efficiency. The nanoparticles morphology was observed by transmission electron microscopy. 8-MOP release from SLNs was investigated using Franz diffusion cells. The 8-MOP accumulation in the different skin layers and permeation through the whole skin after application of free TRC-SLNs or TRC SLNs were investigated using Franz cells and newborn pig skin. *In vitro* biocompatibility of all unloaded and 8-MOP loaded formulations was checked measuring 3T3 fibroblasts viability by using the MTT assay. Finally, the influence of the incorporation of TRC in SLNs on the cellular uptake of

nanoparticles was also evaluated. Freshly prepared nanoparticles showed spherical shape, mean diameters ranging between 120 and 133 nm, a fairly narrow size distribution, highly negative ζ potential values, and high entrapment efficiency. Empty and loaded formulations keep stable in terms of mean diameter (variation lower than 30% compared to the freshly prepared formulations), polydispersity index (variation lower than 0.05 compared to the freshly prepared formulations) and Z potential (variation lower than ±10 mV compared to the freshly prepared formulations) for at least 30 days. In vitro penetration and permeation studies demonstrated a greater 8-MOP accumulation in each skin layer after SLN TRC 2% and TRC 4% application than that after SLN TRC 0% application. Finally, the results of experiments on 3T3 fibroblasts showed that the incorporation of TRC into SLNs could enhance the cellular uptake of nanoparticles, but it did not increase their cytotoxicity.

Chapter 2 focuses on a new class of phospholipid vesicles, called Penetration Enhancer Containing Vesicles (PEVs). Empty or 8-methoxypsoralen loaded conventional liposomes or Penetration Enhancer-containing Vesicles were prepared using the thin film hydration method combined with probe sonication. Two different PEV formulations were developed by varying the % of the penetration enhancer Transcutol® (5% or 10%). Liposomes and PEVs were characterized in terms of size, polydispersity index, zeta potential and encapsulation efficiency. In vitro skin permeation and penetration studies were carried out in order to investigate the % of the drug accumulated in each skin layer or permeated through the skin after the application of the different formulations. Finally, biocompatibility was checked by an MTT assay after the incubation of human keratinocytes with our formulations. PEVs showed a mean diameter lower than conventional liposomes. No statistically significant differences in both size (~135 nm) and encapsulation efficiency (~65%) were found for different Transcutol® concentration. All the formulations had a fairly narrow size distribution and highly negative zeta potential. The amount of 8-MOP accumulated in each skin strata and permeated through the whole skin after application of PEVs was higher than that recovered after the application of conventional liposomes. Finally, biocompatibility checked by an MTT assay, demonstrated that the incubation of human keratinocytes for 24 h with 8-methoxypsoralen loaded Penetration Enhancer-containing Vesicles did not significantly reduce cell viability.

In *Part 2* of the thesis photo-polymerization 3D printing is employed as an innovative method for the manufacturing of solid and hollow microneedles (MNs) patches. Patches containing solid or hollow microneedles of pyramidal or conical shapes were designed, optimized and printed with a DLP 3D printer. MNs patches were observed with Optical and Scanning Electron Microscopy in order to evaluate the conformity of the 3D printed objects with the original designs. Finally, the insertion ability of the optimized patches was tested on a model membrane. The two MNs shapes did not show significant difference in the insertion ability. Even at low applied force, MNs showed a good insertion of ~250 μm. Overall, this work showed that DLP 3D printing can be successfully applied for the development of solid and hollow MNs patches that can be potentially applicable for skin drug and vaccine delivery.

General introduction

1. The skin

The skin (**Fig.1**), the most external part of the human body, is the human most extended organ with an average surface area of 2 m^2. Having a weight of around the 15% of the total weight of the human body, is one of the heaviest human organs [1–3]. It covers continuously the whole surface of the body and it continues with the mucous membrane in the orifices of the digestive, respiratory and urogenital systems. Depending on the area of the body, it shows differences in thickness, color, amount of hairs and glands, innervation and vascularization [1,2].

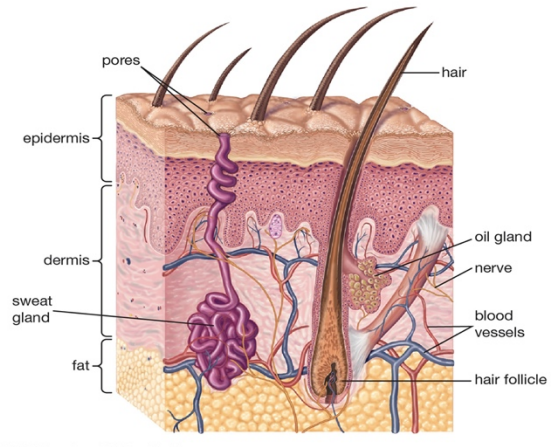

Figure 1. Microanatomy of the human skin [4].

Skin main function is to create a physical barrier between the internal and the external environment of the body. Primarily, it protects the human body from various external stresses: mechanical, chemical, biological and thermal stresses and ultraviolet (UV) radiation [1–3]. Skin protection ability against mechanical stimuli is due to its particular structure that combines rigid and soft tissues. The rigidity is conferred by the stratum corneum and by the collagenous tissue of the dermis, instead, the softness is conferred by the hypodermis. Defects in these structures cause various diseases that lead to physical weakness. The movement of molecules (e.g. water, electrolytes, lipids, and proteins) across the skin is largely limited by the outermost skin layer: the *stratum corneum*. Moreover, skin prevents bacteria, fungi, virus, toxins and allergens from entering the body. The low carbohydrate and water content and a weakly acidic pH (a pH of 5.6

to 6.4) of the skin make difficult the bacterial growth. Continuous turnover of epidermal cells by desquamation prohibits colonization of microorganisms on the skin. The skin is also equipped with antimicrobial proteins and dendritic cells that control immunologic and allergic responses to external insults. Skin also protects from heat and cold stresses, maintaining the internal organs at a certain constant temperature by regulating blood flow, sweat production, thermal storage in the fat layer, and thermogenesis in brown fat cells. Furthermore, the skin is able to reflect, absorb and diffract UV radiation from the sun limiting its penetration into the stratum corneum. These mechanisms protect the genomic DNA of cells from UV-induced damage thereby preventing tumorigenesis [3].

The skin is highly innervated with various sensory nerves that respond to mechanical, thermal and pain stimuli. When these nerve cells are damaged (neuropathy), the affected areas will be characterized by a loss of sensation [1].

In the epidermal layer of human skin occurs the synthesis of vitamin D. In the presence of sunlight, a form of vitamin D_3 called cholecalciferol is synthesized from a derivative of the steroid cholesterol in the skin. Next, the liver converts cholecalciferol to calcidiol, which is then converted to calcitriol (the active chemical form of the vitamin) in the kidneys. Vitamin D is indispensable for normal absorption of calcium and phosphorous, which are necessary for the maintenance of bone mineralization [1,3].

The fat cells in the subcutis represent important storage units for nutrients. Indeed, when the body needs them, they move into the surrounding blood vessels and are carried to where they are required.

Skin is organized in three piled up layers that have different functions, thickness and strength. From the most superficial to the deepest we can find the epidermis, the dermis and the hypodermis.

The **epidermis** (**Fig.2**), the outermost layer of the skin, is a stratified epithelial cellular sheet, cornified into the uppermost part to form the *stratum corneum*. In the epidermis we can find different types of cells: the most numerous are the keratinocytes. A keratinocyte is a cell that produces and stores the protein keratin, an intracellular fibrous protein that gives hair, nails, and skin their hardness and water-resistant properties [1–3].

The epidermis can be subdivided into several strata that from the deepest to the most superficial are: stratum basale, stratum spinosum, and stratum granulosum, stratum lucidum and stratum corneum.

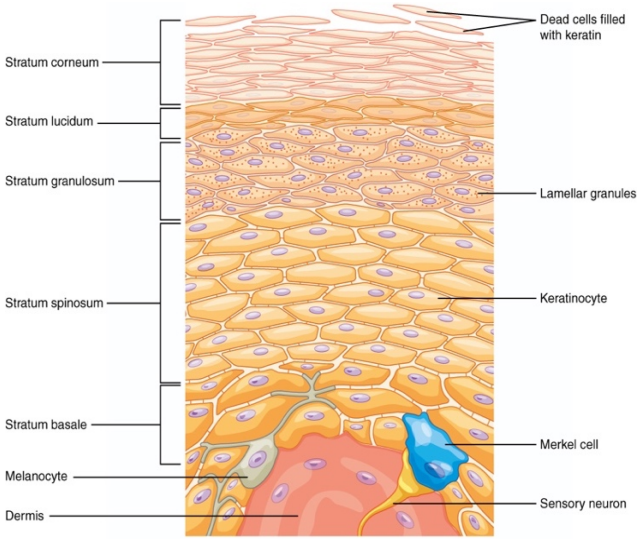

Figure 2. Structure of the epidermis [5].

The stratum basale (also known as stratum germinativum) contains a single layer of prismatic stem cells, precursors of the epidermal keratinocytes. These cells connect the epidermis to the basal lamina, below which lie the layers of the dermis. The main characteristic of the cells of the stratum basale is that they are constantly through mitosis to produce new cells. As new cells are formed, the existing cells are pushed most superficially. Among the stratum basale we can also identify other types of cells such as the melanocytes. The stratum spinosum contains more layers of polygonal cells that become flatter going from the deeper to the more superficial layers. The cells of the stratum spinosum are characterized by protruding processes (spine) that join them via structures called desmosomes [1,2]. The desmosomes main function is to interlock the cells between each other. The "spiny" nature of this layer is much more evident after the staining process. In this stratum begins the keratinization process. In the cytoplasm of the cells that made up the stratum spinosum we can observe aggregates of the fibrillar protein cytokeratin forming tonofribrils. Tonofibrils and desmosomes allow strong connections between adjacent keratinocytes making the epidermis highly resistant to traction. Interspersed among the keratinocytes of this layer we can observe also the Langerhans cells and the melanocytes [2]. The stratum granulosum consists of at least three layers of flattened cells rich of lamellar granules of keratohyalin that give the layer its grainy appearance [1,2]. When the cells die, the nuclei and

other cell organelles break up, leaving lipids and keratohyalin into the intercellular region, contributing to the impermeabilization of the skin. In some parts of the body (thick skin of the palms, soles, and digits) we can found an additional skin stratum known as stratum lucidum which is a smooth and translucent layer located just above the stratum granulosum and below the stratum corneum. The keratinocytes that compose the stratum lucidum are flattened and contain eleidin, a clear protein rich in lipids and sulfur. Eleidin gives to the keratinocytes of stratum lucidum their transparent appearance and provides a barrier to water [2]. The stratum corneum, the uppermost layer of the epidermis, is made of 15-20 layers of dead cornified cells. Cells, known as corneocytes, are flattened with an irregular shape, their desmosomal junctions are altered making the cells less adherent between each other, they lack of nuclei and are rich in keratin. Despite having no organelles and nuclei, they retain some metabolic and signaling functions [1–3]. The stratum corneum can be imagined as a wall of bricks where the bricks are represented by the corneocytes and the mortar is represented by the intercellular lipid lamellae. The most abundant lipids in the stratum corneum are cholesterol, free fatty acids, and ceramides. Thanks to the hydrophobic and structural properties provided by all these components, the epidermis is protected from physical insults as well as water loss [3]. Skin undergoes to a completely renovation through a process called keratinization. Some of the cells produced in the stratum basale gradually migrate into the more superficial layers. During this migration they progressively lost the organelles and nuclei and finally they dead becoming small scales that afterwards left the epidermis through desquamation. Cells need about two weeks to reach the stratum corneum and once reached this stratum they stay there other fifteen days before detaching from the skin [1,2]. The most numerous cells that inhabit the epidermis are the keratinocytes, however we can also find non-keratinocyte cells: melanocytes, responsible for melanin production; Langerhans cells, antigen-presenting dendritic cells that participates to skin's defensive process; Merkel cells, sensory mechanoreceptors. Melanocytes are ramified cells that we can find especially in the deepest layers of the epidermis [1–3]. They produce two different pigments: the eumelanin, a black-dark brown pigment and the pheomelanin, a red-yellow pigment. Both types are derived from the precursor tyrosine [1,3]. The synthesis of the melanin takes place into the melanosomes, ellipsoidal melanocyte's cytoplasmic organelles and it is controlled by the enzyme tyrosinase and stimulated by the melanocyte stimulating hormone and by the exposure to the UV light. The keratinocytes of the deepest strata of the epidermis phagocytise the melanosomes [1–3]. Skin

pigmentation depends on the amount of pigment in the melanosomes. Melanocyte numbers are similar in individuals with different skin colors, and instead differences of pigmentation depend on the amount and quality of melanin in the skin [1,3]. Pigmentation of human skin offers protection against UV-induced sunburn and UV-induced skin cancer [3]. Langerhans cells are star shaped [2] dendritic cells that we can find especially in the intermediate layers of the epidermis [1]. Their main role is to identify the antigen and present it to the lymphocytes T [1,2]. Merkel cells are located in the stratum basale of the epidermis and are in association with the nerve endings [1,2]. They can be isolated or combined into specialized groups. They have round shapes and present numerous vesicles in their cytoplasm grouped nearby the cellular membrane [1]. It is thought that Merkel cells take place to the tactile perception acting as mechanoreceptors [1,2].

The **dermis** (**Fig.3**) is a connective tissue layer situated between the epidermis and the hypodermis. It is mainly composed of collagen and elastin. Moreover, it includes blood and lymph vessels, nerves, and other structures, such as hair follicles and eccrine and apocrine sweat glands. The dermis is organized in two layers: the papillary layer, which is in contact with the epidermis and the reticular layer which is above the hypodermis. The papillary layer is characterized by loose connective tissue. It projects into the epidermis through finger-like dermal papillae [1,2]. It presents a minor density than the reticular layer, but it is rich of cells, blood vessels, nerve fibers, and touch receptors called the Meissner corpuscles. It contains many cell types including fibroblasts, macrophages, and mast cells. Fibroblasts are the principal cells of the dermis. Mast cells are typically found surrounding dermal capillaries of the subpapillary plexus. The vascular network allows to recruit neutrophils, lymphocytes, and other inflammatory cells. The reticular layer is characterized by dense collagen fibers forming a net-like structure. It also contains elastin fibers that provide elasticity to the skin. Moreover, blood vessels, sensory and sympathetic nerves are present in this layer.

The dermis, in addition to the cellular components contains also amorphous extracellular "ground substance". This is made of proteoglycans and glycoproteins. The most abundant not sulphurated proteoglycan is the hyaluronic acid, able to retain high amounts of water. Dermatan sulphate is the most abundant sulphurated proteoglycan, which confers consistency to the connective tissue [1].

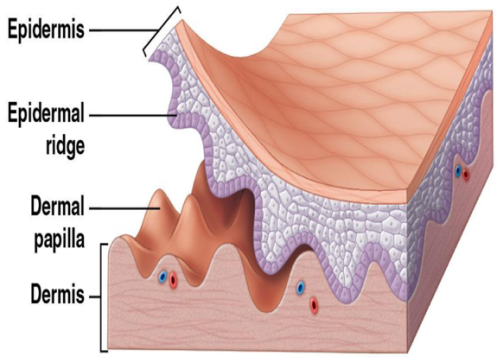

Figure 3. General structure of the dermis [6].

The **hypodermis** (**Fig.4**), also known as subcutaneous layer, is the deepest layer of the skin. The limit between the hypodermis and dermis is difficult to distinguish. It consists of loose connective tissue rich of elastin and collagen fibers and fat-storing cells called adipocytes arranged as lobules [2,7]. Its thickness and distribution depend on ethnic group, age, sex and area of the body. Males have the tendency to accumulate fat in different areas (neck, arms, lower back, and abdomen) than do females (breasts, hips, thighs, and buttocks). Its thickness is between 0.5 and 2 cm. It is absent in the eyelids, auricle, nose and cranial vault, on the contrary it is quite thick in the gluteus, hips and abdominal region [8]. The hypodermis layer works as an energy stock, provides insulation to avoid heat loss, and acts as a cushion to protect underlying structures from trauma [7,8].

Figure 4. The subcutaneous fat [8].

2. Skin drug delivery

Skin represents a promising site of application for a large number of drugs that have a local action in the skin or a systemic effect. Dermal or topical delivery consists in the use of drugs with local actions on the surface of the skin or in the different skin strata. Instead, transdermal drug delivery refers to application onto the skin of drugs that, after diffusion through the different skin layers, have to reach the circulatory system and exert systemic effects [3,9–11]. Once the dosage form is applied on the skin surface, the drug needs first to be released from the dosage form and distributes onto the surface of the skin, then, depending on its target site, it may diffuse through the stratum corneum and reach more deep layers of the skin. If its target site is not the skin, once it reaches the dermis, it is uptaked by the dermis capillaries and transported to its target organ [3,9,11,12]. The first challenge for drugs that have a therapeutic effect in the layers under the stratum corneum or in a site that is not the skin, is to overcome the stratum corneum. The routes that a drug may follow in its diffusion through the stratum corneum are the transepidermal route and the transappendageal route. The transepidermal route can be further subdivided into transcellular and intercellular (**Fig.5**).

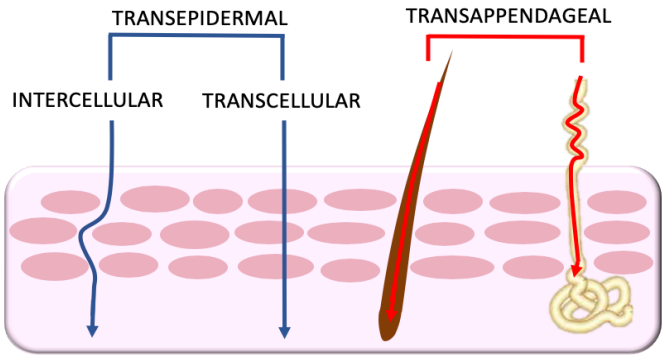

Figure 5. Routes of drug penetration through the *stratum corneum.*

The transcellular route involves the diffusion of the drug through the corneocytes [3,9,11–13]. First, the drug crosses the cell wall of the corneocyte, then, polar molecules migrate to the aqueous sites of the corneocyte, on the contrary, lipophilic molecules migrate to the most lipophilic sites of the corneocyte [9]. The intercellular pathway, consists in the diffusion of the drug through the extracellular matrix around the cells [9,11–13]. The pathway followed by a substance

is mainly dependent on its partition coefficient: hydrophilic drugs usually penetrate the stratum corneum through the transcellular route, instead the lipophilic ones traverse it via the intercellular route [12]. The transappendageal route comprises the transport via the sweat glands and the hair follicles with their associated sebaceous glands. At the beginning this route was considered of minor importance because skin appendages occupy just the 0.1% of the total skin [9,11,12]. Currently it has been reconsidered because it may be the pathway followed by nanoparticles and large polar molecules which hardly penetrate through the stratum corneum [11,12].

The passive diffusion through the *stratum corneum* of a topically applied drug could be described with laws governing diffusion of solutes across a membrane or any homogeneous barrier such as the Fick's first law.

$$J = \frac{dM}{dt}\frac{1}{A} = -D\frac{dc}{dx}$$

Where,

J is the rate of absorption or flux of any substance across a barrier,

D is the diffusion coefficient of the drug across the skin,

$\frac{dc}{dx}$ is the concentration gradient of the permeant at the two sides of the membrane [9].

At steady state conditions, where the amount of drug entering the membrane is equal to the amount leaving the membrane, the flux is given by the following equation [14]:

$$J = \frac{DK}{h}(C_d - C_r)$$

Where,

D is the diffusion coefficient of the drug across the skin,

C_d - C_r is the difference on concentration of the drug at the two sides of the membrane,

K is the partition coefficient of skin/vehicle,

h is the thickness of the membrane [9].

For topically applied drugs, the concentration difference can be simplified as the concentration of the drug in the vehicle [15].

$$J = \left(\frac{DK}{h}\right)C_d = K_p C_d \quad \text{(Adapted from [14–17])}$$

K_p is defined as the permeability coefficient of the drug through the skin from the formulation [16].

From the above equation it can be seen that the rate of permeation of a drug through the skin depends on the solubility and the diffusivity of the drug, on its concentration into the vehicle, indeed, is inversely proportional to the thickness of the biological membrane. The solubility of the drug is expressed with its partition coefficient which is the ratio between the solubility of the drug into the *stratum corneum* and its solubility into the vehicle. This parameter concerns to the drug affinity for the *stratum corneum* and its ability to leave the vehicle. The diffusivity represents the ability of the drug to cross the skin barrier.

The passive diffusion of a compound across the skin barrier is affected by the physicochemical properties of the drug and of the vehicle and by the physiologic and pathophysiologic conditions of the skin (**Fig.6**).

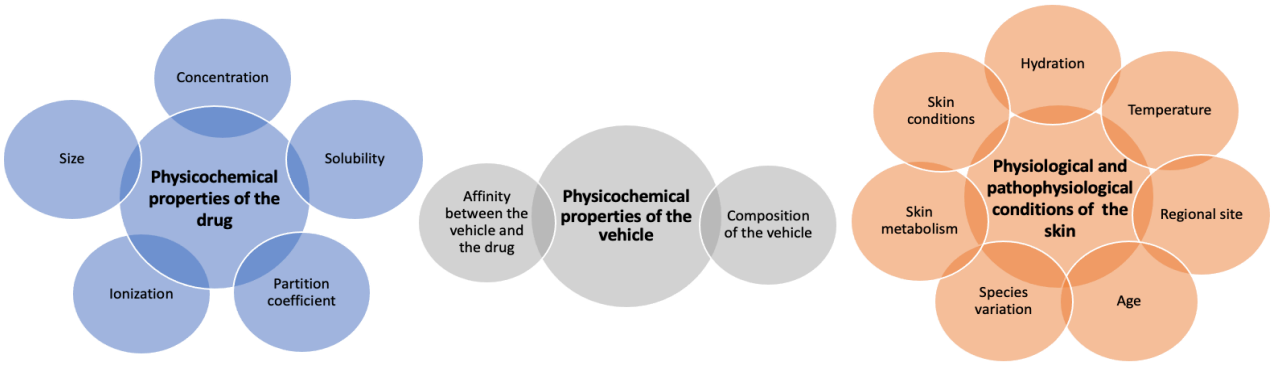

Figure 6. Factors affecting the penetration of a drug through the skin.

According to the Fick's law, the flux of a compound through the skin is affected by its concentration into the vehicle. If we increase the concentration of the drug into the vehicle, the concentration gradient will be higher facilitating the flux of the drug through the skin [9,11,12,18]. The partition coefficient of the drug and its solubility are two other factors that strongly influence the transport of a drug across the skin barrier [9,12,18]. An increase in the drug solubility into the vehicle leads to an enhancement in the concentration gradient facilitating the flux through the skin. However, since the solubility into the vehicle is inversely related to the partition coefficient, the composition of the vehicle must be optimized in order to avoid an excessively decrease of the partition coefficient [9]. Moreover, in order to promote the permeation of the drug across the skin, the drug should have an optimal balance of solubility in both oil and water. The degree of ionization of the drug is another property that influences its diffusion across the skin. It has been reported

that uncharged forms of drugs can penetrate the skin easier than their ionized forms [9,11,18]. According to the pH partition theory, the ionization enhances the hydrophilicity of a compound, thus decreases its partition coefficient between the skin and the vehicle and as a consequence its penetration through the skin [9]. The diffusion of a compound through the skin is also affected by its size. There is an inversional relation between the flux and the molecular size. In particular, small molecules penetrate faster than large ones [12,18]. The affinity of the drug for the vehicle may influence the release of the drug from the vehicle. A high affinity can result in a slow release of the drug from the vehicle. The release of the drug from a vehicle is highly dependent on the solubility of the drug into the vehicle, on its interfacial partition coefficient between the vehicle and the skin and on its concentration. The composition of the vehicle may affect both the release of the drug and the permeability of the skin. The addition of a penetration enhancer in the formulation promotes skin penetration of the therapeutic compound by modifying some physicochemical or physiological properties of the *stratum corneum* [11,18].

In addition to the physicochemical properties of drug and of vehicle, the physiologic and pathophysiologic conditions of the skin should be taken into consideration when a drug is applied in the skin. Hydration of the skin increases the rate of drugs skin penetration [9,18]. Skin water content is usually comprised between the 15 and the 20% [9]. The presence of hygroscopic substances in the stratum corneum allows the skin to retain water and confers it elasticity and softness [19]. The lipid film on the skin surface prevents the removal of natural moisturizing factor from the skin [11]. Skin hydration depends on the water concentration gradient between the dermis and the skin surface but is also dependent on the ability of the *stratum corneum* to retain water. Physiological, environmental and pharmacological factors may affect skin hydration. In addition, occlusivity and environmental humidity may increase the water retention in the stratum corneum and as a consequence skin elasticity and permeability [9]. The natural moisturizing factor (NMF) regulates skin hydration. NMF is composed by hygroscopic water-soluble substances. They are principally free amino acids and various derivatives of these amino acids such as PCA, urocanic acid and inorganic salts, sugars, as well as lactic acid and urea. NMF components are highly efficient humectants with the abilities to attract and bind water from the atmosphere. Hydrated NMF can form ionic interactions with keratin fibers, reducing the intermolecular forces between the fibers and thus increasing the elasticity of the stratum corneum. In addition, the NMF allows the corneocyte cells to balance the osmotic pressure preventing excessive water influx that cause

hyperhydration. Moreover, NMF provides much of the water required for the performance of enzymes that inhabit the skin. It has been reported that the reduction or the lack of NMF is correlated with various stratum corneum abnormalities that manifest clinically as areas of dry skin with scaling, flaking, or even fissuring and cracking [20].

The temperature of the skin is another factor that affects skin permeability. Generally raising skin temperature results into a fluidification of the lipids of the *stratum corneum* increasing its permeability [9]. It may also increase vasodilatation of the skin's blood vessels leading to an increase in percutaneous absorption [11]. The thickness of the skin is another factor affecting the percutaneous absorption. It varies depending on the regional site of the body. It is ticker in the palms and soles and it has a minimum thickness in the postauricular region [9]. There is also a species variation in skin anatomy. The thickness of the *stratum corneum,* the number of sweat glands and hair follicles per unit surface area [11,12], the surface lipids [18], are some skin characteristics that vary from species to species affecting the drug penetration. It has been reported that the skin permeability is dependent on the age of the individual. In particular, children skin is more permeable than adult skin [9,11,12,18]. This is mainly due to the fact that skin barrier is not completely developed [9] and because the water content of young skin is higher than in adult skin which makes it more permeable [18]. Skin contains a wide range of enzymes that may metabolize the drug affecting its topical bioavailability [11,18]. Metabolic activity is found in microorganisms that inhabit the skin-surface, in the appendages, in the stratum corneum, in the viable epidermis, and in the dermis. Generally, compounds that remain in the skin for longer periods of time undergo significantly more metabolism. Skin metabolism should be taken into consideration when designing a drug for topical application. Furthermore, the type of metabolism of a substance may also be influenced by the nature of its formulation. Thus, metabolism in skin compartments plays a significant role in determining the fate of a topically applied active compound [3]. In many dermatological diseases, such as ichthyoses, psoriasis, atopic dermatitis and contact dermatitis [3], have been observed defects in the skin barrier that increase skin permeability. Moreover, skin cut and abrasion increase skin permeability proportionally to the damage's extension [18].

3. Methods to enhance skin permeability

Since the stratum corneum has been recognized as the main barrier to drug penetration, a great effort has been made in order to find ways to overcome it. As a result, several methods to enhance skin permeability have been developed. These methods can be divided into chemical and physical penetration enhancement methods.

3.1 Chemical methods

The most studied chemical method to enhance skin drug delivery consists in the use of penetration enhancers. Penetration enhancers (PEs), also known as permeation enhancers, sorption promoters or accelerants [18], are chemicals capable to reversibly disorganize and fluidify the highly ordered structure of the SC barrier by partitioning into or interacting with the components of the *stratum corneum*. This, temporary reduces the impermeability of the SC, promoting the flux of the penetrant through the skin [11,12,14,16,18,21–25]. Additionally, they can indirectly promote skin drug delivery by interacting with the components of the formulation and modifying their properties [24,25].

In particular, according to the lipid-protein-partitioning theory, PEs could act directly in the skin barrier by three different ways:

1. changing the structural organisation of the lipid bilayers of the SC. It has been reported that PEs could interact with lipid bilayers of the SC at three main sites:
    - interaction with the polar head groups of the lipids forming H bonds and/or ionic forces. This disturbs the hydration spheres of the lipid bilayers and thereby alters their packing order. As a consequence, the intercellular lipids are more fluid. Moreover, the water volume between the lipid layers is increased. Overall, the resistance to drug diffusion is decreased.
    - interaction in the aqueous domain of the lipid bilayers increasing the solubility ability of this site for the drug. These solvents enhance the partitioning of the drug from the vehicle into the SC.

- interaction with the lipid alkyl chain. PEs insert directly between the hydrophobic lipid tails of the bilayer disrupting the packing of lipids and thereby increasing their fluidity. As a result, the drug diffuses through the SC easier [11,24,25].

2. interacting with the intracellular proteins of the SC. Enhancers may interact and binding with the keratin filaments modifying its conformation to cause swelling and increased hydration. Moreover, they can act on the corneodesmosomes to alter cohesion between corneocytes. The diffusion of the drug through the SC is then increased.
3. increasing partitioning of a drug, co-enhancer or co-solvent into the SC. Some PEs can penetrate into the SC and change its chemical properties and thereby its solvent properties. As a consequence, the partitioning and the solubility of a drug, co-enhancer and co-solvent into the SC is increased.

Besides acting directly into the skin barrier, penetration enhancers can modify the drug formulation itself and indirectly enhance drug permeation through the skin. They can modify:

- the thermodynamic activity of the vehicle. Due to the faster solvent permeation into the skin, the permeant drug is left in a more thermodynamically active state. This effect is defined as the “push effect”.
- the drug solubility in the vehicle. The use of enhancers may decrease depletion effects and facilitate the drug permeation through the skin of poorly soluble drugs [24,25].

The majority of the enhancers promote the drug diffusion into the skin through a combination of the aforementioned modes of action.

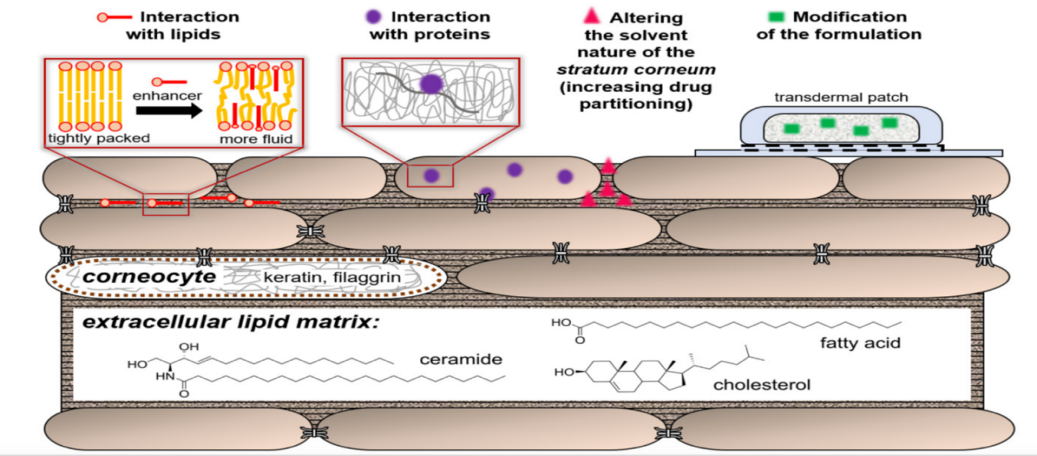

Figure 7. Mechanism of action of permeation enhancers [24].

Penetration enhancers are usually classified into various groups depending on their chemical structure. Based on this classification, we can distinguish alcohols (e.g. ethanol, propylene glycol), esters (e.g. isopropyl myristate), sulfoxides (e.g. dimethyl sulfoxide) [16,24,25], amines (e.g. diethanolamine), hydrocarbons (e.g. squalene) [16,24], amides (e.g. Azone®) [24,25], fatty acids (e.g. oleic acid, lauric acid), surfactants (e.g. sodium lauryl sulphate, polysorbates), terpenes and derivatives (e.g. D-limonene), phospholipids(e.g. phosphatidylcholine) [16,25]. Moreover, according to their origin they can be classified in natural (e.g. water) , synthetic (e.g. Azone®) or semi-synthetic (e.g. terpenes derivatives) [24].

An ideal penetration enhancer should meet the following requirements:

- it should not exhibit any pharmacological activity [11,12,18,23–25]
- it should act quickly and its effect should have a predictable duration [11,12,18,23–25]
- it should not cause toxicity, allergic reactions and irritations [11,12,18,23–25]
- it should be chemically and physically compatible with all the components of the formulation [11,12,18,23–25]
- its action should be unidirectional promoting the penetration into the skin but preventing the loss of body fluids, electrolytes and other endogenous materials [11,12,23–25]
- when the PE is removed from the skin, a fast and full recover of the normal skin barrier properties is expected [11,12,23–25]
- it should not possess any smell or color [11,12,18,25]
- it should be economic [11,12,23]

To date, developing an enhancer that possess all of the aforementioned properties is challenging. The majority of the substances satisfy some, but not all of the criteria [18,25]. Despite being very effective in facilitating drug permeation through the skin, many chemical penetration enhancers have a limited use in topical and transdermal drug delivery systems because they can cause skin irritation [16,21,24]. Karande et al. reported that the irritation behavior of PEs is related to hydrogen bonding and polar interactions. In particular, they believe that the irritation potential is directly proportional to hydrogen bonding ability. In fact, competitive hydrogen bonding can potentially change the native hydrogen bonding in proteins leading to alteration in their structural conformations. Polar interactions are inversely related with the hydrophobicity of a molecule. Hydrophobic molecules may promote partitioning of PEs in the hydrophobic protein

core resulting in the loss of structural conformations and, hence, the inverse dependence of IP on polarity [26].

In order to overcome the toxicity related with some PEs, two strategies could be used: combining enhancers, so that the potency will be superior than the one achieved using single substances and the concentrations of the individual components of such a mixture can be decreased to minimize their toxicities; using biodegradable enhancers, compounds that first interact with the components of the *stratum corneum* barrier increasing the flux of the drug, and then after reaching the viable skin layers get degraded into non-toxic compounds [24].

Despite the problems related to their use, a large group of chemical compounds has been employed for years safely and effectively in dermal and transdermal drug delivery [18,25].

3.2 Physical methods

Physical methods enhance drug transport through the skin by using external energy that acts as a driving force for drug transport or physically reduces the barrier nature of the SC [27–29]. These methods are gaining importance as a result of the progress in precision engineering (bioengineering), computing, chemical engineering and material sciences [29]. In contrast to passive methods, they enable delivery of large molecular weight (> 500 Da) and also hydrophilic molecules (e. g., peptides and proteins) into and through the skin [27–29]. In addition, they offer more control over delivery profile and the possibility to adjust the device and application parameters in accordance to individual's skin properties [28]. In the following paragraphs the most used techniques are briefly described.

3.2.1 Electrically assisted methods

Iontophoresis

Iontophoresis is a method that involves the application of a continuous low-voltage electric current, either directly to the skin or indirectly via the dosage form, enhancing the transport through the skin of a topically applied therapeutic agent [10,27,29,30]. Generally, an iontophoretic device includes a microprocessor controller [7,31], a power source and two electrode compartments named anodal (positively charged) and cathodal (negatively charged) [7,31,32]. The drug formulation is placed in the electrode compartment that possess the same charge: a positively charged drug would be placed in the anodal compartment, whilst a negatively charged

drug in placed in the cathodal compartment [7,32]. The electrode compartment with a charge opposite to the charge of the applied drug is placed at a distal site on the skin [32]. When the current is applied, ions migrate out from the reservoir and into the skin, driven by the electric field. Positive charges in the anodal compartment move towards the cathode whereas anions move in the opposite direction [7,31,32]. The dermal blood supply carries away the drug before it is transported back to the receiving electrode [18].

Iontophoresis enhances drug delivery through the skin by one or a combination of the following mechanisms:

- electrorepulsion: charged drugs move through the skin driven by electronic repulsion of similar charges. In particular, anionic drugs can cross the skin by using a negatively charged electrode. On the contrary, cationic drugs enter the skin more successfully when a positively charged electrode is used [31];
- electroosmosis: the applied electric field generates an electroosmotic flow of water that can transports weakly charged and uncharged compounds along with it [21,31,33–36];
- electroperturbation: the electric current reduces the skin barrier function enhancing the permeation of charged and uncharged drugs [7,31,36,37].

This process follows the Faraday's law: D=IT/(IZI)F where D is the drug to be permeated, I is the current (amperes), IZI is the valence and F is the Faraday's constant (coulomb/Mol) [35].

This equation shows the direct proportionality between the current applied and the rate of drug that permeates through the skin [14,15,18,21,27,32,34–36]. The efficiency of the transport of drugs by iontophoresis depends on the electrode type [10,27,29,30], the current intensity [7,10,14,18,27,29,30,32,36], formulation factors (pH of the system [7,10,18,27,29,30,32], presence of competing ions [10,18,27,29,30,36]) and properties of the permeant (polarity [14,18,27], molecular weight [36] and concentration in the delivery system [7,18,32,36]).

The main advantage of iontophoresis is the possibility to accurately control the rate and profile of drug delivery [7,17,27,32,35]. Moreover, it provides rapid onset of action and offset time [27,32]. In addition, its application is relatively painless [17,33] and not irritating [33]. However, iontophoretic systems are associated with some limitations. There are regulatory limits that set the amount of electric current that can be used in humans at 0.5 mA/cm^2 [10,29,30]. The electric current can irreversibly damage the skin barrier [10,29,30,37]. Finally, iontophoresis is not able to

improve the transdermal delivery of macromolecules that possess a molecular weight higher than 7000 Da [10,29,30].

In the late 1970s the Food and Drug Administration approved the first iontophoretic system: the Phoresor™ device (Iomed Inc., Salt Lake City, UT) [10,14,29,30,36]. This device is combined with a topical solution of 2% lidocaine hydrochloride with 0.001% epinephrine (Iontocaine®) and hydrogel electrodes (Numby Stuff™) to induce local anesthesia [14]. After the first device approved, iontophoretic systems have been under intense development over the years in order to be more patient-friendly and more efficient. An interesting development is GlucoWatch® (Cygnus) which is used to monitor blood glucose concentrations in diabetics [14,34,37]. This device uses reverse iontophoresis as a diagnostic tool. Reverse iontophoresis is a technique by which molecules in the systemic circulation (such as glucose) can be extracted at the skin surface using the electroosmotic effect [14,37].

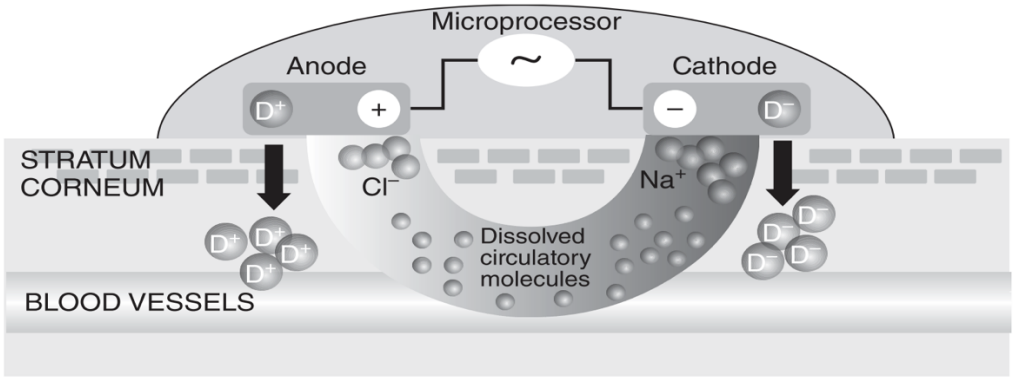

Figure 8. Schematic representation of an iontophoretic patch system [7].

Electroporation

Electroporation is a technique that employs short-duration, high-voltage electric pulses to the skin [7,10,14,15,17,21,29–31,33–39]. Voltages higher than 100V microseconds to milliseconds are typically employed [10,15,29–31,33,34,36,37]. As a result, the structure of lipid bilayer membranes of the skin is perturbated leading to an increased permeability of the skin [10,14,17,21,27,29,30,33,38]. It is believed that the increase in skin permeability is caused by the generation of transient pores in phospholipid bilayers of cell membrane [7,14,15,27,29–31,34,36–39]. The pores are generally smaller than 10 nm and occupy a surface area of about 0.1% [7,38]. Molecular transport through transiently pathways created through the skin by electroporation,

occurs by different mechanisms at different times: enhanced diffusion (during and after pulses), electrically driven transport (during pulses) and very slightly electroosmosis [7,17,27,38].

Electroporation enhances the transport through the skin of molecules of different size, different grade of hydrophobicity [7,10,17,27,29–31] and charge [7,21]. This technique has also shown the ability to successfully deliver therapeutics with a molecular weight greater that 7 kDa, the current limit for iontophoresis [10,27,29–31].

Some parameters need to be optimized to obtain a successful delivery. These includes: electrical parameters (pulse voltage, pulse number and pulse length) [10,27,29–31,36,38], physicochemical properties of the drug (charge, molecular weight, conformation and lipophilicity) [36,38] and formulation of drug reservoir (competitive ions, ionization, pH and viscosity) [38].

A major concern related to the use of electroporation is the pain and muscle stimulation that may be associated with the electrical pulses [7,21,27,36]. In fact, as a result of electroporation, the resistance of stratum corneum rapidly goes down and the electric field distributes into the deeper tissues, which contain sensory and motor neurons [21,27]. This can be avoided paying attention to the design of the electrodes and patch [36] and carefully selecting the pulses [27]. Moreover, molecular transport into and out of the skin during electroporation is relatively nonspecific, which makes dose control more difficult [27].

To date, a number of devices have been tested in clinical studies for various therapies. In 2005 Genetronics Inc. (San Diego, CA, USA) has developed a prototype electroporation transdermal device, that has been tested with various compounds for gene delivery, for improving drug delivery, and aiding the application of cosmetics. Over the years various devices have been developed to enhance transdermal delivery by electroporation, however, to reach the marked more information on safety and efficacy need to be provided [10,29].

Sonophoresis

Sonophoresis is a technique that employs ultrasound waves, sound of frequency greater than 20 kHz [14,27,35], to increase drug permeation through or into the skin [7,10,14,17,27,29–31,34–36]. This approach can be applied as a pretreatment to make the skin more permeable before the drug administration or simultaneously with the application of the drug [10,29,30,40].

Sonophoresis has shown to enhance skin permeability through a combination of a variety of alterations within the skin tissue such as thermal and mechanical alterations [10,27,31,34].

Cavitation is reported to be the major effect of sonophoresis. On exposure to ultrasound waves, air/gas bubbles are generated within the lipid bilayers of the SC [7,10,14,15,17,21,27,29,30,35,37,40]. These bubbles oscillate and collapse producing localized shock waves and/or liquid microjets. This results in sub-microscopically transient alterations to the stratum corneum lipid structure, thereby increasing drug diffusion through the skin of compounds of various sizes, charges, and lipophilicities [7,15,17,21,27,37,40].

The efficacy of the enhancement in percutaneous absorption promoted by sonophoresis depends on the intensity, frequency and duration of the treatment [10,29,30,40].

Ultrasound is typically classified as high-frequency or diagnostic ultrasound (> 3 MHz), medium-frequency or therapeutic ultrasound (1–3 MHz) and low-frequency or power ultrasound (20–100 kHz) [27]. Even though frequencies in the range of 20 kHz to 16 MHz increase skin permeation, ultrasound at low frequencies (20–100 kHz) has shown more effectiveness than the use of higher frequencies inducing a greater perturbation of the skin barrier and thereby more efficiency at enhancing drug delivery [7,10,14,27,29–31,33,34,40].

The SonoPrep® device (Sontra Medical Corporation) is one example of the devices employed in low-frequency ultrasound. It contains a control unit, ultrasonic horn with control panel, a disposable coupling medium cartridge, and a return electrode. It uses low-frequency ultrasound (55 kHz) for an average duration of 15 s to enhance skin permeability [10,29].

During the last decade, the use of ultrasound at low frequencies has emerged as a powerful tool for facilitating transport of various compounds across the skin, thus is increasing the interest of device manufacturers in designing devices more and more efficient.

Magnetophoresis

Enhancing skin permeability through skin exposure to a magnetic field is known as ***magnetophoresis*** [10,17,29,30,35]. The magnetic field acts as an external driving force that facilitates the diffusion of a diamagnetic solute across the skin. In addition, it may creates structural alterations in the skin that further increase its permeability [10,29,30]. This technique only facilitates skin drug delivery of diamagnetic materials. This fact limits significatively its application [10,29].

Radiofrequency

Radiofrequency is the application of high frequency alternating current (~100 kHz) in the skin [10,29,30]. This locally heats the skin creating microchannels, thereby enhancing drug delivery through the skin [10,17,27,29,30]. This effect is similar to the one obtained when laser radiation is employed. The amount of drug delivered is regulated by the number and depth of the microchannels formed by the device, which depend on the properties of the microelectrodes used in the device [10,29,30].

3.2.2 Mechanical methods

Skin abrasion

Skin abrasion techniques involve the direct removal or disruption of the superficial layers of the skin to enhance the permeation of topically applied therapeutic agents [7,10,21,29–31]. Abrasion may be obtained by rubbing the skin with abrasive paper; motor-driven devices using abrasive wheels, pads, or brushes; a "sand-blasting" process using various crystalline particles such as aluminum oxide; or other patented abrasive devices [7]. Many of these techniques are widely used by dermatologists for superficial skin resurfacing (e.g. microdermabrasion) in the treatment of acne, scars, hyperpigmentation, and other skin blemishes [7,10,29–31]. The main advantage of employing these techniques in skin drug delivery, is that their use is not restricted by the physicochemical properties of the drug and thereby they are also able to enhance and control the delivery of a hydrophilic permeant [7,10,29,30].

Suction ablation

Suction ablation implies the application of a vacuum or negative pressure to selectively remove the epidermis without affecting the basal membrane. As a consequence, this method avoids pain and bleeding [10,29,30]. However, this method is associated with some drawbacks. First, the prolonged length of time required to achieve a blister (2.5 h), although this can be reduced to 15-70 min by warming the skin to 38°C. In addition, although there is no risk of systemic infection when compared with the use of intravenous catheters, there is a potential for epidermal infections [10,29].

Microneedles

Microneedles (MNs) are arrays constituted by micron-scale projections that originated from a base substrate. Upon their application into the skin, they create micron-channels through which a wide range of molecules and nanoparticles could be transported [41–43]. MNs were first proposed in 1976 by Gerstel and Place [44], however the first work that involves the MNs application in transdermal drug delivery dates to the late 1990s when Henry et al. described the application of silicon MN to facilitate the delivery of the model drug calcein across excised human skin in vitro [45]. Since then, as a result of the progress in microfabrication technologies, MNs of different sizes, shapes and materials have been developed. MNs are commonly classified into five categories: solid microneedles, hollow microneedles, coated microneedles, dissolving microneedles and hydrogel forming microneedles. There are four general approaches (**Fig.9**) of (trans)dermal drug delivery by microneedles.

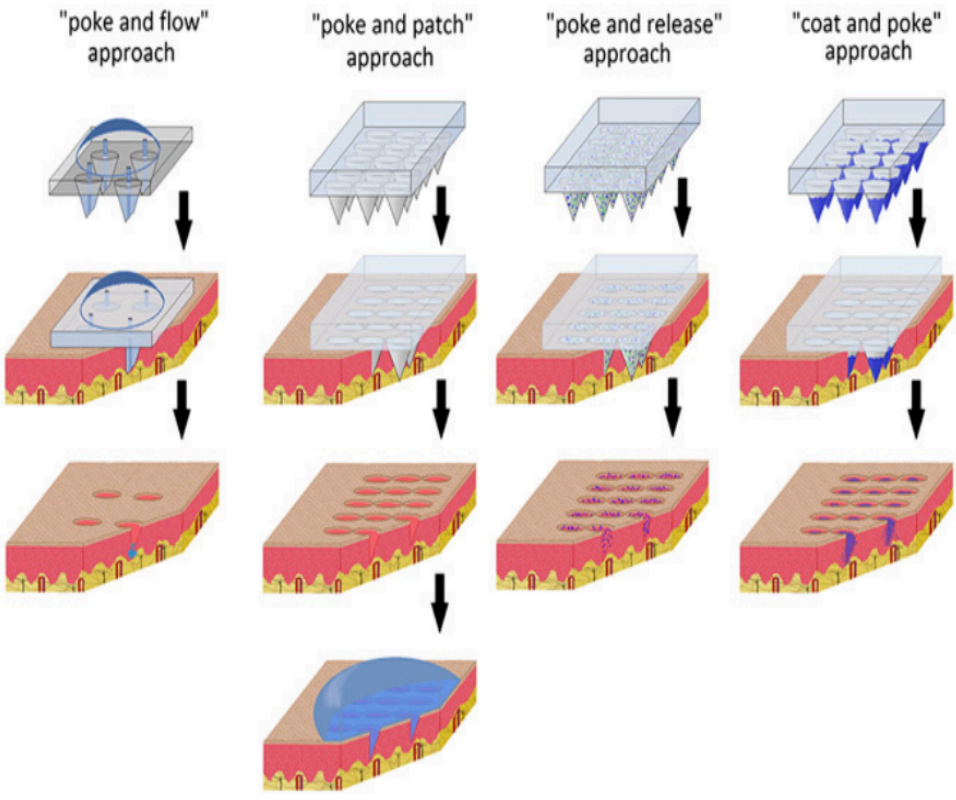

Figure 9. Schematic representations of drug delivery using Microneedles [46].

The first strategy of MN-mediated (trans)dermal drug delivery is the “poke and patch” approach. In this strategy solid MNs are first applied into the skin and subsequently removed leading to the

formation of transient microchannels upon which a conventional drug formulation (transdermal patch, solution, cream or gel) is applied, creating an external drug reservoir. The drug, after being released from the formulation, pass through these microchannels via passive diffusion [41–43,46,47]. The requirement of an application in two-step represents the main disadvantage of this approach [42,43]. A variation on the "poke and patch" approach is the "scrape and patch" approach. In this approach microneedles are first scraped over the skin to generate micro-abrasions, over which a patch with a drug solution is applied [46].

Another way to employ MNs is through the "coat and poke" approach. In this method solid microneedles are coated with a drug formulation before being applied to the skin. After the coated MNs are inserted into the skin, the drug formulation which coats the microneedles dissolves and is deposited in the skin [42,43]. The main advantage of this technique is that allows a simple one-step application process [43]. Unfortunately, the MNs surface can be coated with small amount of drug (the maximum drug dose is less than 1 mg), therefore their use is limited to potent molecules/drugs [43,46,47].

The third approach is known as "poke and release". This approach employs dissolving or biodegradable microneedles. These microneedles contain the drug encapsulated within their matrix. After their application, microneedles degrade or dissolve in the skin allowing a sustained release of the incorporated drugs [42,43,46]. The release kinetic of the drug is affected by the polymers' dissolution rate [42,43,47]. Therefore, in order to obtain a controlled drug delivery is necessary to carefully select the polymer of the MN array, or modify the MN fabrication process [42,43]. The main advantages of this types of microneedles are the low cost of polymeric materials and the easiness of fabrication [43]. Moreover, they do not leave any biological waste into the skin that could constitute a hazard to humans and enable a safe elimination of the residual device. The main drawbacks associated with these types of MN are that the drug loading can affect the mechanical strength of the microneedles and the method used to fabricate the MNs could negatively affect the stability of the incorporated drug or macromolecule [42,43].

Finally, the "poke and flow" approach consists in the application of hollow microneedles. Hollow MNs are characterized by micron-sized channels through the needle's length. This type of MNs allows continuous delivery of molecules across the skin through the MN bore using by simple diffusion through the MNs' bores or by pressure or electrically driven flow combining the MNs with a syringe, a pump or pressurized gas [41–43,46]. These systems allow the delivery of larger

amounts of drug substances in comparison to solid, coated and dissolving MNs [42,43]. The main limitation of hollow MNs is the potential obstruction of the bore of the needle during skin insertion. In addition, the infusion rates are quite low (50-300 nL/min). Moreover, the dense dermal tissue compressed around the MN tips could make resistance to the drug's flow [43]. However, this limitation can be overcome by partial retraction of the needles allowing a relaxation of the compressed tissue around the tips or adding hyaluronidase to the infusion solution, which breaks down hyaluronic acid within skin collagen fibers [46].

MNs allow an easy and patient-friendly administration of APIs into and across the skin. MNs have been shown to penetrate the skin and cross the SC into the viable epidermis without causing any pain and bleeding. This is due to the fact that their length does not allow them to reach nerve fibres and blood vessels that reside primarily in the dermal layer. Since their discovery, extensive research has been carried out concerning MN design with the use of a wide range of materials and fabrication methods [42].

3.2.3 Velocity based enhancement techniques

Jet Injections

Jet injections involve the use of a needle-free device to deliver a drug (in liquid or solid form) intradermally, subcutaneously or intramuscularly. They are proposed as an alternative to conventional injections. Compared to conventional injections, this method provides numerous advantages. It avoids needle-phobia, prevents the risk of needle stick injuries [17,29,30,48–50] and makes easier the self-administration [49,50]. However, its use is also associated with some drawbacks including the high cost of both the device and dosage form and the inability to program or control drug delivery in relation to interindividual variability in skin permeability. In addition, to date is not known which effects might have a long-term bombardment of the skin with drug particles at high speed. Thus, such systems may not be suitable for drugs that require frequent administration but may be appropriate for these that do not require frequent dosing [17,29].

Typically, needle-free injector devices consist of three components:

- Injection device: is made up of plastic and is designed to allow self-administration
- Nozzle: usually in plastic, contains an orifice with size typically ranging between 150 and 300 µm. It is the only part of the device that will enter in contact with the skin

- Pressure source: the pressure can be generated by compressed gas (i.e. carbon dioxide or nitrogen) contained into a gas cartridge or alternatively pressing a plunger to release a spring [48,49,51,52].

Basically, we can identify three types of needle-free injectors: powder injectors, liquid injectors and depot or projectile injectors.

In liquid injectors, after the device is activated, the power source pushes the piston against the drug-containing reservoir, enhancing the pressure inside the device. This forces the formulation at high speed through the micron-sized orifice of the nozzle. After being ejected, it impacts the skin creating a channel through which it penetrates into the deeper skin layers eventually reaching the subdermal tissues including fat and muscles [28,51].

In power injection systems, the powdered formulation contained in a cartridge is extruded by the compressed gas allowing its deliver to the skin tissue [28,48,51]. In particular, once the device is activated, the compressed gas expands and breaks the membranes that closed each side of the drug compartment. The flow of gas forces at high speed the drug particles outside the nozzle making them impact on the skin. As a result, particles puncture micron-sized holes into stratum corneum and some of them are contained in stratum corneum while a high percent reach the viable epidermis for the desired therapeutic effect [28]. The powder must possess specific characteristics and size to guarantee its stability and adequate dispersion into the tissue. This offers the advantage of a higher stability API and it may not require cold storage. Moreover, it offers the chance to the single administration of a fast acting and a delayed-release form [28,48,51].

Depot injections are administered intramuscularly where they create a depot of the drug from which is released continually for a controlled period of time [48].

Over the years there have been numerous examples of needle-free injector systems. Nowadays, they are a steadily developing technology that promises to make the administration of medicine more efficient and less painful.

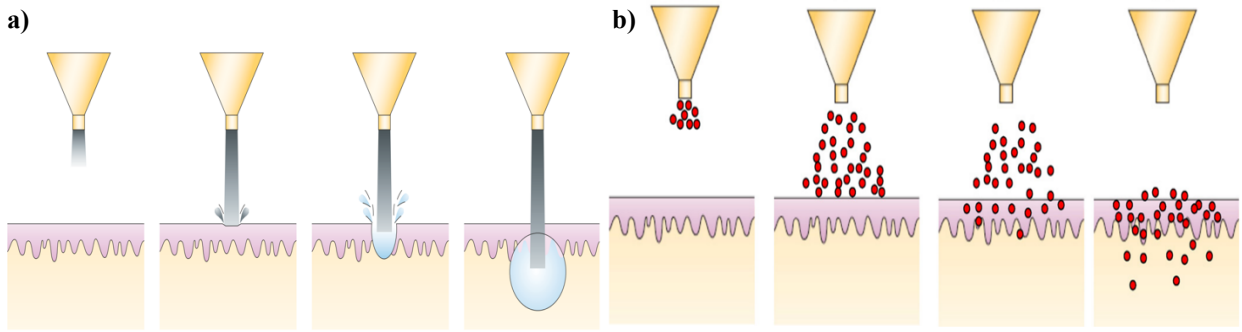

Figure 10. Schematic representations of drug delivery using a liquid jet injector (**a**) and powder injector (**b**) [28].

3.2.4 Thermal and laser ablation

Thermal Ablation

Thermal ablation is a method that consists in the heating to hundreds of degrees, for short-time, localized regions of the skin surface. In details, pulses of heat of microsecond- to millisecond-long are applied [10,17,21,28] . Due to the short duration of the treatment, there is not enough time for heat to propagate into the deepest skin layers where are localized the pain receptors, thereby pain sensation is minimized [10,15,21,28]. As a result of the heat application, skin permeability is increased due to the formation of microchannels in the stratum corneum [7,17,21,28]. In addition, an increase in drug diffusivity in the vehicle and in the skin due to increased lipid fluidity are observed. [10,30]. Moreover, vasodilation of the subcutaneous blood vessels as a homeostatic response to an increased skin temperature is another factor that plays an important role in enhancing the transdermal delivery of topically applied compounds [29–31]. Generally, microarrays containing heating elements or radiofrequency sources are employed for this purpose. A certain number of systems for thermal ablation are in an advanced stage of development. Among these, the PassPort™ system from Altea Therapeutics Corporation (Atlanta, GA, USA) uses an array of resistors as a source of localized heating. The ViaDerm system (TransPharma Medical Ltd., Lod, Israel) uses an array of radiofrequency microelectrodes to create microchannels. The system is composed by a reusable and rechargeable control unit along with a disposable microelectrode array designed for a single use [7].

Laser Ablation

Laser ablation consists in a direct and controlled exposure of the skin to laser radiations. This induces microablations in the stratum corneum without reasonably affecting underlying skin layers [7,10,17,27,29–31,33,36]. This has been shown to promote the delivery of lipophilic and hydrophilic drugs [10,27,29–31,36]. The extension of the skin barrier disruption could be controlled carefully setting laser parameters such as wavelength, pulse length, pulse energy, pulse number, and pulse repetition rate [7,10,27,29,30]. Intense laser radiation has recently been reported to generate high-amplitude pressure waves (photomechanical waves) that enhance skin permeability. This effect is believed to be a consequence of the formation of temporary hydrophilic channels due to expansion of the lacunae domains in the SC. [7,29,30,36]. The application of lasers to enhance skin drug delivery offers numerous advantages such as controlled removal of the stratum corneum, short treatment time, absence of pain and mild adverse effects [10,27,31]. However, the safety and clinical efficacy of this technique need to be further investigated [27,31].

3.3 Nanodelivery systems

Looking at the drawbacks related to physical and chemical methods as strategies to enhance skin permeability to topically applied drugs, a novel approach of nanotechnology-based drug delivery system is being investigated by researchers all around the world. **Figure 11** shows nanocarriers that have been developed for the purpose to promote skin drug delivery. Among these systems, lipid carriers such as liposomes and analogues, solid lipid nanoparticles (SLN) and nanostructured lipid carriers (NLC) have gained a major attention.

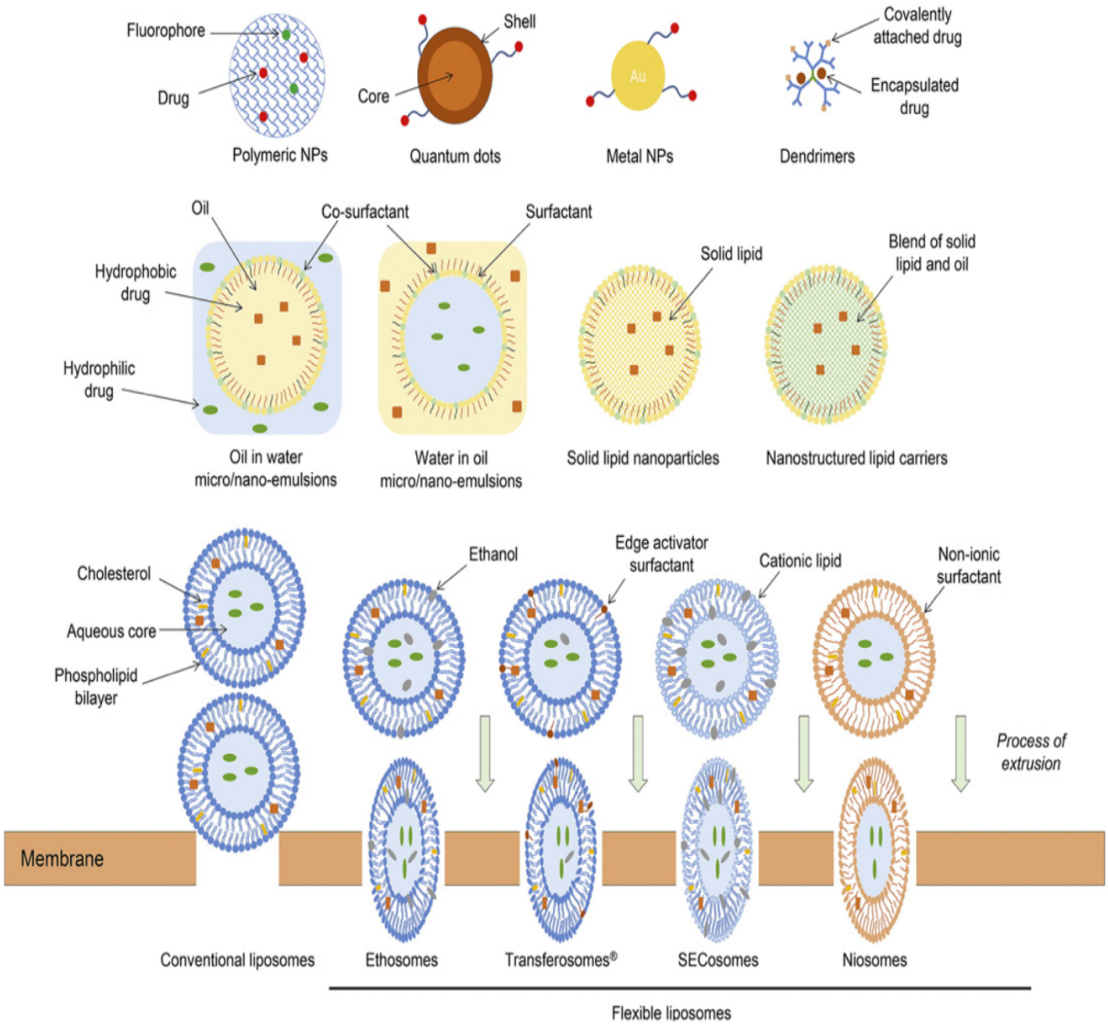

Figure 11. Nanodelivery systems investigated for dermal and transdermal drug delivery [53].

Vesicular lipid-based nanocarriers

Liposomes are spherical vesicles formed by the spontaneous assembly of amphipathic phospholipids in aqueous environments. When exposed to aqueous environments, phospholipids originate these structures in order to minimize the contact with water of their hydrophobic domains. They can assembly forming one or several bilayers delimiting one or several aqueous compartments [54]. Depending on their size and the number of lamellae, they can be classified into several types: MLVs (multilamellar vesicles) with a size > 0.5 µm, SUVs (small unilamellar vesicles) with a size ranging from 20 nm to 100 nm, the LUVs (large unilamellar vesicles) with a size > 100 nm [55]. Due to their structure and composition, they can be used as drug carriers for hydrophilic and lipophilic molecules. More in details, hydrophilic compounds can be dissolved in the aqueous compartment, while lipophilic compounds can insert into the lipid bilayers [52, 53]. They can be prepared using different methods such as thin-film hydration, reversed phase evaporation, solvent injection, dual asymmetric centrifugation, supercritical fluid and microfluidic [56]. They are characterised by high biocompatibility, low toxicity, biodegradability, and can be produced on a large scale [54]. Several theories about the mechanism through which liposomes can promote skin drug delivery have been proposed. Liposomes can promote skin drug delivery interacting with the SC lipids and causing partial fluidization of the lipid bilayer. This promotes their skin penetration without losing their original structure. As a consequence, they deposit in the deepest skin layers from where the API is released. Alternatively, liposomes may break at the SC surface allowing phospholipids penetration within the SC which would promote skin permeation of the active payload. According to another theory, vesicles might be adsorbed to the surface of the skin, merge with the lipid matrix in the SC and then the active molecule diffuses through the skin layers [55]. It is commonly admitted that conventional liposomes cannot penetrate deeply into the skin layers [54,55]. This may be a consequence of their rigid structure [56].

In order to overcome this drawback and further enhance skin permeation of encapsulated molecules, modifications in the composition and structure of conventional liposomes were made to generate new generations of lipid vesicles with flexible and ultradeformable properties such as Transfersomes® and ethosomes.

Transfersomes® are phospholipid-based vesicles that differ from conventional liposomes for the presence of an additional component named “edge activator” (EA). The edge activator, usually

a single-chain surfactant with a large radius of curvature, destabilises the bilayers, thereby making the system more elastic and therefore more deformable. The most conventionally used EAs are sodium cholate, sodium deoxycholate, Span 60, Span 65, Span 80, Tween 20, Tween 60, Tween 80 and dipotassium glycyrrhizinate. Two possible mechanisms have been identified as possible explanations of the ability of transfersomes® to cross the skin membrane. The first mechanism is related to the degree of flexibility of the vesicle. It has been reported that the addition of edge activator in amounts ranging from 10 to 20% to the composition of phospholipid vesicles makes them able to deform and fit into the intercellular channels of the SC, even if their size is higher than SC channels. The second mechanism proposes that transfersomes® may pass through the SC driven by the transepidermal osmotic gradient. The water gradient is generated as a result of the difference in water content between the SC (15%) and the other layers of the epidermis (75%) [54,55].

Ethosomes are liposomes analogues developed in 2000 by Touitou et al. They are composed of phospholipids and a large amount of ethanol (20-45%) [55,56]. They have shown effectiveness in increasing skin drug delivery in both non-occlusive and occlusive conditions. It has been suggested that ethanol and phospholipids act synergistically to promote drug delivery through the skin. Ethanol disturbs the organization of the SC lipids by both fluidifying SC lipids and decreasing the density of the intercellular lipid domains. In addition, ethanol increases the vesicle fluidity and flexibility. Vesicles interact with the disorganised SC, alter the intercellular lipid lamellae thus creating new pathways across the SC to the deep skin layers [54,55].

Penetration enhancer containing vesicles (PEVs) are liposomes that contain penetration enhancers (PEs) in order to promote skin passage but also to solubilize active molecules that are poorly soluble in water and others commonly employed solvents such as ethanol or methanol [53]. They were first introduced in 2009 by Manconi et al. who add in liposome formulation two hydrophilic additives consisting of a glycol group, i.e. propylene glycol, and, for the first time, the penetration enhancer (PE) diethylene glycol monoethyl ether (Transcutol®). These innovative vesicles were characterized by high stability during storage and the capability to encapsulate high amounts of diclofenac acid [57]. The same group proposed the mechanism with which these vesicles may increase skin drug delivery. They suggested that it is related to intact penetration of PEVs into the epidermis due to a synergistic action of penetration enhancer/intercellular skin lipids and the enhanced PEVs' bilayer fluidity allowing transport and accumulation of the active

ingredient loaded. After vesicles disintegration, according to its solubility, the active ingredient continues to diffuse into the skin layers [58].

Solid lipid nanoparticles (SLN) and Nanostructured Lipid Carriers (NLC)

SLN were first introduced in 1991 as a promising alternative to the antecedent lipid systems and polymeric nanoparticles [53,58,59]. The main advantages of SLNs are the reduced toxicity of its components that are characterized by high degree of biocompatibility and biodegradability [55,59–63]; their ability to enhance the stability of chemically labile drugs through protection from the external environment [53,58–60]; the higher loading capacity compared to other drug delivery systems [59]; their chemical versatility that enables the incorporation of both hydrophilic and lipophilic drugs [59,60,63]; their ability to offer controlled release of the loaded drug [55,59,60,63]; the possibility of large-scale production [55,59,60,62,63].

Basically, SLNs consist in one or more solid lipids dispersed into an aqueous medium [55,59,62,64,65]. In order to ensure the stability of the system over the time, surfactants at a concentration ranging from 0.5% (w/w) to 5% (w/w) are added to the formulation [55,59,62,64]. The wide variety of lipids used in the formulation of SLN may be classified as fatty acids, waxes, steroids, partial glycerides, and triglycerides [59,61,62]. SLNs have been prepared using a wide range of methods such as high pressure homogenization technique [59–61,63,64], high shear homogenization [60,61,63,64], solvent emulsification evaporation or diffusion technique [59–61,63,64], microemulsion [59,60,63,64], sonication methods [59–61,63,64], solvent injection and membrane contractor method [59,61]. Depending on the type of API, lipids and surfactants used, on the solubility of the drug in the melted lipids and on the fabrication method, SLNs can be classified into three types:

- Homogenous matrix model: is generated from a solid solution of lipid and API. This SLN type is usually obtained when SLNs are prepared by a cold homogenization technique without using a surfactant. In this model the active constituent in a molecularly dispersed in the lipid mixture.
- Drug enriched shell model: SLN type II consists in a lipid core surrounded by an outer shell containing both lipid and drug. It is produced using the hot high-pressure homogenization technique and applying a small concentration of the drug in the lipid matrix. In the cooling process, the lipid is precipitated first leading to an increase in the concentration of the

drug molecules, which remained in the melt. Then, the outer shell is solidified containing both lipid and drug.

- Drug enriched core model: this type of SLN is obtained when the concentration of the API in the lipid melt is near to its saturation. In this method, cooling process leads to the precipitation of the drug due to super saturation at low temperatures. Further cooling leads to the precipitation of the melted lipid and surrounding the precipitated drug particles [61].

Besides the numerous advantages, SLNs are related to some drawbacks. First, the dispersions have a high (70–90%) water content. In addition, polymeric transitions of the lipids may occur during storage leading to drug expulsion. Moreover, SLNs present a compactly packed lipid matrix that limits the space available for drug encapsulation and thereby their drug loading capacity [60,61,63].

In order to overcome these limits, in 1999 a second generation of lipid nanoparticles has been developed. These systems are known as nanostructured lipid carriers (NLC). In contrast to SLNs, the lipid matrix of NLCs is composed by a mixture of solid and liquid lipids at a ratio varying from 70:30 to 99.9:0.1. As for SLNs, the system is stabilized by a surfactant or a mixture of surfactants [55,59,64]. The methods of production are the same reported for SLNs. NLCs can be classified into three different types:

- Imperfect type: NLCs are prepared by mixing spatially different lipids. As a result, the distance between the fatty acid chains is higher leading to imperfections in the crystal structure. This offers more space for drug inclusion and thereby a high drug loading.
- Multiple type: the amount of oily lipids used is high. The drug that shows higher solubility in the liquid lipids than in solid lipids can be dissolved into the liquid lipid and then protected from degradation by the solid lipids.
- Amorphous type: NLCs contain additional specific lipids e.g., isopropyl myristate, hydroxyl octacosanyl, hydroxyl stearate etc. to prevent crystallization of solid lipid upon cooling. Thus, expulsion of drug caused by crystallization of solid lipids is avoided [63].

The introduction of liquid lipids determines a depression of the melting point of the solid lipid. Despite that, the matrix still remains solid at both room and body temperatures [55,59,64]. In

addition, the presence of the liquid lipid reduces the high order of the lipid matrix creating imperfections in the crystal structure. This offers more space for drug inclusion and consequently enhances drug loading in comparison to SLNs [55,64]. Moreover, the recrystallization of solid lipids is prevented leading to a more thermodynamically stable system. As a result, the risk of drug expulsion during storage is reduced [59]. Finally, nanostructured lipid carriers require a lower amount of water in comparison to SLNs. This enables the production of concentrated systems which can be directly incorporated in dermal formulations [55].

Among the different applications that have been proposed for SLN and NLC, the cutaneous use seems to be one of the most promising, for both therapeutic and cosmetic purposes. Solid lipid nanoparticles and nanostructured lipid carriers offers chemical protection of the incorporated drug, allowing the skin application of labile molecules that are difficult to transport in traditional semi-solid formulations [64,65]. Moreover, due to its small particle sizes and large surface area, SLNs and NLCs are able to adhere to the skin surface for a prolonged time forming a hydrophobic film that has an occlusive effect highly reducing the transepidermal water loss [39,53,55,65]. As a consequence, there is a rearrangement of the corneocyte packing and a size increasing of the inter-corneocytes gaps. That, enhances drug transport through the skin [55].

To summarize, several enhancement strategies can be used as tools to enhance dermal and transdermal drug delivery.

Starting from this background, the aim of this thesis is to investigate if the combination of nanocarriers and both a chemical or a physical enhancement method could have a synergistic effect in improving skin drug delivery.

Part 1: Combination of Lipid Nanocarriers and Transcutol® P to promote 8-MOP skin delivery

1. General introduction

8-methoxypsoralen (8-MOP) (**Fig. 12**), also known as methoxsalen or xanthotoxin, is an organic molecule belonging to the furanocoumarin class. It appears as white to cream-colored soft needles, its odourless and its characterized by a bitter taste [66]. It is insoluble in water, slightly soluble in ether and freely soluble in common organic solvents such as chloroform, boiling alcohol, acetone and acetic acid [66].

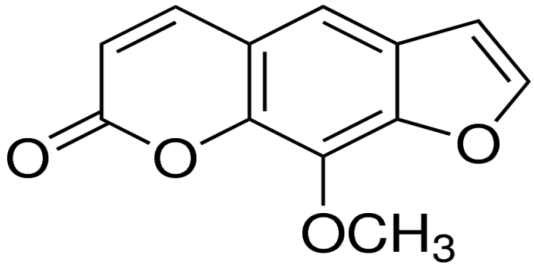

Figure 12. 8-Methoxypsoralen (8-MOP).

Among with psoralen and its derivatives, 8-MOP is commonly employed in the photo-chemotherapeutic treatment of numerous skin diseases characterized by abnormally high rate of cell proliferation or by lack of skin pigmentation such as psoriasis and vitiligo [67]. The photochemotherapy of these diseases involves the oral or topical administration of psoralen or its derivatives followed by patient's exposure to long-wave ultraviolet A radiation (320–400 nm). This treatment is defined as PUVA therapy [68]. 8-MOP, due to its planar aromatic structure and hydrophobic nature, is able to intercalate between DNA base pairs of the epidermal keratinocytes remaining quiescent in the absence of ultraviolet radiation. Once exposed to UVA light, 8-MOP bonds to DNA forming monofunctional or bifunctional adducts. Thus, leads to inhibition of DNA synthesis and cell division. In addition, activated 8-MOP interacts with molecular oxygen forming reactive oxygen species which damage cell membrane by lipid peroxidation, disrupts mitochondria

and activates eicosanoid pathways [68]. Nowadays, systemic PUVA that requires the oral administration of 8-MOP is most commonly used due its effectiveness and the ease of its achievement. In systemic PUVA, a crystalline form of 8-MOP in the dosage of 0.6 mg/kg is commonly administered 2 hours before the patient is irradiated with UVA. Alternatively, an encapsulated form at a dose of 0.4 mg/kg is administered 90 min before irradiation [69]. However, systemic PUVA therapy is associated with acute gastrointestinal side-effects such as nausea and vomiting. Moreover, a long-term exposure to UVA light may increase the risk of photocarcinogenesis and glaucoma [70,71]. In addition, 8-MOP is characterized by a high variability in absorption from the gastrointestinal tract with significant inter-individual dissimilarities in peak blood concentrations, as well as a strong first-pass effect through the liver [70]. In order to minimize the systemic PUVA adverse effects, in some dermatological treatments topical PUVA therapy is preferred. The maximum therapeutic effects in PUVA are obtained if the skin is exposed to UVA when 8-MOP level reaches the highest concentration in the skin [67]. In topical PUVA, an emollient base containing 0.1% 8-MOP is commonly employed. It should be applied 30 min before exposure to UVA starting at a dose of 0.25 to 0.5 J/cm2 (Joule/cm2) and increasing the dose up to 0.5 J/cm2 depending on the patient's tolerance [68]. 8-MOP has been employed into many formulations such as ointments, lotions, tinctures, emulsions and creams. Unfortunately, these conventional vehicles produce poor skin accumulation and weak skin permeability of psoralens [70,72]. As a consequence, to reach the maximum therapeutic effect will be necessaries more frequent treatment sessions, however this might increase the risk of side effects [72]. With the aim of overcoming the issues associated with conventional vehicles, 8-MOP has been formulated in a variety of nanocarriers such as nanoemulsions [73–75]; microemulsions [76,77]; liposomes [67,72,78,79]; ethosomes [79]; niosomal carriers [67,70]; lipid nanoparticles (solid lipid nanoparticles (SLN) and nanostructured lipid carriers (NLC)) [80] and polyamidoamine dendrimers [71]. Indeed, it has been demonstrated that the use of nano-delivery systems presents several advantages over the classical delivery systems such as the ability to improve the solubility of the delivered drug, ensure a controlled or sustained release, enhance drugs' stability and facilitate the delivery to the target site, which make the therapy more effective and reduce the toxicity. Among all the different types of nanodelivery systems, lipid-based nanoparticles have been the most studied by scientists of all over the world since the first nanotechnology approaches were employed in the field of drug delivery. Indeed, they offer several advantages such as being highly biocompatible and cost-effective. Moreover, the encapsulation of various APIs in these

systems can improve their physico-chemical stability, reduce the serious side effects of skin irritation, enhance topical absorption improve the solubility and bioavailability of poorly water-soluble and/or lipophilic drugs. Since 8-MOP is reactive with oxidizing agents, sensitive to light (it gradually darkens on exposure to light) and it is characterized by a high lipophilicity which makes challenging its topical bioavailability, its encapsulation in lipid-based nanosystems could be a promising approach to overcome this issue.

In order to promote the skin accumulation of 8-MOP we encapsulated this drug in two different lipidic nanocarriers (PEVs and SLNs) introducing in our formulations the penetration enhancer Transcutol® P. Transcutol® is an hydroalcoholic solvent, reported as diethylene glycol monoethyl ether under EP and USP/NF monographs. It is available as a clear liquid characterized by low viscosity and it is almost odourless [81]. Due to its high safety profile and its miscibility with both polar and non-polar solvents, it is an attractive skin penetration enhancer [82]. Transcutol® skin penetration enhancing effect may be attributed to a wide range of mechanism. It may increase thermodynamic driving force and decrease drug charge. Moreover, due to its ability to penetrate the stratum corneum and interact with the water of the intercellular region, it modifies the skin barrier in a reversible way. Thus, makes the skin more permeable to the topically applied API [81].
In ***Chapter 1*** we compare the ability of free-Transcutol® P and Transcutol® P solid lipid nanoparticles (SLNs) to promote skin accumulation of 8-MOP.
In ***Chapter 2*** we employed Transcutol® P for the formulation of penetration enhancer containing vesicles (PEVs).

Chapter 1: Combination of Solid Lipid Nanoparticles (SLN) and Transcutol® P to promote 8-MOP skin delivery

The majority of this chapter has been directly copied or modified from *Pharmaceutics* **2020**, *12(10), 973;* "Transcutol® P Containing SLNs for Improving 8-Methoxypsoralen Skin Delivery" by **Pitzanti, G.**; Rosa, A.; Nieddu, M.; Valenti, D.; Pireddu, R.; Lai, F.; Cardia, M.C.; Fadda, A.M.; Sinico, C.*; *https://doi.org/10.3390/pharmaceutics12100973*

ABBREVIATIONS

8-MOP	8-methoxypsoralen
DMSO	Dimethyl Sulfoxide
EE%	Entrapment Efficiency
FA	Fluocinolone Acetonide
FC	Free Cholesterol
HPLC	High Performance Liquid Chromatography
M3-PALS	Phase Analysis Light Scattering
MD	Mean Diameter
MTT	3-(4,5-dimethylthiazol-2-yl)-2,5-diphenyltetrazolium bromide
MTX	Methotrexate
NLC	Nanostructured Lipid Carriers
P-PL	Polyunsaturated Phospholipids
P188	Poloxamer 188
PBS	Phosphate-Buffered Saline
PC 16:0/16:0	1,2-dipalmitoyl-sn-glycero-3-phosphocholine
PC 16:0/18:1	1-palmitoyl-2-oleoyl-sn-glycero-3-phosphocholine
PC 16:0/18:2	2-linoleoyl-1-palmitoyl-sn-glycero-3-phosphocholine
PC 16:0/20:4	2-arachidonoyl-1-palmitoyl-sn-glycero-3-phosphocholine
PC 18:1/16:0	1-oleoyl-2-palmitoyl-sn-glycero-3-phosphocholine
PC 18:1/18:1	1,2-dioleoyl-sn-glycero-3-phosphocholine
PC 18:2/18:2	1,2-dilinoleoyl-sn-glycero-3-phosphocholine
PC 20:5/20:5	1,2-dieicosapentaenoyl-sn-glycero-3-phosphocholine
PCS	Photon Correlation Spectroscopy
PDI	Polydispersity Index
S/M–PL	Saturated/Monounsaturated Phospholipids
SLNs	Solid Lipid Nanoparticles
TEM	Transmission Electron Microscopy
TRC	Transcutol® P
ZP	Zeta Potential

1. Introduction

Solid lipid nanoparticles (SLNs) were first introduced in 1990s as a promising alternative to the pre-existing lipid systems (emulsions and liposomes) and polymeric nanoparticle systems. Their matrix is constituted by lipids being solid either at room and at body temperature, dispersed in an external aqueous phase, stabilized by one or more surfactants. SLNs have been studied for parenteral, oral, ocular, pulmonary and cutaneous drug administration. Among the different applications of SLNs, their use for skin drug delivery represents one of the most promising [65]. Solid lipid nanoparticles have shown a great potential for the treatment of different skin disorders such as psoriasis [80,83,84], acne vulgaris [85,86], atopic dermatitis [87], skin infections [88–90] and skin cancers [91–93]. In the management of skin disorders is desirable the creation of drug depots in the skin from which the drug is slowly released over a period of time. SLNs have shown the ability of maintaining the required drug concentration in the skin for a prolonged time [94]. Moreover, their small particle size ensures a high adhesion to the uppermost epidermal layer and the formation of a highly hydrophobic film with occlusive effect avoiding the transepidermal water loss. As a result, the skin penetration of the encapsulated agent is facilitated [55,65,80,81,95]. Furthermore, their components are highly biocompatible lowering the risk of skin irritation [55,65,95]. In addition, they offer the possibility to a controlled drug release [55,65,80,95]. Thus, SLNs represent an attractive drug delivery system for topical/transdermal use.

In psoriasis topical therapy the main challenges are related to the stratum corneum thickening and scaling which make it an even harder barrier to be crossed by different active ingredients. Different research groups have demonstrated the potential of SLNs in psoriasis topical therapy. For instance, Pradhan et al. evaluated the potential of solid lipid nanoparticles (SLNs) as a topical delivery system for the synthetic hydrocortisone derivative Fluocinolone acetonide (FA). The formulations were optimized using Box–Behnken design of Design Expert software and evaluated for particle size, polydispersity index, zeta potential, drug encapsulation efficiency and drug loading. Shape and surface morphology of the SLNs were investigated under a transmission electron microscope. Powder X-ray diffraction and differential scanning calorimetry demonstrated the complete encapsulation of the drug in the nanoparticles. SLNs led to a prolonged release of Fluocinolone acetonide whilst pure drug suspension exhibited faster drug release. SLNs remained

stable for 3 months at 4 °C. Finally, in vitro skin distribution studies showed a higher amount of FA on the epidermis when treated with FA loaded SLNs suspension than when a plain FA suspension is applied to the skin. Moreover, the amount of FA detected in the receptor fluid after the application of FA loaded SLNs suspension was quite low as compared to the plain FA suspension suggesting a minimal distribution of the drug in systemic circulation which might eliminate adverse side effects associated with systemic exposure [96].

Ferreira et al. developed solid lipid nanoparticles for the co-delivery of methotrexate and etanercept. The SLNs were incorporated in a Carbopol hydrogel and their potential for delivering the drugs into the skin was evaluated. Pig ear was used as a model for the in vitro permeation studies. When incorporated within solid lipid nanoparticles methotrexate showed a higher skin accumulation than when the free drug was applied. The incorporation of the SLNs in a Carbopol hydrogel increased the MTX retention time within the skin. Moreover, the amount of drug permeated the skin was reduced thus limiting the % of MTX and etanercept which reached the systemic circulation. The results were confirmed by preliminary studies using human skin biopsies from healthy and psoriatic regions.

In 2008 Fang and his co-workers were the first to investigate the potential of solid lipid nanoparticles (SLN) as vehicles for topical psoralen delivery [80]. The group of Fang demonstrated the ability of SLNs to enhance the skin permeation and ensure a controlled release of topically applied psoralen-loaded SLNs [80].

Starting from their promising results, we decided to develop penetration enhancer containing SLNs in order to enhance 8-MOP skin accumulation. For this purpose, we added to the conventional SLNs the penetration enhancer Transcutol® P (TRC). Transcutol® has been successfully combined with numerous nanocarriers in order to enhance skin delivery [82,97–99]. However, to the best of our knowledge, its ability of promote skin delivery of compounds encapsulated into solid lipid nanoparticles has not been highly investigated.

In this work, empty and drug loaded SLNs including the penetration enhancer Transcutol® (TRC) at different concentrations (2% or 4%) were obtained by hot homogenization followed by ultrasonication. Moreover, the respective loaded and unloaded formulations without the penetration enhancer were prepared as control. The prepared formulations were characterized in terms of size, polydispersity index, zeta potential and encapsulation efficiency. The stability of

the SLNs was monitored for 90 days. Moreover, the nanoparticles morphology was evaluated by transmission electron microscopy. 8-MOP release from SLNs was investigated using Franz diffusion cells. The 8-MOP accumulation in the different skin layers and permeation through the whole skin after application of free TRC-SLNs or TRC SLNs were assessed by Franz diffusion experiments. *In vitro* biocompatibility of all unloaded and 8-MOP loaded formulations was checked measuring 3T3 fibroblasts viability by using the MTT assay. Finally, the influence of the incorporation of TRC in SLNs on the cellular uptake of nanoparticles was also evaluated.

2. Materials and Methods

2.1 Materials

8-MOP and Pluronic F68 (Poloxamer 188) were purchased from Sigma Aldrich (Milan, Italy). Compritol 888 ATO and Transcutol® P were kindly supplied by Gattefossé (Lyon, France). Cell culture materials were purchased from Invitrogen (Milan, Italy). Cholesterol, standards of fatty acids, 3-(4,5-dimethylthiazol-2-yl)-2,5-diphenyltetrazolium bromide (MTT), 1,2-dipalmitoyl-sn-glycero-3-phosphocholine (PC 16:0/16:0), 1,2-dioleoyl-sn-glycero-3-phosphocholine (PC 18:1/18:1), 1-palmitoyl-2-oleoyl-sn-glycero-3-phosphocholine (PC 16:0/18:1), 1-oleoyl-2-palmitoyl-sn-glycero-3-phosphocholine (PC 18:1/16:0), 2-linoleoyl-1-palmitoyl-sn-glycero-3-phosphocholine (PC 16:0/18:2), 2-arachidonoyl-1-palmitoyl-sn-glycero-3-phosphocholine (PC 16:0/20:4), 1,2-dilinoleoyl-sn-glycero-3-phosphocholine (PC 18:2/18:2), and 1,2-dieicosapentaenoyl-sn-glycero-3-phosphocholine (PC 20:5/20:5) were purchased from Sigma–Aldrich (Milan, Italy). All the other compounds and solvents were of analytical grade and used as received from Sigma Aldrich (Milan, Italy).

2.2. SLN preparation

SLNs were prepared by hot homogenization followed by ultrasonication. The lipid phase, containing 8-MOP and the solid lipid Compritol 888 ATO, was heated until a temperature of ten degree above the solid lipid melting point was reached. A hot aqueous solution of Poloxamer 188

and Transcutol® P (when present in the formulation) was separately heated at the same temperature of the lipid phase and subsequently dispersed into the drug-containing melt. The obtained pre-emulsion was homogenised using a high share homogenizer (Ultra Turrax T25 basic) for 1 minute at 6500 rpm and then sonicated for 4 minutes with a Soniprep 150 (MSE Crowley, UK) thermostated at 85 °C. Thereafter, the produced hot O/W nanoemulsion was left cooling down to room temperature in order to allow the lipid re-crystallisation and the development of SLNs. Additionally, empty control SLNs were prepared using the same technique and the same surfactant concentration of loaded formulations.

2.3. Characterization of Solid Lipid Nanoparticles

Particle size and Z potential Analysis

The average diameter (nm±SD) and polydispersity index (PDI, a measure of the size distribution width) of the SLNs were determined by photon correlation spectroscopy (PCS) using a Zetasizer nano (Malvern Instruments, Worcestershire, United Kingdom). Samples were backscattered by a helium-neon laser (633 nm) at an angle of 173° and a constant temperature of 25 °C.

The zeta potential (ZP) was estimated by means of the M3-PALS (Phase Analysis Light Scattering) technique using the same instrument. Each sample was properly diluted with bidistilled water just before the analysis. All the measurements were made in triplicate.

A medium-term stability study of SLN stored at 25 ± 1 °C was performed by monitoring average size, polydispersity index, and surface charge for 90 days.

Encapsulation Efficiency

The total amount of 8-MOP encapsulated within nanoparticles, known as entrapment efficiency (EE%), was determined by an indirect method. Briefly, 500 µL of 8MOP-SLN dispersions were placed in the upper chamber of an Amicon® Ultra-0.5 (30 kDa) centrifugal filter unit and centrifuged at 15000 rpm for 30 min using a cooling centrifuge (Scilogex mod. D3024R, Rocky Hill, CT, USA) to separate the lipid and aqueous phase. The unentrapped drug collected in the filtrate in the lower chamber was assayed by HPLC after being properly diluted with methanol.

Entrapment efficiency (EE%) was calculated according to the following equation:

$$EE\% = \frac{(\text{Amount of drug added} - \text{Amount of free drug})}{(\text{Amount of drug added})} \times 100$$

Transmission electron microscopy (TEM)

The morphology of 8-MOP SLNs was studied using a transmission electron microscopy (TEM) Jeol JEM 1400 Plus (Jeol, Milan, Italy) operating at 120 kV. A drop of SLN dispersion was placed on the surface of a carbon-coated copper grid and subsequently stained with an equal volume of an aqueous 1% phosphotungstic acid solution. Finally, the grid was dried at room temperature and the sample was observed.

2.4. 8-MOP quantification

8-MOP was quantified using a liquid chromatograph Alliance 2690 (Waters, Milan, Italy) equipped with a multi λ fluorescence detector and a computer integrating software (Empower 3). The excitation wavelength was set at 317 nm and emission wavelength at 445 nm. The column was a X Terra RP18 (3.5 µm, 4.6 mm × 100 mm, Waters), and the mobile phase was a mixture of water: methanol: acetonitrile (40:40:20, v/v) eluted at a flow rate of 0.5 mL/min. A standard calibration curve was built up by using standard solutions. Calibration graphs were plotted according to the linear regression analysis, which gave a correlation coefficient value (R2) of 0.999.

2.5. In Vitro Release Experiments

In vitro release experiments of 8-MOP from the SLNs under investigation were carried out using Franz-type diffusion cells (LGA, Berkeley, CA, USA). Cellulose membranes were soaked in water for 1h at room temperature. After 1h, they were mounted in Franz-type diffusion cells between the donor and the receptor compartment. A hydroalcoholic solution composed of water: ethanol in the ratio of 50:50 (v/v) was used as release medium to ensure pseudo-sink conditions by increasing the active compound solubility in the receiving phase. The release medium was constantly stirred using a magnetic stirrer and thermostated at 37 °C throughout the study. In total, 200 µL of each formulation were applied on the membrane surface under non occlusive

conditions and the experiments were run for 24 h. At regular time intervals, the solution contained into the receiving compartment was withdrawn and replaced with an equivalent volume of pre-thermostated (37 °C) fresh medium. The 8-methoxypsoralen concentration in the receptor medium samples was determined by HPLC by using the method described in the paragraph 2.4.8. Each experiment was performed at least on three replications.

2.6. In vitro skin penetration and permeation studies

Experiments were performed non-occlusively using vertical diffusion Franz cells with an effective diffusion area of 0.785 cm^2 and newborn Goland-Pietrain hybrid pig skin. The pigs (~1.2 kg) died of natural causes a few hours after birth and were provided to us by a local slaughterhouse. The pig hair was shaved and the skin was excised using a surgical sterile scalpel and the subcutaneous fat was removed. The skin was carefully observed to visualize any wounds, punctures, holes, bleeding, or skin disease. The skin was cut into squares of 3 × 3 cm^2, randomized, and stored −80 °C until the experiments. 24 hours before the experiment, the skin was defrosted and pre-equilibrated in saline solution (0.9% w/v of NaCl) at 25 °C. Newborn pig skin specimens were placed between donor and receptor compartments of the Franz cells, with the epidermis' side facing the donor compartment. The receptor compartment was filled with 5.5mL of hydroalcoholic solution (ethanol: phosphate buffered saline solution 50:50) which was kept under continuously stirring with a small magnetic bar and thermostated at 37±1 ◦C throughout the experiments to keep the skin temperature at the physiological conditions (32±1 ◦C). Since 8-MOP is a lipophilic drug, ethanol was added into the receptor media in order to enhance 8-MOP solubility into the more hydrophilic skin strata and therefore promote its diffusion through the skin following the gradient created by ethanol. In previous works of our research group, it has been demonstrated that the skin integrity was not affected after in vitro skin penetration and permeation studies where a hydroalcoholic solution was used as receptor medium.

100 µL of either 8-MOP loaded SLNs with or without PE were placed onto the skin surface (n=6 skin specimens per tested formulation). At regular intervals of 2 h up to 8 h, the solution contained into the receiving compartment, was withdrawn, replaced with an equivalent volume of pre-thermostated fresh solution and analysed by HPLC for its 8-MOP content. Fang et al. reported that when 8-MOP loaded SLN are administered in vitro in newborn pig skin, the flux of 8-MOP through

the skin is low (14.5 µg cm^{-2} h^{-1})[80]. Since we expected a low permeation of 8-MOP we decided to perform sampling at regular intervals of 2 hours from the beginning of the study. After 8 h, the skin surface of specimens was washed with distilled water then dried with filter paper. The stratum corneum (SC) was removed by stripping with an adhesive tape Tesa® AG (Hamburg, Germany). A piece of the adhesive tape was firmly pressed on the skin surface and rapidly pulled off with one fluent stroke. Ten stripping procedures were performed consecutively. The epidermis was separated from the dermis with a surgical sterile scalpel. Tape strips, epidermis, and dermis were cut and placed into separated flask with methanol and sonicated (Soniprep 150, MSE Crowley, UK) for 4 min for 8-MOP extraction. The tapes and tissue suspensions were centrifuged for 10 min at 10.000 rpm, the supernatant was filtered and assayed for 8-MOP content by HPLC.

2.7. Cell culture

Mouse 3T3 fibroblasts (ATCC collection) were grown at 37 °C in Dulbecco's modified Eagle's medium (DMEM, Invitrogen, USA), supplemented with 10% (v/v) fetal bovine serum, penicillin (100 U mL^{-1}), and streptomycin (100 µg mL^{-1}) (Invitrogen) in a 5% CO_2 incubator at 37 °C.

2.8. Cytotoxicity assessment, MTT assay

The cytotoxic effect of the SLNs was evaluated in 3T3 fibroblasts by the MTT [3(4,5-dimethylthiazolyl-2)-2, 5- diphenyltetrazolium bromide] colorimetric assay. 3T3 cells were seeded in 96-well plates at a density of 3×10^4 cells/well in 100 µL of serum-containing media. Experiments were carried out two days after seeding when cells had reached 90% confluence. Different concentrations (1.25, 2.5 and 5 µL/mL) of SLNs formulations were added to the cells in 100 µL of complete medium. Cell were then incubated at 37 °C for 24 h. At the end of the incubation time, cells were subjected to the MTT test as previously reported [100]. Colour development was measured at 570 nm with an Infinite 200 auto microplate reader (Infinite 200, Tecan, Austria). The absorbance is proportional to the number of viable cells. Results are shown as percent of cell viability in comparison with non-treated control cells. Cytotoxicity of pure 8-MOP at the dose of 5 µg/mL (from a 1 mg/mL DMSO solution) was also evaluated in 3T3 cells (24 h of incubation) for comparison. Evaluation of the cell morphology after 24 h of incubation with different SLNs was also performed by microscopic observation.

2.9. Lipid Profile Modulation in 3T3 Fibroblasts

3T3 fibroblasts, 2 days post-seeding (at a density of about 106 cells/10 mL of complete medium) in Petri dishes, were treated with 5 µL/mL of SLNs formulations in fresh medium. After 24 h of incubation at 37 °C, the cells were washed with PBS and scraped. After centrifugation (1200 g at 4 °C for 5 min), cell pellets were separated from supernatants and used for the extraction and analyses of lipid compounds.

2.10. 3T3 Cell Lipid Extraction and Analysis

Total lipids were extracted from 3T3 cell pellets using the mixture $CHCl_3$/MeOH/H_2O 2:1:1 as previously reported. Dried aliquots of the $CHCl_3$ fraction, from each cell sample, dissolved in MeOH, were injected into the HPLC system for the direct analysis of lipid components (phospholipids, PL, and free cholesterol, FC) [101,102]. Another aliquot of dried $CHCl_3$ fractions, dissolved in EtOH, was subjected to mild saponification [101]. The saponifiable phase with free fatty acids was collected and a portion of the dried residue was dissolved in CH_3CN/0.14% CH_3COOH (v/v). Analyses of lipid compounds were carried out with a 1100 HPLC equipped with a DAD and an Agilent 1100 HPLC-DAD/1260 ELSD system, equipped with an Inertsil ODS-2 column, for the direct analysis of lipid components (phospholipids, PL, and free cholesterol, FC) with MeOH as the mobile phase, at a flow rate of 2 mL/min and ELSD detection, as previously reported [101,102]. Another aliquot of dried $CHCl_3$ fractions, dissolved in EtOH, was subjected to mild saponification. The mixture of free fatty acids (saponifiable phase) was collected, dissolved in CH_3CN/0.14% CH_3COOH (v/v), and injected into the 1100 HPLC-DAD/1260 ELSD system according to the literature [101]. Unsaturated (DAD detection, 200 nm) and saturated fatty acids (ELSD detection) were separated with an XDB-C18 Eclipse column with the mixture CH_3CN/H_2O/CH_3COOH (75/25/0.12, v/v/v) as the mobile phase (at a flow rate of 2.3 mL/min) as previously reported [100,101]. The Agilent OpenLAB Chromatography data system was used for the recording/integration of the chromatogram data. Lipid components were identified using standard compounds and UV spectra. Calibration curves, constructed using standard compounds, were linear (DAD) and quadratic (ELSD) for unsaturated and saturated fatty acids, respectively [101].

2.11. Statistical analysis

Data analysis was carried out with the software package Microsoft Excel, version 2020. Results are expressed as mean±standard deviation (3 independent samples). Evaluation of statistical significance of differences for the experiments on 3T3 cells was performed using Graph Pad INSTAT software (GraphPad software, San Diego, CA, USA). Comparison between groups was assessed by Student's unpaired t test with Welch's correction or one–way analysis of variance (One–way ANOVA) followed by the Bonferroni Multiple Comparisons Test.

3. Results and Discussion

In the present study, different SLN formulations were prepared by hot homogenization followed by ultrasonication.

Empty and 8-MOP loaded SLNs were obtained using Compritol 888 ATO (4% wt/wt) as solid lipid and different concentrations (2%, 4%) of the penetration enhancer Transcutol® P (TRC). Empty and 8-MOP loaded SLN without Transcutol® P were also prepared as a control. Compritol 888 ATO is a solid lipid which is composed of mono-, di- and triglycerides of behenic acid (C22) and is one of the most used solid lipid for the development of SLN. All the formulations were stabilized with the non-ionic surfactant Poloxamer 188 (P188). When developing dermatological products, non-ionic surfactants are preferred over ionic surfactants because of their better skin tolerability. The composition of the SLNs described in this work is the result of pre-formulation studies where the influence of different concentrations of the solid lipid and of the penetration enhancer on the stability of the SLN (in terms of mean diameter, polydispersity index and zeta potential) was evaluated. The maximum concentration of Transcutol we were able to add to the formulation of SLN was 4% (wt/wt). At higher %, we observed significative changes in the physicochemical characteristics of the SLNs short time after the preparation. In **Table 2** is reported the composition of the optimized SLNs.

Table 2. Composition of 8-MOP loaded and unloaded SLN.

	Compritol 888 ATO (%wt/wt)	P188 (%wt/wt)	8-MOP (%wt/wt)	Transcutol®P (%wt/wt)	Water (%wt/wt)
Empty SLN TRC 0%	4	2.2	–	–	93.8
SLN TRC 0%	4	2.2	0.1	–	93.7
Empty SLN TRC 2%	4	2.2	–	2	91.8
SLN TRC 2%	4	2.2	0.1	2	91.7
Empty SLN TRC 4%	4	2.2	–	4	89.8
SLN TRC 4%	4	2.2	0.1	4	89.7

In order to determine the SLN mean diameter, PDI and zeta potential, PCS analysis were performed on all empty and loaded formulations at the same day of preparation (**Table 3**). We can observe that the incorporation of the penetration enhancer does not significantly affect the mean diameter of the empty nanoparticles. Empty SLNs exhibit a mean diameter ranging between 120.1 nm and 132.9 nm. 8-MOP incorporation does not directly influence the nanoparticle size, although they were prepared with different TRC concentrations. Polydispersity index values for all formulations were always smaller than 0.3, thus indicating a fairly narrow size distribution. Both empty and loaded formulations showed highly negative ζ potential values ranging between −30 and −37 mV (no statistically significant difference was found for all empty and loaded SLNs). These values should be adequate to prevent aggregation or fusion phenomena between the nanoparticles during storage. Entrapment efficiency (EE%) was always higher than 90% and independent of the TRC concentration.

Table 3. Mean diameter (MD), polydispersity index (PDI), zeta potential (ZP) and % entrapment efficiency (EE%) observed for freshly prepared 8-MOP loaded and unloaded SLN using different amounts of Transcutol® P. Mean values ± standard deviation, obtained from at least 3 independent samples, were reported.

	MD (nm) ± S.D.	PDI ± S.D.	ZP (mV) ± S.D.	EE% ± S.D.
Empty SLN TRC 0%	132.9 ± 3.8	0.238 ± 0.010	-35.5 ± 1.5	-
SLN TRC 0%	125.8 ± 5.2	0.234 ± 0.010	-35.4 ± 2.0	97.2 ± 0.2
Empty SLN TRC 2%	120.1 ± 13.8	0.233 ± 0.009	-35.2 ± 1.7	-
SLN TRC 2%	126.0 ± 1.0	0.225 ± 0.013	-36.9 ± 1.5	97.4 ± 0.3
Empty SLN TRC 4%	125.0 ± 5.5	0.251 ± 0.018	-30.3 ± 5.1	-
SLN TRC 4%	130.5 ± 1.2	0.234 ± 0.012	-35.6 ± 1.4	99.6 ± 0.6

We evaluated experimentally the stability of the SLNs monitoring the mean diameter, the PDI and the zeta potential for 90 days storing the formulations at room temperature. Figures 1 A and B show the results of the stability study.

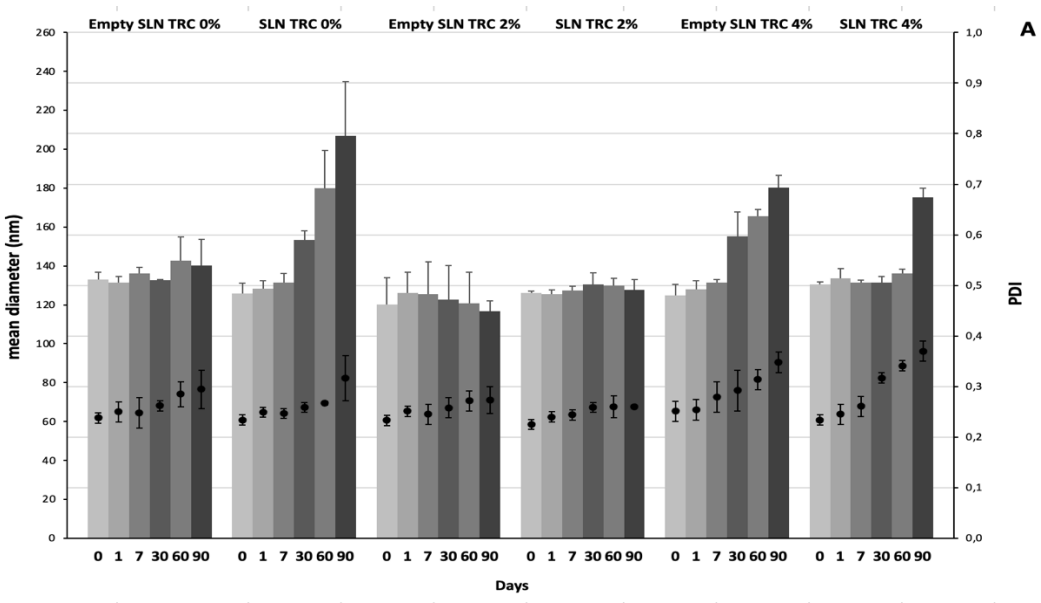

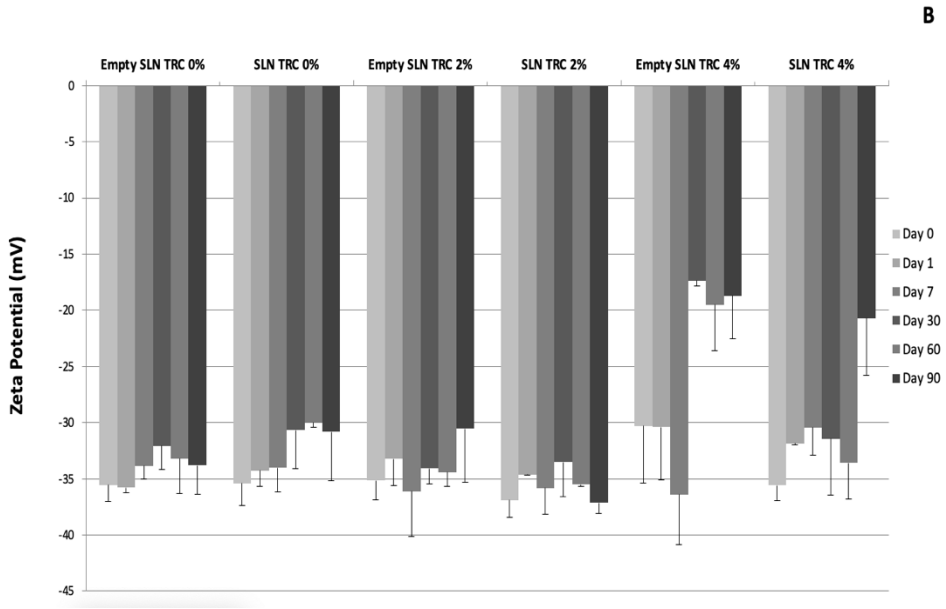

Figure 1. Values of mean diameter, polydispersity index (**A**), and zeta potential (**B**) of 8-MOP loaded and unloaded SLN collected over 90 days of storage at 25 ± 1 °C. Mean values ± standard deviation (error bars) were reported from at least 3 independent samples.

All the formulations keep constant the mean particle size during the first 30 days of storage. Empty SLN TRC 0%, empty and 8-MOP loaded SLN TRC 2% do not show any growth in their size after 90 days of storage. On the contrary, SLN TRC 0% and empty SLN TRC 4% show a progressive increase of this parameter starting from day 30. At day 90, SLN TRC 4% shows an increase in particle size of around the 35% in comparison to the freshly prepared formulation.

As concern to the polydispersity index, empty and 8-MOP SLN TRC 0% show a slight increase of this parameter from day 60 and day 90 respectively. The formulations with the lowest concentration of the penetration enhancer (empty and 8-MOP loaded SLN TRC 2%) do not show any increase of this parameter during the stability study. On the contrary, empty and 8-MOP loaded formulations with the highest concentration of Transcutol® P (empty and 8-MOP loaded SLN TRC 4%) exhibit a gradually increase in the polydispersity index during the 90 days of storage. The Z potential values were always highly negative (from ∼−30 to ∼−37mV), indicative of a good stability against nanoparticle aggregation and fusion. However, empty SLN TRC 4% shows a Z potential of ∼−18 mV after 30 days of storage. Since after 30 days of storage this formulation shows also an increase in size and polydispersity index, probably some aggregation phenomena

have occurred. The same behaviour was observed for the correspondent loaded formulation at day 90.

The evaluation of the morphology of the SLN was performed using transmission electron microscopy (TEM). **Figure 2** shows a representation of the SLN TRC 0% and SLN TRC 2%. The SLNs show diameters lower than the values obtained by DLS analysis. However, we would like to point out that this result is in accordance with the literature data [103,104], and can be explained by the ability of DLS to measure the hydrodynamic diameter of hydrated particles, which is also influenced by all substances adsorbed on the nanoparticle surface (hydration layer, polymer shell, or surfactants). Thus, it is always larger than the dry particle diameter obtained with TEM or SEM, which measure the geometrical size.

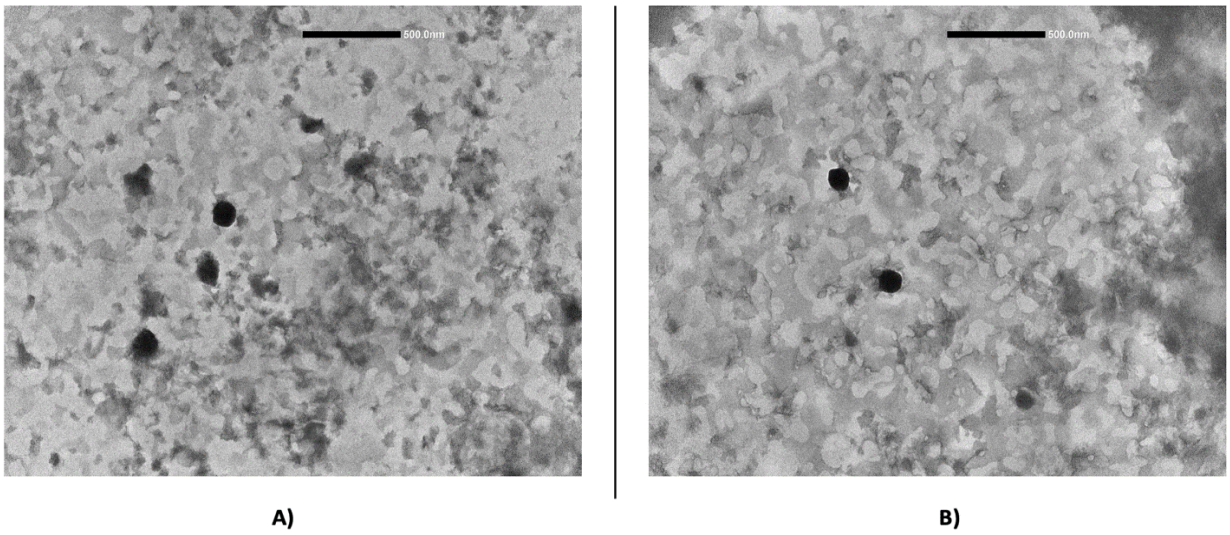

Figure 2. TEM micrograph of 8-MOP loaded SLN TRC 0% (**A**) and SLN TRC 2% (**B**).

Before studying the skin permeation behaviour, an 8-MOP release study through a cellulose membrane was performed. In **Figure 3** are reported the μg/cm^2 of 8-MOP released from SLNs during 24h.

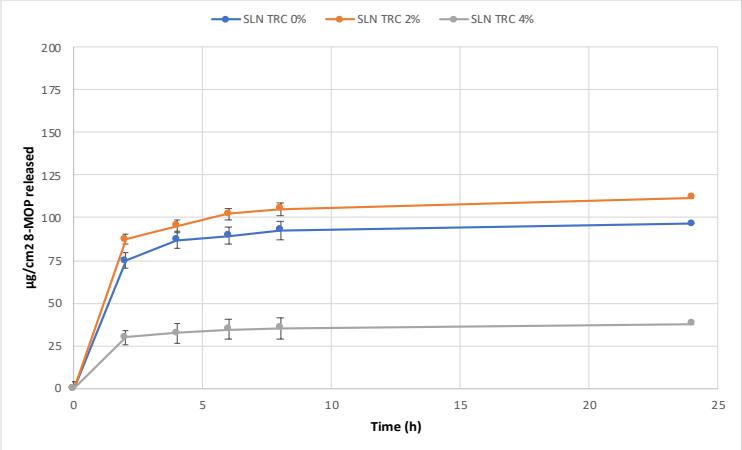

Figure 3. µg/cm^2 of 8-MOP released from SLNs during 24h. Each value is the mean ± standard deviation of six experimental determinations.

Since 8-MOP is a poorly water-soluble drug, an increase of its release from SLN should result in an increase of its thermodynamic activity and, therefore, in an increase in its diffusion rate. However, the 8-MOP release rate from the studied SLNs was really slow for all the studied formulations, even using a hydroalcoholic solution as receptor fluid. All the formulation showed an initial burst release followed by a sustained release which levelled off after 8h in the case of the formulation SLN TRC 0% and SLN TRC 2%, and after 6h in the case of the formulation SLN TRC 4%. SLN TRC 4% exhibited a lower initial burst release and was able to release less 8-MOP over the 24h of the experiment compared to the other two formulations (SLN TRC 0% and SLN TRC 2%). We hypothesize that this behaviour is related to the high stability and high entrapment efficiency of this formulation (SLN TRC 4%).

In order to clarify the influence of SLNs with increasing concentration of TRC on 8-MOP cutaneous delivery, *in vitro* penetration and permeation studies were carried out using newborn pig skin and vertical Franz diffusion cells. Experiments were performed in non-occlusive condition for 8 h and using the whole skin, since this model enabled us to measure both drug skin flux as well as drug accumulation in skin strata. Previous studies with newborn pig skin demonstrated that this animal model provides reliable information to predict drug permeation through human skin. Indeed, newborn pig stratum corneum possess a lipid composition and a thickness very similar to that of human [105,106].

In **Figure 4** the amount of permeated 8-MOP per area is plotted against time. Examination of the permeation graphs suggests that all the studied carriers reached steady-state conditions, but after

different lag times. In a previous work Fang et al. investigated the skin permeation of 8-MOP from an aqueous suspension, a lipid emulsion and nanoparticulate lipid systems (SLN and NLC). Compared to the lipid emulsion and aqueous control, enhanced psoralen permeation was achieved with the SLN and NLC. In particular, the flux was found to be higher for both NLC vehicles (21.0 μg cm^{-2} h^{-1}), SLN (14.5 μg cm^{-2} h^{-1}) and aqueous suspension (13.1 μg cm^{-2} h^{-1}), and lower for lipid emulsion (8.3 μg cm^{-2} h^{-1}). In this study, SLN TRC 0% and SLN TRC 2% formulations provided a lower flux (1.00 and 0.83 μg cm^{-2} h^{-1} respectively) than the formulations studied by Fang et al [80]. Indeed, after 8h only 5% (SLN TRC 0%) and 6 % (SLN TRC 2%) of the drug is released through the skin. This aspect is of great interest because it suggests that the drug is retained into the skin for a long time and systemic effects are minimized. By contrast, the mean amount of the drug permeated after 8 h experiment from SLN TRC 4% was 37.4 μg, with a steady-state flux 4.75 μg cm^{-2} h^{-1}. This is not surprising, given the different concentration of penetration enhancers between the tested SLNs. In these experiments, we did not use control formulations, such as emulsions or other lipidic nanocarriers, since 8-MOP solubility in different vehicles is different and, therefore, also its thermodynamic activity would be different. As consequence, comparisons between in vitro skin permeation results would be unreliable [80].

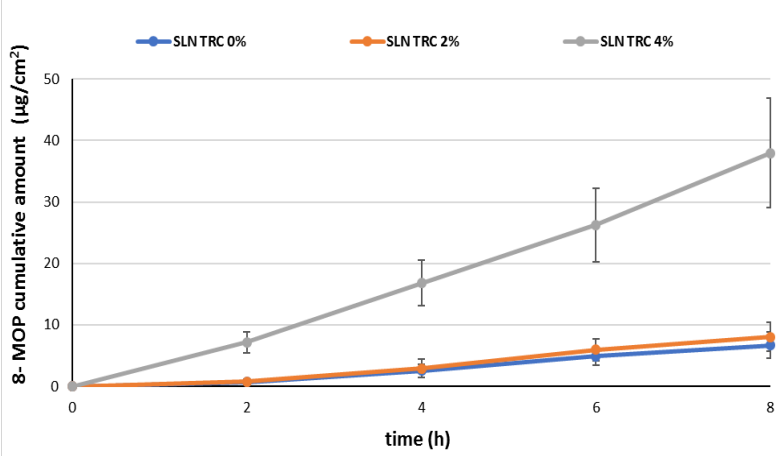

Figure 4. Cumulative amount of permeated 8-MOP per area against time.

The 8-MOP accumulation in the different skin layers (stratum corneum, epidermis and dermis) and permeation through the whole skin after application of Transcutol-free SLNs or SLN TRC are reported in **Figure 5**.

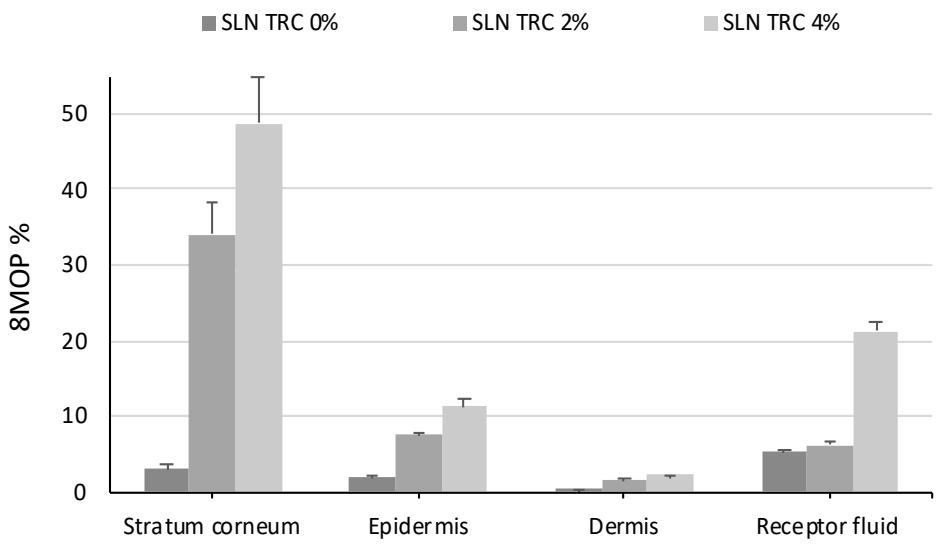

Figure 5. *In vitro* skin permeation studies: amount of 8-MOP accumulated in the skin layers (Stratum corneum; Epidermis; Dermis) and Receptor fluid after 8 h of non-occlusive application of the SLN. Each value is the mean ± standard deviation of six experimental determinations.

In accordance with the results obtained with others lipidic nanocarriers [73], all formulations showed higher drug accumulation in stratum corneum as compared to viable epidermis and dermis, since these strata have higher hydrophilic characteristics than stratum corneum. Therefore, lipophilic substances such as 8-MOP, tend to accumulate in this tissue. After SLN TRC 2% and TRC 4% application, the % of the drug accumulated in each skin layers was greater than that found after SLN TRC 0% application. In particular, Transcutol® P containing SLNs determine a greater 8-MOP accumulation in the stratum corneum than the formulation without Transcutol® P (SLN TRC 0%: 3%; SLN TRC 2%: 34%; SLN TRC 4%: 49%). SLN TRC 4% allows the highest 8-MOP accumulation into the epidermis (11%). This value is around six folds higher than the one obtained after the application of Transcutol-free SLN (2%).

The ability of different lipidic nanocarriers to enhance 8-MOP skin delivery has been previously reported in the literature [67,70,73,74,76,78,80,107–110]. For instance, in our group previous study, we incorporated 8-MOP into vesicular carriers (liposomes and niosomes) positively or negatively charged and we investigated their effect on 8-MOP diffusion through the skin and on its distribution within the skin layers. In comparison to the drug hydroalcoholic solution, all the vesicular carriers increased both the skin permeation and accumulation [67]. The results obtained

in this work with Transcutol SLNs revealed up to around a three-fold higher skin accumulation as compared by the data obtained with vesicles.

In a very recent work, Oliveira et al. investigated 8-MOP nanoemulsions for topical treatment of skin diseases. The ex vivo permeation study showed that 8.5% of the applied 8-MOP permeated through the skin, with a flux of 1.35 μg cm−2 h−1. The skin drug retention was almost two-fold higher than a commercial cream (∼23% and 14%, respectively) [74]. Once again, our formulations lead to a higher accumulation into the whole skin, reaching the maximum values for the formulation with the highest concentration of Transcutol (∼62% of the applied dose).

Indeed, the penetration enhancer is able to interact with the network of keratin and lipids (free fatty acids, cholesterol, and long-chain ceramides) that makes up the stratum corneum (SC), thus reducing its barrier effect. Moreover, it has been reported that Transcutol is a hygroscopic compound that can absorb water from the skin and can change the solubility of many drugs, thus improving their skin penetration into the inner skin strata [111]. The higher 8-MOP accumulation into the skin obtained after the application of Transcutol SLNs as compared to the drug skin accumulation obtained after the application of free-Transcutol SLNs may be a consequence of the combination of the two mechanisms of action of this penetration enhancer.

The overall results of the transdermal experiments clearly suggest that the higher the TRC%, the higher the flux and the skin accumulation. Higher skin accumulation of 8-MOP obtained with Transcutol P-containing SLNs might improve the efficacy of topical PUVA in psoriasis and minimize the risk of serious adverse effects.

If we compare the results obtained in the in vitro release experiments with the ones obtained in the *in vitro* penetration and permeation studies, we can notice that the formulation with the highest concentration of TRC is characterised by a low release. By contrast, the total amount of 8-MOP accumulated and permeated through the porcine skin is higher than the amount released when the formulation is applied onto a cellulose membrane. We hypothesize that the high amount of TRC allows an interaction of the formulation with the SC lipids which promotes the 8-MOP release. These does not happen when an inert membrane is employed.

SLNs formulations were tested in murine 3T3 fibroblasts by using the MTT assay. MTT assay has been previously used to test the cell viability and mitochondrial activity after treatment with biocompatible nanoparticles [101,112]. **Figure 6** shows the viability, expressed as % of the control,

induced in 3T3 fibroblasts after 24 h of incubation in the presence of different concentrations (1.25, 2.5, 5 µL/mL) of unloaded SLN (U-SLN) (**Fig. 6A**) and 8-MOP loaded SLN (L-SLN) (**Fig. 6B**) without or with different % of Transcutol® (TRC 2 or 4%). The treatment with all formulations did not induce a significant reduction in cell viability in the tested range with respect to the control cells. Pure 8-MOP, added to cells at the maximal dose present in the tested formulations, was not toxic for 3T3 cells, and the cell viability was 96% (data not shown).

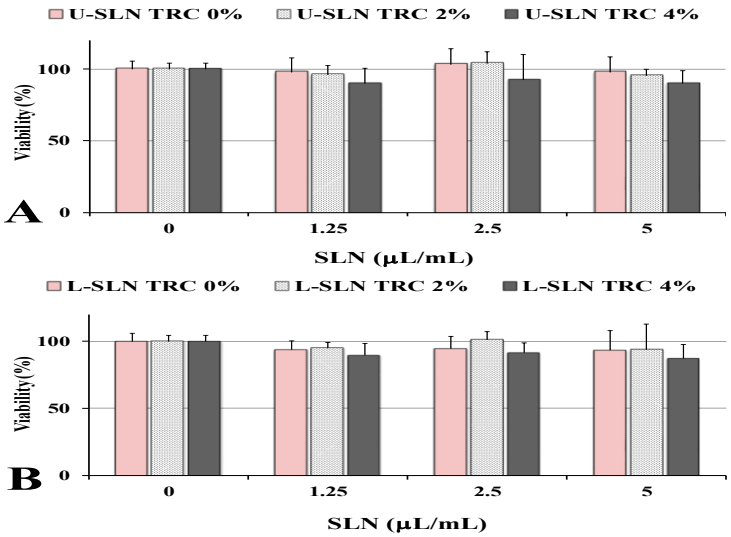

Figure 6. Viability (expressed as % of the control) (MTT assay) measured in control 3T3 fibroblasts (0) and cells treated for 24 h with three aliquots (1.25, 2.5, 5 µL/mL) of unloaded SLN (U-SLN) (**A**) and 8-MOP loaded SLN (L-SLN) (**B**) with different % of Transcutol® (TRC: 0, 2, 4%). Data are expressed as a mean ± standard deviation (SD) of three independent experiments involving triplicate analyses for each sample (n=9).

A study has been undertaken to investigate the impact of SLNs on 3T3 lipid profile as a marker of the cellular internalization of lipid nanoparticles. **Figure 7A** shows the chromatographic profile, obtained by HPLC-ELSD analysis, of polar lipid compounds (saturated/monounsaturated phospholipids, S/M–PL; polyunsaturated phospholipids, P-PL; free cholesterol, FC) measured in control 3T3 fibroblasts and cells treated for 24 h with unloaded SLN without TRC (Empty SLN TRC 0%) (5 µL/mL). The chromatographic region for each lipid class was assigned by using standard mixtures of saturated, monounsaturated, and polyunsaturated phosphatidylcholines and FC. The equivalent carbon number ECN =CN−2n, (CN is the number of acyl group carbons and n the number of double bonds) was used for the chromatographic separation of lipid components [101]. Control 3T3 cells showed a polar lipid profile characterized by two main peaks of PL, corresponding

to S/M-PL and P-PL, and a peak of FC. 3T3 cells treated with Empty SLN TRC 0% showed a slight change in the lipid profile, with a significant decrease in the % peak area of P-PL ($p < 0.05$ versus untreated cells) and a small increase in the % of S/M-PL (Fig. 7A). Figure 7C shows the values of the main fatty acids (expressed as µg/plate) measured in control 3T3 and fibroblasts treated with Empty SLN TRC 0% (24 h). Control 3T3 showed a lipid composition characterized by a high level of 18:1 isomers (18.96 ± 1.40 µg/plate; mainly oleic acid 18:1 n-9), palmitic acid (16:0), stearic acid (18:0), arachidonic acid (20:4 n-6) and linoleic acid (18:2 n-6). The incubation (for 24 h) of 3T3 cells with Empty SLN TRC 0% did not induce evident changes in fatty acid levels, with treated cells showing a profile similar to that of control cells.

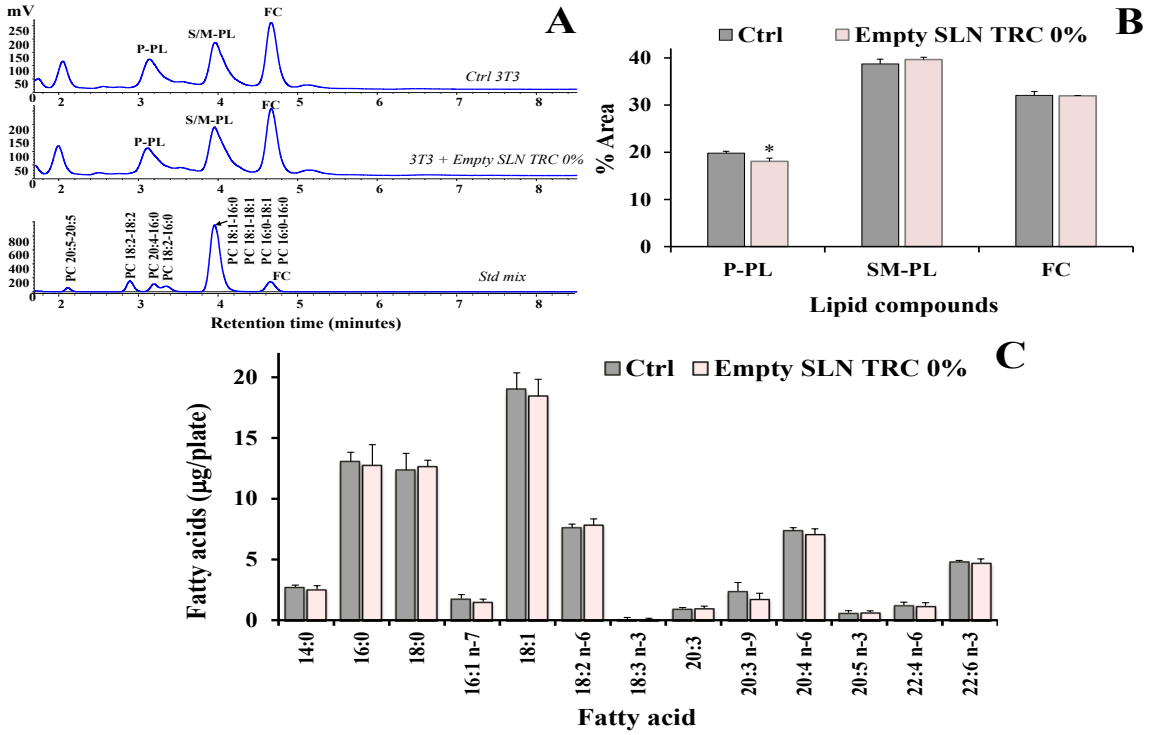

Figure 7. (A) Chromatographic profile, obtained by HPLC-ELSD analysis, of lipid compounds (saturated/monounsaturated phospholipids, S/M–PL; polyunsaturated phospholipids, P-PL; free cholesterol, FC) measured in control 3T3 fibroblasts (Ctrl) and cells treated for 24 h with unloaded SLN without TRC (Empty SLN TRC 0%) (A); the chromatographic region for each lipid class was assigned by using standard mixtures of saturated/monounsaturated (mix PL: PC 16:0/16:0, PC 18:1/18:1, PC 16:0/18:1, PC 18:1/16:0, ECN 32) and polyunsaturated phosphatidylcholines (PC 16:0/18:2, ECN 30, PC 16:0/20:4, PC 18:2/18:2, ECN 28, PC 20:5/20:5, ECN 20). Values of PL and FC (% area) (B) and the main fatty acids (expressed as µg/plate) (C) measured in control 3T3 and fibroblasts treated with Empty SLN TRC 0% (24 h). Two independent experiments and tree replicates for each condition are performed and data are presented as mean ± SD (n = 6); * = $P < 0.05$ versus respective Ctrl (Student's unpaired t test with Welch's correction).

Figure 8 shows the values of polar lipid compounds (S/M–PL, P-PL, FC) (% area) (Fig. 8A) and main fatty acids (µg/plate) (Fig. 8B) measured in 3T3 fibroblasts treated for 24 h with empty and 8-MOP loaded SLNs with 4% of TRC (Empty SLN TRC 4% and SLN TRC 4%) compared to the respective control cells. Both formulations (at the dose of 5 µL/mL) induced in 3T3 cells a change in the profile of polar lipids, in particular a marked ($p < 0.001$ versus untreated cells) decrease was observed in the % of peak corresponding to P-PL with respect to the other peaks, coupled to an increase in the % of S/M-PL (Fig. 8A), with the latter effect more marked in cells treated with SLN TRC 4%. The 24 h-treatment of fibroblasts with both formulations also affected the cell fatty acid profile. A remarkable increase in the cell levels of 18:1 n-9 ($p < 0.05$ versus untreated cells), 16:0 ($p < 0.05$), and 18:0 was detected in fibroblasts incubated with SLN TRC 4%, while the treatment did not seem to affect the levels of the other unsaturated fatty acids, with respect to control cells. The fatty acid profile modulation was less marked in 3T3 cells treated with Empty SLN TRC 4%, with an evident, but not significant, increase of 18:1 n-9.

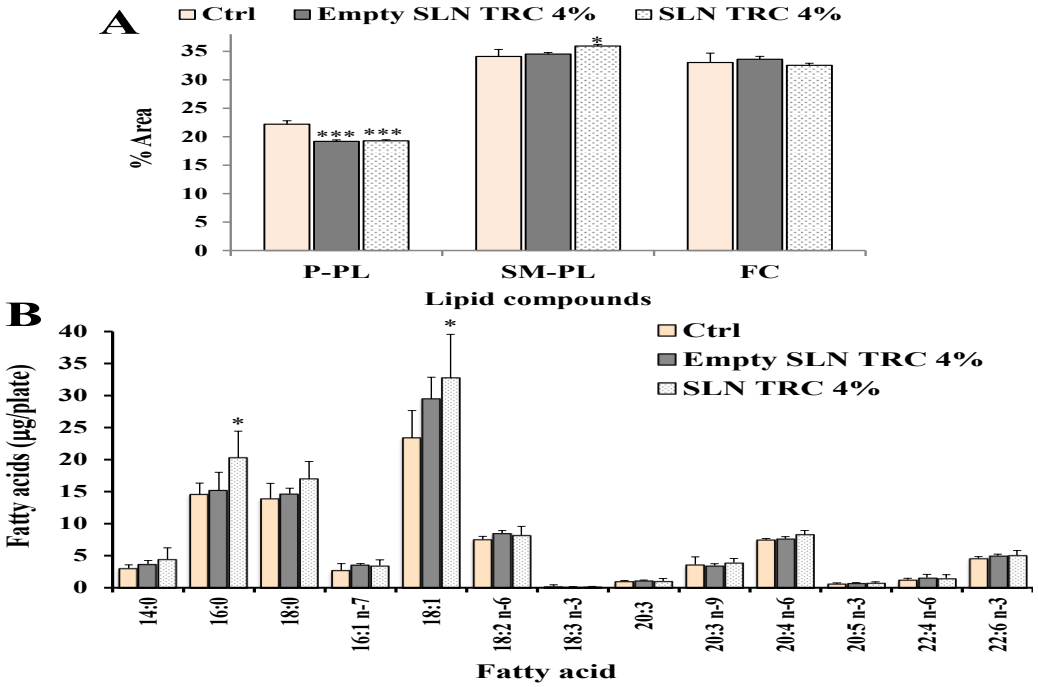

Figure 8. Values of lipid compounds (saturated/monounsaturated phospholipids, S/M-PL; polyunsaturated phospholipids, P-PL; free cholesterol, FC) (% area) (A) and the main fatty acids (expressed as µg/plate) (B) measured in control 3T3 (Ctrl) and fibroblasts treated for 24 h with unloaded (Empty SLN TRC 4%) and 8-MOP loaded SLN with 4% TRC (SLN TRC 4%). Two independent experiments and tree replicates for each condition are performed and data are presented as mean±SD (n= 6); *** = $P < 0.001$; * = $P < 0.05$ versus Ctrl (One-way ANOVA followed by the Bonferroni Multiple Comparisons Test).

The modulation of the fatty acid profile was compatible with a potential intracellular uptake of the SLN formulation and the metabolism of behenic acid, the main fatty acid of Compritol® 888 ATO that is constituted by a mixture of glycerol tribehenate, dibehenate and monobehenate. A previous study reported the cellular uptakes of SLNs composed of different lipid materials and the order of cellular uptake ability was: glycerol tristearate SLN > monostearin SLN > stearic acid SLN > Compritol® 888 ATO SLN [113]. Our results showed that the incorporation of TRC into SLNs could enhance the cellular uptake of nanoparticles, but it did not increase their cytotoxicity. Presumably, after the addition to the culture media, SLNs with 4% of TRC were taken up by 3T3 cells by endocytosis [112], and behenic acid, derived from the lipolysis of its derivatives, was possibly metabolized/oxidized and its oxidation products were used for the synthesis of phospholipids incorporating 18:1 n-9, 16:0 and 18:0.

4. Conclusions

In this study, a new safe and efficient lipid drug delivery system for 8-MOP has been obtained, using the hydrophilic penetration enhancer Transcutol® at different concentration (2 and 4%). The enhancement activity of treatment of different TRC concentrations was evaluated on porcine skin. The overall results of the in vitro skin penetration and permeation studies highlight that these systems are able to enhance drug accumulation in the skin layers when compared to conventional SLNs. In addition, the higher the TRC %, the higher the flux and the skin accumulation of 8-MOP. Finally, SLNs formulations were tested on fibroblasts to investigate both the cytotoxicity and their impact cell lipid profile. These studies demonstrated that the incorporation of TRC into SLNs could enhance the cellular uptake of nanoparticles, but it did not increase their cytotoxicity. In conclusion, overall results suggest the potential use of Transcutol®-SLNs as carriers for 8-MOP in topical treatment of skin disorders, including PUVA therapy. Further research is needed to analyze the effectiveness of this delivery system in epidermal hyperproliferation simulating psoriasis-affected animal skin.

Chapter 2: Nanoliposomes@Transcutol for in vitro skin delivery of 8-methoxypsoralen

This work will be published in the Volume 21, Number 5 (May 2021) of the Journal of Nanoscience and Nanotechnology as "Nanoliposomes@Transcutol for *in vitro* skin delivery of 8-methoxypsoralen" by Sinico C., Fadda A.M., Valenti D., Pireddu R., Corrias F., Schlich M., **Pitzanti G.**, Lai F.*; https://doi.org/10.1166/jnn.2021.19047.

ABBREVIATIONS

8-MOP	8-methoxypsoralen
DMSO	Dimethyl Sulfoxide
EE%	Entrapment Efficiency
HPLC	High Performance Liquid Chromatography
LIPO	Conventional Liposomes
MTT	3(4,5-dimethylthiazolyl-2)-2, 5- diphenyltetrazolium bromide
P90G	Phospholipon 90G
PBS	Phosphate-Buffered Saline
PCS	Photon Correlation Spectroscopy
PDI	Polydispersity Index
PE	Penetration Enhancer
PEVs	Penetration Enhancer-containing Vesicles
PUVA	Psoralen + long wave ultraviolet-A radiation
TRS	Transcutol®
ZP	Zeta Potential

1. Introduction

During the last three decades there has been a large interest in nanocarriers as effective approach to delivery active molecules through the different administration routes, and among them liposomes have been the most studied to improve drug delivery into and through the skin [114,115]. However, since conventional liposomes have often failed fail to penetrate the skin layers deeply, an intensive research has been devoted to the development of new classes of lipid vesicles, which have been generally obtained by adding new additives in the classic composition of liposomes (i.e. phospholipids with or without cholesterol). In particular, the addition of an "edge activator" such as sodium cholate led to the highly deformable, elastic liposomes, i.e. Transfersomes ,introduced in 1992 by Cevc and Blume [116] while Touitou et al. [117] developed ethosomes, introducing in the composition of the phospholipid vesicles high amount of ethanol.

In this context, our research group has been studying for years the so-called Penetration Enhancer-containing Vesicles (PEVs), liposomes with a penetration enhancer in their composition, as carriers for dermal delivery of different drugs. PEVs can be prepared by using the several methods commonly used in the preparation of conventional liposomal carriers. In previous studies it has been demonstrated that the method used for their preparation and the structure of the vesicles (multi-, oligo-, or unilamellar), do not affect their mean diameter which was always in the nanometer range and their homogeneity. Only when the PE Transcutol was employed at concentrations higher than 40%, vesicles showed a mean diameter higher than 1 μm, were not homogeneous and were characterized by a high instability. It has been reported that the PEVs' EE% was affected by the type and the concentration of the PE and by the lipophilicity of the drug [118].

Manconi et al. proposed the mechanism through which PEVs could promote skin drug delivery. According to them, PEVs are able to penetrate into the epidermis intactly due to a combination of two different mechanisms: the interaction between the penetration enhancer and the intercellular skin lipids and the enhanced PEVs' bilayer fluidity. Once vesicles disintegrate, depending on its solubility, the drug continues to diffuse through the skin [58].

During the years, PEVs have been prepared using various penetration enhancers, different for physicochemical properties and mechanism of enhancement, with the aim of finding new stable and efficient vesicular carriers for dermal drug delivery [98,99,119]. A special attention has been

dedicated to PEVs prepared by using hydromiscible cosolvents, such as Transcutol® (TRS), which have shown peculiar properties and mode of action. TRS (diethylene glycol monoethylether) is a well-known and efficient permeation enhancer, non-toxic and biocompatible, soluble both in water and in oil (KO/A = 0.7) and used in several dosage forms. It works as a powerful solubilizing agent, which swells the intercellular lipids of the stratum corneum, thus allowing drug to penetrate into the reversibly modified skin barrier [58].

In this work 8-MOP loaded PEVs were prepared with the aim to develop new carriers for skin delivery of therapeutic amounts of the drug, useful for PUVA treatment of psoriasis [67,70,72,77,78,120].

For this purpose, empty and drug loaded vesicles were obtained using a combination of Phospholipon 90G and TRS at different concentrations (5% or 10% PEVs) or phosphatidylcholine alone as control (conventional liposomes, LIPO). The composition of liposomes was selected on the basis of the promising results obtained in a previous work of our research group where drugs with different degree of lipophilicity where encapsulated in conventional liposomes and PEVs [58]. The prepared formulations were characterized in terms of size, polydispersity index, zeta potential and encapsulation efficiency. The 8-MOP accumulation in the different skin layers and permeation through the whole skin after application of LIPO or PEVs were assessed by Franz diffusion experiments. In vitro biocompatibility of all unloaded and 8-MOP loaded formulations was checked by the MTT assay measuring the viability of human keratinocytes.

2. Materials and Methods

2.1 Materials

Enriched soy phosphatidylcholine (Phospholipon 90G, P90G) was kindly supplied by AVG S.r.l. (Garbagnate Milanese, Milan, Italy). 2-(2-Ethoxyethoxy) ethanol (Transcutol®, TRS) was a gift from Gattefossè, (Saint Priest, France). 8-methoxypsoralen (8-MOP) and all the other products and solvents of analytical grade were purchased from Aldrich (Milan, Italy).

2.2 8-MOP solubility studies

8-MOP solubility was measured in water and in Transcutol® water solution (50 and 100 µg/mL). An excess of 8-MOP bulk powder was added to the water or Transcutol® solution and the suspension was kept under constant stirring for 72 h in a thermostatic bath at 25°C. At preselected time intervals, samples were withdrawn and centrifuged. Clear supernatants were diluted with methanol and analysed by HPLC for 8-MOP content. Solubility studies were performed in triplicate.

2.3 Vesicles preparation

Conventional liposomes and PEVs, empty or loaded with 8-MOP, were prepared by the thin film hydration method, combined with probe sonication (complete compositions are reported in **Table 1**). Briefly, weighed amounts of P90G and 8-MOP were dissolved in a 3/1 (v/v) chloroform and methanol mixture in a round bottom flask. The mixture was evaporated under reduced pressure and a thin film was formed. The thin film was hydrated with 10 mL of ultrapure water or TRS solution and mechanically shaken for 1 h at room temperature.

The vesicles suspensions were then sonicated (10 seconds on and 10 seconds off for 5 cycles, 13 µm of probe amplitude,) with a Soniprep 150 ultrasonic disintegrator (MSE Crowley, UK). A clear opalescent dispersion was obtained.

2.4 Vesicles characterization

The average diameter (nm±SD) and polydispersity index (PDI) of loaded and empty formulations have been determined by Photon Correlation Spectroscopy (PCS), using a Zetasizer nano-ZS (Malvern Instruments, Worcestershire, United Kingdom) and dispersant refractive index value of 1.350. 0.2 mL of each formulation was diluted with bidistilled water up to 1 mL and backscattered by a helium-neon laser (633 nm) at an angle of 173° and a constant temperature of 25°C.

ζ potential (ZP) was determined using the same instrument by means of the M3-PALS (Mixed Mode Measurement-Phase Analysis Light Scattering) technique, which measures the particle electrophoretic mobility. Before the analysis, 0.2 mL of each formulation was diluted with bidistilled water up to 1 mL All the measurements were made in triplicate.

Entrapment efficiency (EE%) of liposomes and PEVs, expressed as the percentage of the amount of 8-MOP in the unpurified vesicles, was evaluated on the same day of preparation. Each vesicle dispersion was purified from the nonincorporated 8-MOP by exhaustive dialysis. Briefly, 1 mL of vesicles dispersion was loaded into a dialysis bag (Spectra/Por membranes: 12– 14 kDa MW cut off, 3 nm pore size; Spectrum Laboratories Incorporation, USA) and dialysed against 2000 mL of distilled water for 4 hours, at room temperature, replacing the water after each hour. Purified and unpurified liposomes or PEVs were disrupted by the addition of 9 parts of methanol to 1 part of vesicles dispersion. The obtained mix was vortexed and centrifuged at 8000 rpm for 5 minutes on a Mikro 200 Centrifuge (Hettich, Tuttlingen, Germany). The supernatant (1 mL) was recovered, and quantitative determination of 8-MOP content was carried out by reverse phase chromatography using a liquid chromatograph Alliance 2690 (Waters, Milano, Italy), equipped with a photodiode array detector and a computer integrating apparatus (Millennium 32). The column was a Nova-Pack C18 (60 Å 4 µm, 3, 9×150 mm Waters). Samples were injected using an auto sampler. The mobile phase was methanol and water (70:30 v/v), at a flow rate of 0.8 mL/min.

2.5 Functional tests

In vitro skin delivery studies were performed under non-occlusive conditions using vertical Franz diffusion cells (diffusion area 0.785 cm^2) and newborn pig skin. One-day-old Goland–Pietrain hybrid pigs (about 1.2 kg) were provided by a local slaughterhouse [121]. The skin (n=6 per formulation) stored at –80°C, was pre-equilibrated in saline solution at 25°C for 12 hours and then sandwiched between donor and receptor cells. The receptor was filled with 5.5 ml of hydroalcoholic solution (ethanol: phosphate buffered saline solution 50:50) thermostated at 37±1°C and continuously stirred. Samples (100 µL) were applied onto the skin surface, and at regular intervals, up to 8 h, the receiving solution was withdrawn, replaced with pre-thermostated, fresh hydroalcoholic solution and analysed by HPLC for 8-MOP content. At the end of the experiment (8 h), the skin surface was gently washed (3 times) with 1 mL of distilled water, then dried with filter paper. The stratum corneum was removed by stripping with adhesive tape Tesa® AG (Hamburg, Germany), and epidermis was separated from dermis with a surgical scalpel. Skin strata were cut, placed each in a flask with methanol and sonicated for 2 minutes in an ice bath to extract 8-MOP. The tapes and tissue suspensions were filtered out and assayed for drug content by HPLC.

For in vitro biocompatibility studies human keratinocytes, at passages 3-2, were grown as monolayer in 75 cm^2 flasks, incubated in 100% humidity and 5% CO_2 at 37°C, using RPMI 1640 supplemented with foetal bovine serum, penicillin/streptomycin and fungizone, as culture medium. Cells were seeded into 96-well plates (7.5x103 cells/well) and, after 24 h, different concentrations (0, 1.25, 2.5 and 5 µL/mL) of loaded and empty liposome and PEVs were added to the cells in 100 µL of complete medium for 24h. After incubation, cells were washed 3 times with fresh medium and their viability was determined by the MTT [3(4,5-dimethylthiazolyl-2)-2, 5-diphenyltetrazolium bromide] colorimetric assay, adding 200 µL of MTT reagent (0.5 mg/mL in PBS) to each well. After 2-3 h, the formed formazan crystals were dissolved in DMSO and their concentration was spectrophotometrically quantified at 570 nm with a microplate reader (Synergy 4, Reader BioTek Instruments, AHSI S.P.A, Bernareggio, Italy) [122]. All experiments were repeated at least three times. Results are shown as percent of cell viability in comparison with non-treated control.

2.6. Statistical analysis

Results are expressed as mean±standard deviation. Multiple comparisons of means (one-way ANOVA) were used to substantiate statistical differences between groups, while Student's t-test was used to compare two samples. Data analysis was carried out with the software package XLStatistic for Excel (Microsoft, Redmond, WA, USA). Significance was tested at the 0.05 level of probability (p).

3. Results and Discussion

In the present study, different liposome formulations were prepared by a thin film hydration/probe sonication combined method. Empty and 8-MOP loaded liposomes were obtained using Phospholipon 90G (conventional liposomes, LIPO) or a combination of Phospholipon 90G and TRS at different concentrations (5%, 10%) (PEVs). In Table 1 vesicles composition has been showed. Prepared vesicles were deeply characterised by measuring some physico-chemical features as well as biocompatibility.

Table 1. Composition of liposomes (LIPO) and PEVs, empty or loaded with 8-MOP. The mg of different components are reported for 1 ml of vesicles dispersion.

Formulations	P90G (mg)	8-MOP (mg)	TRS (mg)
LIPO (empty)	90	-	-
LIPO	90	1.25	-
PEV5 (empty)	90	-	50
PEV5	90	1.25	50
PEV10 (empty)	90	-	100
PEV10	90	1.25	100

In order to determine the liposomes mean diameter, PDI and zeta potential, PCS analysis were performed on all empty and loaded formulations at the same day of preparation (Table 2). Empty and 8-MOP loaded LIPO exhibited a mean diameter value greater (168nm and 152nm respectively)

than that of PEV formulations, which ranged between 131nm-137nm. Concerning the conventional liposomes, we can observe a difference on the mean diameter between empty and 8-MOP loaded liposomes. 8-MOP, being characterized by a hydrophobic nature, is expected to reside in the acyl hydrocarbon chain of the liposome. Probably the reduction in size observed when 8-MOP is encapsulated in the conventional liposomes is due to the fact that the presence of a lipophilic drug decreases the bilayer hydrophilicity and hardens the cohesion between the apolar domains of the bilayers. This effect seems to be nullified when Transcutol is added to the formulation. Indeed, no statistically significant difference in size was found for all empty and loaded PEVs, although they were prepared with different TRS concentration. As previously reported [58,123], the smaller mean diameter of PEVs in comparison with conventional liposomes could be attributed to the modification of the bilayer packing due to the TRS intercalation into the phospholipid chains.

Table 2. Mean diameter (nm), polydispersity index (PDI) and zeta potential (ZP, mV) of freshly prepared 8-MOP loaded and empty conventional liposomes (LIPO) and PEVs. Results are expressed as means of 3 independent measurements ± standard deviations.

Formulation	Mean diameter (nm±SD)	PDI (±SD)	ZP (mV±SD)	EE%
LIPO (empty)	168±7	0.22±0.03	-24±3	-
LIPO	152±5	0.25±0.05	-32±2	76±4
PEV5 (empty)	137±6	0.22±0.06	-30±5	-
PEV5	136±8	0.24±0.07	-34±3	63±6
PEV10 (empty)	131±8	0.24±0.04	-32±4	-
PEV10	135±9	0.27±0.05	-33±1	64±4

Polydispersity index values for all formulations were always smaller than 0.27, thus indicating a fairly narrow size distribution. Both conventional and PEVs vesicles showed a highly negative zeta potential values, always smaller than -24mV. Entrapment efficiency of 8-MOP LIPO (EE%≈75%) was greater than that of both PEVs vesicles (EE%≈65%). This behaviour can be explained taking into account the increased 8-MOP water solubility in the presence of TRS, which affect drug partition between the hydrophilic phase (TRS water solution) and the hydrophobic phase (vesicle

bilayers) thus consequently reducing the amount of the loaded drug [124]. The calculated 8-MOP water solubility (45 ±3 µg/mL) increased in the presence of TRS but not proportionally with the rise of TRS concentration. Indeed, the 8-MOP solubility in both TRS water solutions showed very closed values (59±3 µg/mL and 58±3 µg/mL for 100 and 50 g/ml TRS water solution respectively) as well as similar entrapment efficiencies (63% and 64%).

In order to clarify the influence of PEVs with increasing concentration of TRS on 8-MOP cutaneous delivery, *in vitro* permeation studies were carried out using new-born pig skin and vertical diffusion Franz cells. TRS is a well-known and effective permeation enhancer, non-toxic and biocompatible, soluble both in water and in oil ($K_{O/A}$ = 0.7) and used in many topical dosage forms. It is also a useful solubilizing agent able to reversibly modify the skin barrier function, thus improving drug penetration.

The 8-MOP accumulation in the different skin layers (stratum corneum, epidermis and dermis) and permeation through the whole skin after application of LIPO or PEVs are reported in **Figure 1**. As expected, all formulations showed higher drug accumulation in stratum corneum as compared to viable epidermis and dermis, since these strata have higher hydrophilic characteristics than stratum corneum. Therefore, lipophilic substances such as 8-MOP, tend to accumulate in this tissue. Furthermore, as reported in literature, in vivo 8-MOP skin deposition should be higher than in vitro due to the increased cellular uptake [125].

After PEV application, the drug accumulated in each skin layers was greater than that found after LIPO application. In particular, the drug recovered in stratum corneous was 0.40 µg/cm^2 and 0.23 µg/cm^2 for PEV and LIPO respectively. Conversely, this difference on 8-MOP accumulation between PEVs and LIPO is less pronounced in the deeper layers. Moreover, no significant difference was found between the amount of 8-MOP recovered in the different skin layers for different PEVs formulations. This behaviour could be due to the synergic action of the nanocarrier and the penetration enhancer which reversible reduce the barrier properties of the stratum corneum. Indeed, in an interesting investigation, authors demonstrated that a nanoemulsion prepared using a terpene rich essential oil, were able to modulate 8-MOP transdermal delivery and skin retention [75].

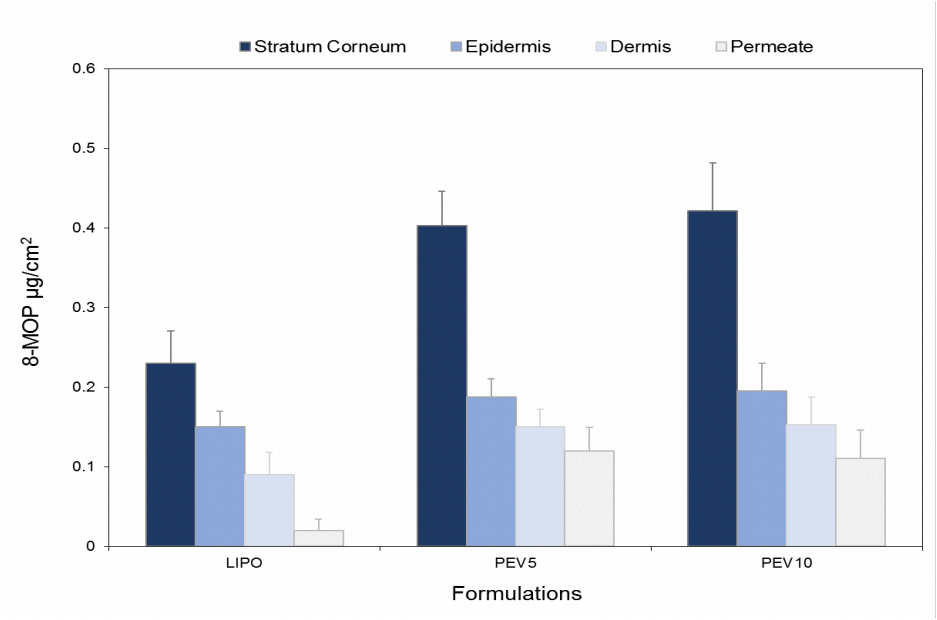

Figure 1. Cumulative amount of 8-MOP permeated and accumulated in stratum corneum, epidermis and dermis after 8 h application of different vesicles formulations. Data represent the means ± standard deviation (SD) of at least six experimental determinations.

It is worth to notice that when PEVs are applied, the increased 8-MOP accumulation in skin strata produced an increasing drug permeation if compared to the LIPO formulation. Indeed, the amount of 8-MOP permeated through the whole skin after 8-hours LIPO application was 0.02 µg/cm, a value more than six-fold smaller than that observed for both PEVs (approximately 0.12 µg/cm^2).

In vitro biocompatibility of all unloaded and 8-MOP loaded formulations was checked measuring the cell viability by using the MTT assay. Experiments were carried out on human keratinocytes at different vesicle concentration (1, 1.25, 2.5 and 5 µL/mL). The obtained results are shown in **Figure 2**, as percentage of cell viability in comparison with non-treated control cells (100% cell viability). Toxicity studies were performed with both empty and loaded vesicles in order to verify if the formulation components could affect cell viability.

Moreover, liposomes are carriers useful for improving cellular uptake and therefore, they could further influence drug toxicity. At the tested concentrations, all formulations (empty and loaded), incubated for 24 h, did not determine a significant reduction in cell viability (always greater than 93%) with respect to the control cells (100%, $p>0.05$).

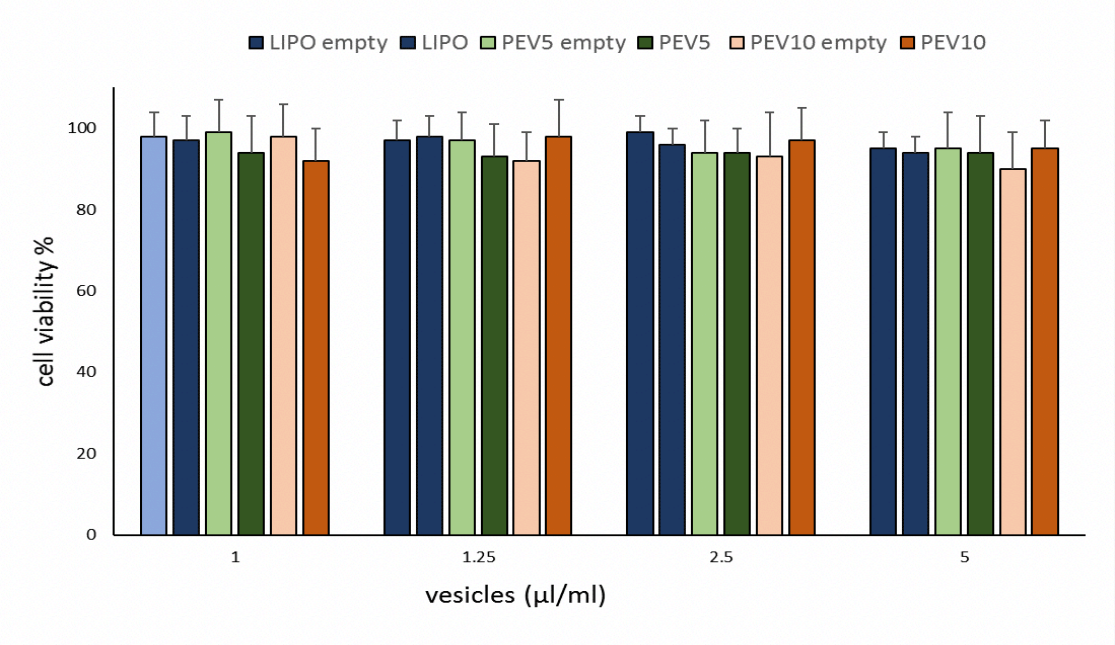

Figure 2. In vitro cytotoxic effect of empty an 8-MOP loaded vesicles on keratinocytes after 24 hours of coincubation at different concentrations (0, 1.25, 2.5 and 5 µL/mL).

4. Conclusions

In this study, a new safe and efficient vesicular drug delivery system for 8-MOP was obtained, using the hydrophilic penetration enhancer Transcutol® at different concentration (5 and 10%). Results highlight that these so-called Penetration Enhancer Vesicles (PEVs) enhance drug accumulation in the epidermal skin layers when compared to conventional liposomes. However, no significant difference was found between the amount of 8-MOP recovered in the skin layers for different Transcutol® concentrations. Finally, biocompatibility assays demonstrated that the incubation of human keratinocytes for 24 h with empty and 8-MOP loaded PEVs did not significantly reduce cell viability. In conclusion, overall results suggest the potential use of PEVs as carrier for 8-MOP in topical treatment of skin disorders, including PUVA therapy. Further research is needed to optimize the nanoformulations and to analyse the effectiveness of this delivery system in *in vivo* models.

Part 2: 3D printed hollow microneedles

ABBREVIATIONS

3DP	Three-dimensional Printing
AM	Additive Manufacturing
CAD	Computer Aided Design
DLP	Digital Light Processing
FDM	Fused Deposition Modelling
IPA	Isopropyl alcohol
MNs	Microneedles
SEM	Scanning Electron Microscopy
SLA	Stereolithography
TDD	Transdermal Drug Delivery

1. Introduction

Three-dimensional printing (3DP), also known as additive manufacturing (AM), includes a range of techniques that build a physical object layer-by-layer based on a Computer Aided Design (CAD) model. Since its introduction in the 1980s, 3DP has revolutionized the field of pharmaceutical, biomedical and material sciences due to its ability to fabricate complex structures in a fast and cost-effective manner [126–128]. Variety of 3DP technologies have been developed, with the main methods based on: powder solidification, liquid solidification, or extrusion [129].
Among the various 3DP technologies, vat photo-polymerization techniques enable the fabrication of structures through the consecutive layer-wise polymerization of liquid UV-sensitive polymers, through a curing process named photo-polymerization. Stereolithography (SLA) and Digital Light Processing (DLP) are two examples of these technologies [128,130].
SLA is based on the solidification of a liquid resin by photo-polymerisation. First, the object is designed using a CAD software (**Fig. 1-1**) and subsequently converted in the desired file format, and finally sliced using the 3D printer model specific software (**Fig.1-2**). The photopolymer resin is poured into a large vat (**Fig.1-3**). The building platform moved downward, and the

photopolymer resin exposed to a radiation source from the top or the bottom (Fig.1-4). As a result, the light-cured layer polymerizes on the support platform (Fig.1-5). After photo-polymerisation of the first layer, the building platform moved upwards, the cured layer peeled off from the bottom surface and the built layer recoated with liquid resin, following by another layer in a similar way until the object is completed (Fig.1-5&6). Following the printing process, the object is accurately washed with an appropriate solvent in order to remove the excess resin (Fig.1-7) and post-cured with ultraviolet light to improve its mechanical properties (Fig.1-8) [131].

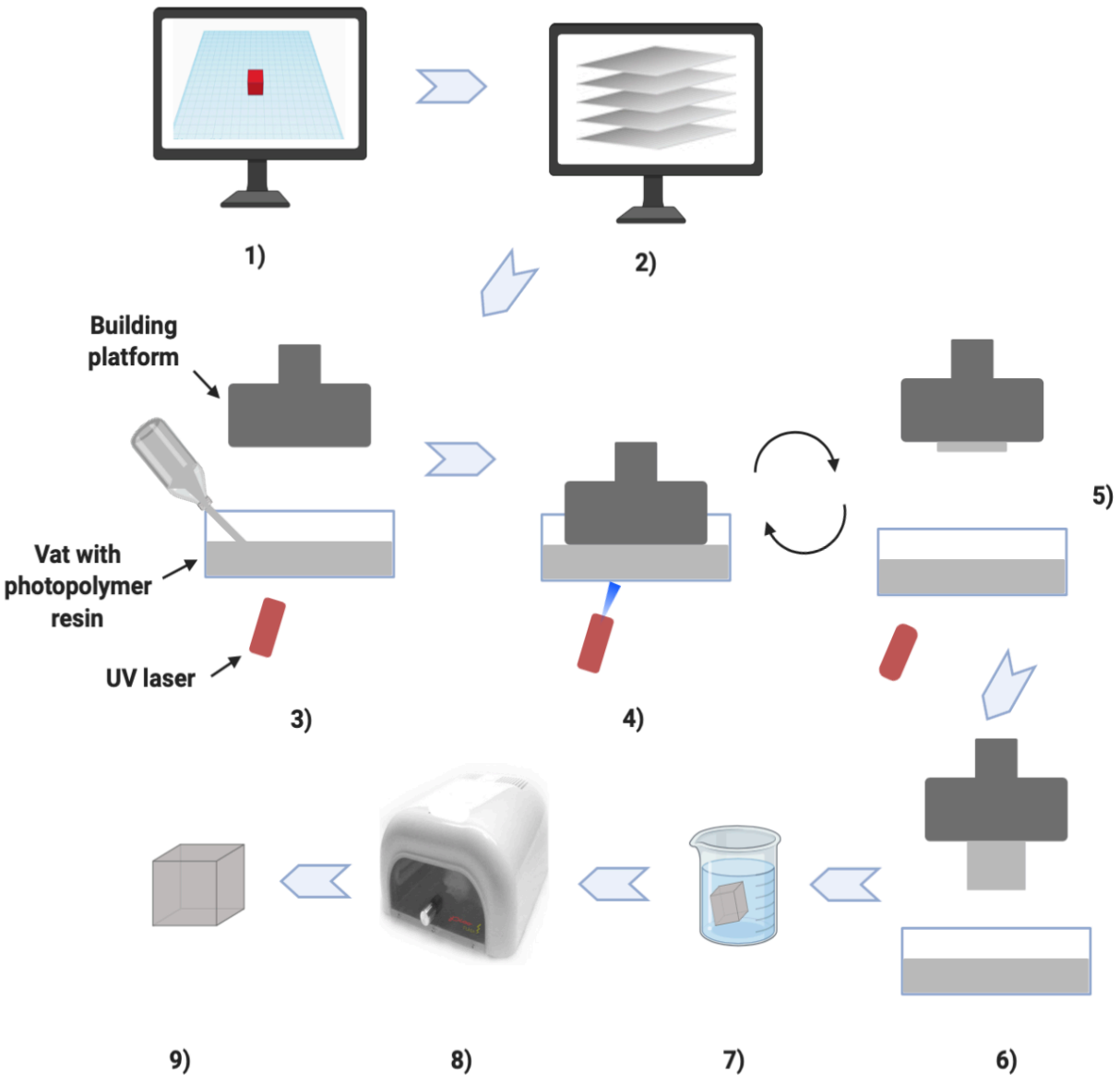

Figure 21. Schematic representation of SLA printing process.

Digital Light Processing (DLP) mainly differs from SLA for the light source that employs. Indeed, SLA uses an UV laser beam while DLP uses UV light from a digital projector. Moreover, in the DLP technique the digital projector displays and cure an entire cross-sectional slice of the object at once. Instead, in the SLA technique the laser beam has to individually cure the resin in a "point to point" manner. As a result, DLP printing speed is increased in comparison to SLA [132].

The application of vat photopolymerization in the pharmaceutical field is very recent and it is mostly employed for the development of oral dosage forms [133–138]. Its potential in fabricating dermal and transdermal drug delivery (TDD) systems has little been explored. In 2016 Goyanes et al. used two different 3D printing technologies, Fused Deposition Modelling (FDM) and SLA to produce patches/masks personalised to the nose anatomy of the patient loaded with the anti-acne drug salicylic acid. The devices printed with SLA showed higher resolution, higher drug loading and faster drug diffusion than those printed by FDM. Moreover, SLA did not lead to drug degradation [139].

More recently, vat photopolymerization has been employed for the manufacturing of microneedles (MNs) [127,128,140–142]. MNs are microscale intradermal/transdermal drug delivery systems that enable drug delivery without causing pain to the patient as the small needles can penetrate the stratum corneum (SC) without reaching the dermal nerves and pain receptors. MNs can be prepared small enough (less than 1mm in length) to avoid reaching the blood supply of the skin and causing bleeding. MNs can overcome the issues highlighted with hypodermic needles such as needle phobia, risk of needle stick injuries and requirement of well-trained healthcare practitioners. Moreover, bypass first pass metabolism, which is a major issue associated with oral dosage. Swallowing issues for elderly and paediatrics patients, as well as stability and drug absorption issues in the stomach, are some of the common issues that can be overcome with the use of MNs. Current manufacture of MNs involves the micromoulding process, in which laser engineered silicone moulds are used to cast MNs or the use of the injection moulding technique [143–147]. Other common MN fabrication techniques include laser cutting and lithography. Conventional methods of fabrication often limit the fabrication of MNs with complex geometries therefore MN designs are limited to conventional shapes and sizes [148,149]. AM, allowing the manufacture of devices with precise geometries, should be a promising method for MNs fabrication. Using CAD software, the needle height, width, shape etc. can be altered more

readily allowing faster production of MNs [130]. Unlike micromoulding of MNs, 3DP allows a larger range of MN designs to be explored in a shorter period. To date, differently to the other 3DP technologies, few works have highlighted the potential of vat photo-polymerization 3DP in MNs manufacturing [127,128,140]. Vat photo-polymerization 3DP can be particularly advantageous to MN fabrication due the ability to print structures <100 µm. 3D printed MNs using the SLA technique have been explored for insulin delivery and treatment of skin tumors, both of these require printing of the needles and addition of compound by inkjet dispensing onto the needle post printing [127,128,140].

The aim of this work, is to investigate if solid and hollow MNs patches could be successfully manufactured by DLP, opening the potential to deliver via the skin both high and low molecular weight (MW) drugs.

2. Materials and Methods

2.1 Materials

PlasGRAY resin was purchased from Asiga (US) and Isopropyl alcohol ((CH3)2CHOH; IPA 99.9%) from Sigma Aldrich.

2.2 MN design and fabrication

The CAD software Autodesk® Tinkercad™ was employed to design hollow MNs of pyramidal and conical shape [128]. The designs were converted into .stl files and pre-processed in the Asiga 3D-printer preparation software Composer. In order to optimise the printing quality, supports were generated with the software and adjusted in order to stay away from the critical parts of the design. The design was oriented with the needles facing the resin tray. The duration of the printing process was 2h. After the end of the printing, the printed patch was carefully peeled-off from the building platform and the supports removed. In order to remove the excess resin, the printed MNs were washed with IPA for 5 min using a bath sonicator. Then, the MNs were left to dry at room temperature and subsequently cured in a 385 nm wavelength UV chamber (Asiga Flash) for 20 min in order to maximize stiffness and strength.

2.3 Scanning electron microscopy (SEM)

Each MNs array, was examined by SEM (Hitachi TM3030) in order to evaluate the correspondence of the parameters of the printed patches with the design made with the CAD software. Energy Dispersive X-Ray (EDX) observation conditions were used. The MNs patches were fixed to a metal sample holder with a double-sided carbon tape and then placed inside the SEM's vacuum chamber.

2.4 Parafilm® insertion test

Parafilm® insertion test was performed according to a method previously described by Larrañeta et al. [150]. Briefly, Parafilm M® was cut to obtain squares of approximately 1cm^2, which were placed one on the top of the other in order to obtain a layer of ~1mm, afterwards the MNs array was carefully positioned on top. The test was performed using a TA.XTPlus Texture Analyzer (Stable Micro Systems, Surrey, UK) in compression mode. The insertion ability of the MNs was evaluated by applying three different forces: 10N, 20N and 32N, which were selected taking into account the fact that the force required to apply manually a MN array is between 10N and 50N [150]. The forces were kept for 30s, which is the time required for an effective MNs insertion [150,151]. Following the insertion test, the MNs patches were removed from the Parafilm and the Parafilm layers were separated. Then, the number of holes left in each layer was counted using a Leica EZ4-D digital microscope (Leica, Wetzlar, Germany) and two polarized lenses. The Parafilm sheet was considered pierced when the hole was visible through the layer. Membrane deformation was not considered as a pierced hole. At least three replicates of each array were tested.

2.5. Statistical analysis

Data analysis was carried out with the software package Microsoft Excel, version 2020. Results are expressed as mean±standard deviation (3 independent samples).

3. Results and Discussion

Arrays containing 25 MNs designed using the CAD software Autodesk® Tinkercad™ using pyramidal and conical MNs designs (**Fig. 2**).

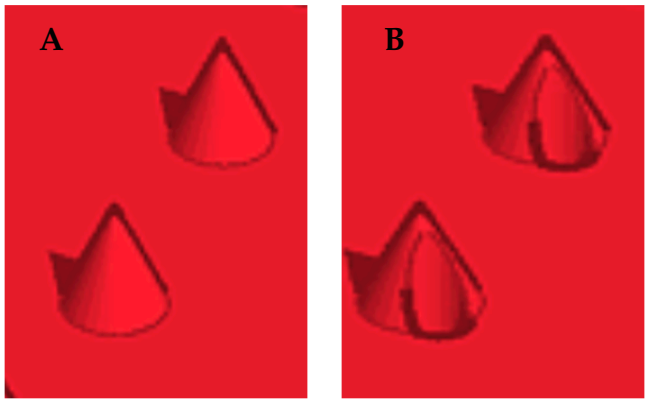

Figure 2. Computer-aided design (CAD) of Solid **(A)** and hollow **(B)** conical MNs.

Arrays with conical and pyramidal needles 1x1 mm height and width were created. First, solid MNs were printed using both shapes in order to assess the printing quality (**Figure 3)**. MNs with well-defined sharp tips and uniform surface post washing and curing were obtained. Next, hollow MNs, with a bore of 0.5 mm and with same parameters (e.g. shapes and dimensions) as the solid MNs, were designed and printed. The holes were placed on the sides of the needles in order for the sharpness of the needles to be maintained and avoid any MNs blockage upon insertion into the skin.

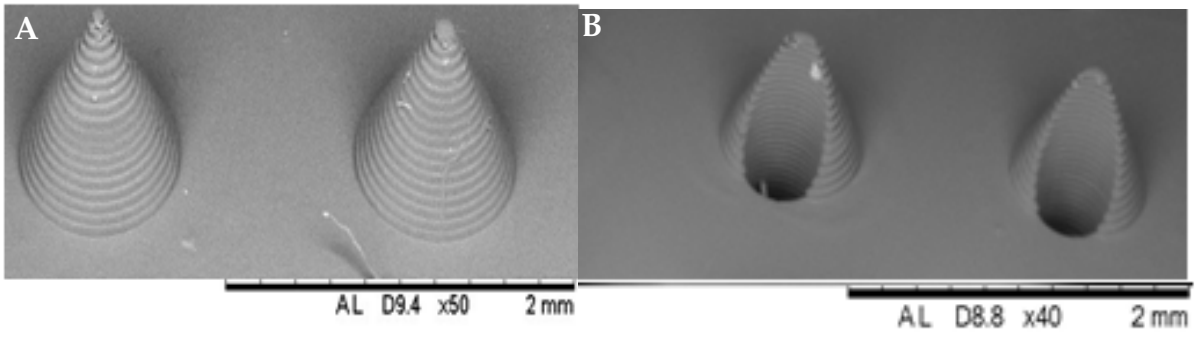

Figure 3. SEM images of MN arrays with Conical solid **(A)** or hollow **(B)** MNs.

The SEM images revealed that the sharpness of the tip was affected by the addition of the bore, with needles losing sharpness, which is due to the bore being too large and close to the tip (**Fig. 3 B)**. Therefore, MN arrays of the same dimensions with the bore size reduced to half were created (**Fig.4**). The tips maintained sharpness and effectively printed without compromising on print quality.

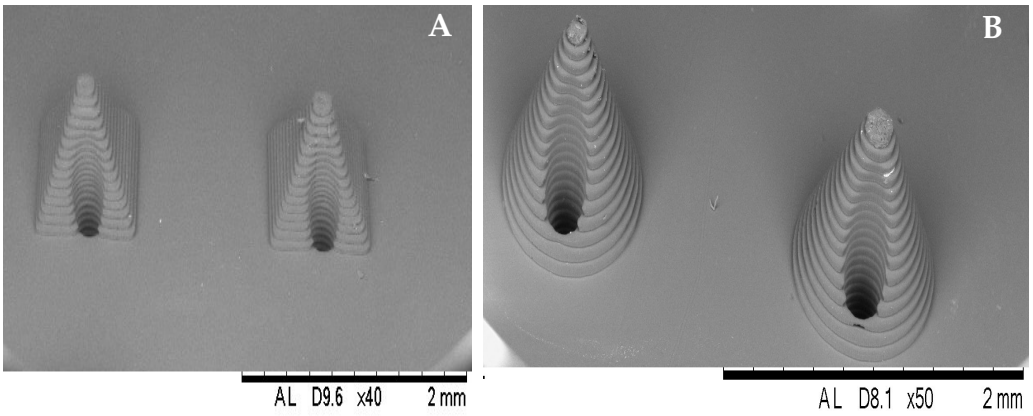

Figure 4. SEM images of hollow Pyramidal **(A)** and Conical **(B)** MN arrays with 0.25mm bore size.

However, the positioning of the bore needed to be changed as it was too close to the bottom of the needle, as MNs rarely achieve 100% insertion it was important to position the hole higher on the needle to ensure that leakage onto the skin does not occur during delivery. Therefore, designs with the bore positioned higher on the needle were created and analysed using VHX digital microscope and SEM (**Fig.5**). Microscopic analysis of the patches confirmed a high conformity of the printed objects to the original designs. In fact, for all the printings the difference between the high of the MNs designed and the printed one was less than 10%. Moreover, positioning the bore higher in the needle did not affect the high of the needles and the sharpness of the tip.

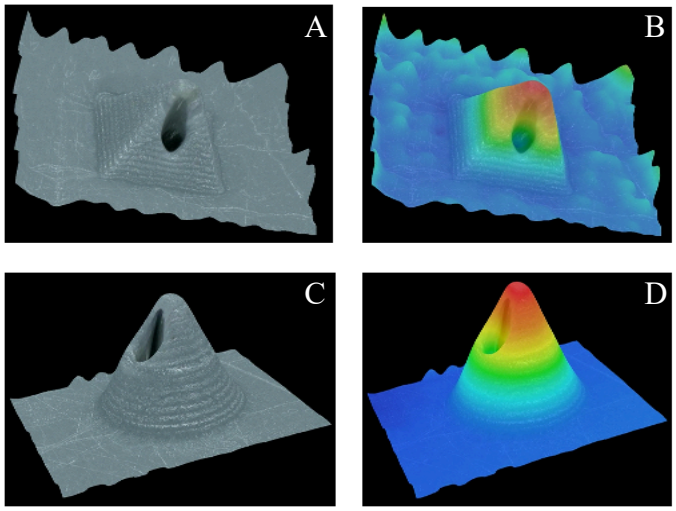

Figure 5. VHX digital microscope images of hollow pyramidal (**A** and **B**) and conical (**C** and **D**) MNs.

The insertion ability of the final designs of the needles was evaluated using the Parafilm method developed in 2014 by Larrañeta et al. In this method Parafilm® M is used as an alternative to biological tissue [150]. In this study, a model membrane with a thickness of about 1270 µm was obtained by piling up 10 Parafilm sheets. The tests were performed applying three different forces: 10N, 20N and 32N. As expected, the insertion depth increased proportionally with the increase of the applied force (**Fig. 6**). The patches with Pyramidal shaped MNs were completely inserted into one Parafilm layer when an insertion force of 10N was applied (**Fig. 6 A**). Less than 50% of the MNs were able to reach the second layer. At forces of 20N and 32N MNs reached the third and the fourth layer respectively (**Fig. 6 A**). The insertion ability of the patches with Conical shaped MNs did not show significantly differences to the patches with Pyramidal shaped MNs. When a force of 10N was applied, Conical shaped MNs reached the second Parafilm layer and created few holes in the third layer (**Fig. 6 B**). At a force of 20N, three Parafilm layers were pierced and few holes were left in the fourth one (**Fig. 6 B**). Finally, at a force of 32N four Parafilm layers were pierced (**Fig. 6 B**). It's to be noted that, independently on the MNs shape, at a force of 10N, a significant difference between the % of holes left in the first and the second layers was shown. As the force was increased, this difference was gradually less noticeable. These data were congruent to the ones obtained for hollow polymeric MNs by Lhernould et al [147].

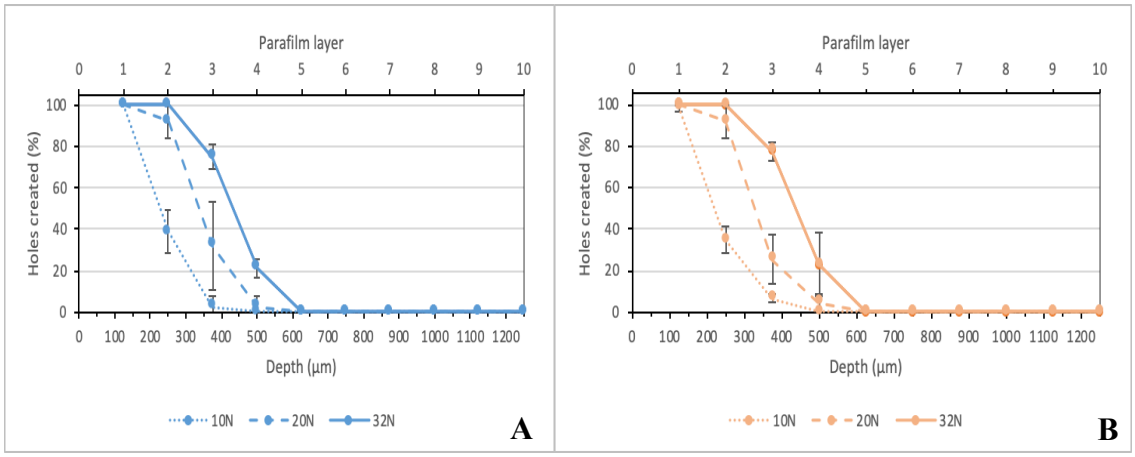

Figure 6. % of holes created in each Parafilm layer under different insertion forces (10N, 20N and 32N): 5x5 Pyramidal 10N, 20N and 32N **(A)**; 5x5 Cones 10N, 20N and 32N **(B)**.

4. Conclusions & Future Directions

In this work we investigated the ability of DLP in printing micron-scale structures. Solid and hollow MNs with pyramidal and conical shapes were designed following previous published designs from the QUB group that optimized and successfully printed using SLA. The printed structures were analysed by SEM. Finally, the ability of the optimized MNs patches, to insert into an artificial membrane was assessed by the Parafilm method. There was not significant difference in the insertion ability of the two MNs shapes as was expected. Even at low applied force, MN show a good insertion of ~250 µm. Overall, this work showed that DLP 3DP can be successfully applied for the development of solid and hollow MNs patches that can be potentially applicable for skin drug and vaccine delivery. *In vitro* and *in vivo* experiments can be conducted in order to verify the effectiveness of the systems in skin drug and vaccine delivery.

This work was conducted at the School of Pharmacy in Queen's University Belfast, and managed and funded by the Lamprou Research Group. Due to the COVID-19 lockdowns, it was not possible to perform further experiments.

During my visiting research period at Queen's University Belfast, I had the opportunity to contribute to the editorial of the special issue "3D Printing of Pharmaceuticals and Drug Delivery Devices" of the journal Pharmaceutics.

Mathew, E.; **Pitzanti, G.**; Larrañeta, E.; Lamprou, D.A. 3D Printing of Pharmaceuticals and Drug Delivery Devices. *Pharmaceutics***2020**, *12*, 266. https://doi.org/10.3390/pharmaceutics12030266

References

1. Ambrosi, G.; Cantino, D.; Castano, P.; Correr, S.; D'Este, L.; Donato, R.; Familiari, G.; Fornai, F.; Gulisano, M.; Iannello, A.; Magaudda, L.; Marcello, M.; Martelli, A.; Pacini, P.; Rende, G. *Anatomia dell'uomo*; 2nd ed.; Edi.Ermes, 2006; ISBN 8870512886.
2. Bentivoglio, M.; Bertini, G.; Cavaletti, G.; Del Fiacco, M.; Esposito, V.; Geuna, S.; Giacobini, G.; Giannetti, S.; Granato, A.; Maffione, A.; Marmiroli, P.; Ottani, V.; Papa, M.; Passiatore, C. *Anatomia umana e istologia*; 2nd ed.; Minerva Medica, 2010; ISBN 8877116706.
3. Kang, S.; Amagai, M.; Bruckner, A.; Enk, A.; Margolis, D.; McMichael, A.; Orringer, J. *Fitzpatrick's Dermatology*; McGraw-Hil, 2019; ISBN 9780071837798.
4. Montagna, W.; Ebling, F.J.G. Human skin Available online: https://www.britannica.com/science/human-skin (accessed on May 31, 2020).
5. Figure 4. Layers of the Epidermis Available online: https://opentextbc.ca/anatomyandphysiology/chapter/5-1-layers-of-the-skin/ (accessed on May 31, 2020).
6. https Available online: https://www.palmbeachstate.edu/slc/Documents/AandPch05LecturePearson.pdf (accessed on Jun 2, 2020).
7. Benson, H.A.E.; Watkinson, A.C. *Transdermal and Topical Drug Delivery: Principles and Practice*; 2012; ISBN 9780470450291.
8. https Available online: http://it.nextews.com/2fdb1486/ (accessed on Jun 24, 2020).
9. Colombo, P.; Alhaique, F.; Caramella, C.; Conti, B.; Gazzaniga, A.; Vidale, E. *Principi di Tecnologia Farmaceutica*; 2nd ed.; Casa Editrice Ambrosiana, 2015;
10. Brown, M.B.; Martin, G.P.; Jones, S.A.; Akomeah, F.K. Dermal and transdermal drug delivery systems: Current and future prospects. *Drug Deliv. J. Deliv. Target. Ther. Agents* 2006, *13*, 175–187.
11. Ramteke, K.H.; Dhole, S.N.; Patil, S.V. Transdermal drug delivery system: A review. *J. Adv. Sci. Res.* 2012, *3*, 22–35.
12. Tanwar, H.; Sachdeva, R. Transdermal Drug Delivery System: a Review. *Int. J. Pharm. Sci. Res.* 2016, *7*, 2274–90.

13. Tayar, N. El; Tsai, R. -S; Testa, B.; Carrupt, P. -A; Hansch, C.; Leo, A. Percutaneous penetration of drugs: A quantitative structure-permeability relationship study. *J. Pharm. Sci.* 1991, *80*, 744–749.
14. Naik, A.; Kalia, Y.N.; Guy, R.H. Transdermal drug delivery: Overcoming the skin's barrier function. *Pharm. Sci. Technol. Today* 2000, *3*, 318–326.
15. Prausnitz, M.R.; Elias, P.M.; Franz, T.J.; Schmuth, M.; Tsai, J.-C.; Menon, G.K.; Holleran, W.M.; Feingold, K.R. Skin Barrier and Transdermal Drug Delivery. *Med. Ther.* 2012, 2065–2073.
16. Mishra, D.K.; Pandey, V.; Maheshwari, R.; Ghode, P.; Tekade, R.K. *Cutaneous and transdermal drug delivery: Techniques and delivery systems*; 2018; ISBN 9780128179093.
17. Dragicevic-Curic, N.; Maibach, H.I. *Percutaneous Penetration Enhancers Chemical Methods in Penetration Enhancement-Drug Manipulation Strategies and Vehicle Effects*; 2015; ISBN 9783662450123.
18. Singh, S.; Singh, J. Transdermal drug delivery by passive diffusion and iontophoresis: A review. *Med. Res. Rev.* 1993, *13*, 569–621.
19. Rawlings, A. V.; Harding, C.R. Moisturization and skin barrier function. *Dermatol. Ther.* 2004, *17*, 43–48.
20. Fowler, B.J. Understanding the Role of Natural Moisturizing Factor in Skin Hydration. *Pract. Dermatology* 2012, 36–40.
21. Prausnitz, M.R.; Langer, R. Transdermal drug delivery. *Nat Biotechnol.* 2009, *26*, 1261–1268.
22. Bolzinger, M.A.; Briançon, S.; Pelletier, J.; Chevalier, Y. Penetration of drugs through skin, a complex rate-controlling membrane. *Curr. Opin. Colloid Interface Sci.* 2012, *17*, 156–165.
23. Finnin, B.C.; Morgan, T.M. Transdermal penetration enhancers: Applications, limitations, and potential. *J. Pharm. Sci.* 1999, *88*, 955–958.
24. Kováčik, A.; Kopečná, M.; Vávrová, K. Permeation enhancers in transdermal drug delivery: benefits and limitations. *Expert Opin. Drug Deliv.* 2020, *17*, 145–155.
25. Dragicevic, N.; Maibach, H.I. *Percutaneous Penetration Enhancers Chemical Methods in Penetration Enhancement-Modification of the Stratum Corneum*; 2017; ISBN 9783662532737.
26. Karande, P.S.; Jain, A.K.; Mitragotri, S. Design principles of chemical permeation enhancers for transdermal drug delivery. *AIChE Annu. Meet. Conf. Proc.* 2005, *2005*, 8372.

27. Zorec, B.; Préat, V.; Miklavčič, D.; Pavšelj, N. Active enhancement methods for intra- and transdermal drug delivery: A review. *Zdr. Vestn.* 2013, *82*, 339–356.
28. Arora, A.; Prausnitz, M.R.; Mitragotri, S. Micro-scale devices for transdermal drug delivery. *Int. J. Pharm.* 2008, *364*, 227–236.
29. Brown, M.B.; Traynor, M.J.; Martin, G.P.; Akomeah, F.K. Transdermal drug delivery systems: Skin perturbation devices. *Methods Mol. Biol.* 2008, *437*, 119–139.
30. Mathur, V.; Satrawala, Y.; Rajput, M.S. Physical and chemical penetration enhancers in transdermal drug delivery system. *Asian J. Pharm.* 2010, *4*, 173–183.
31. Kumar, R.; Philip, A. Modified Transdermal Technologies: Breaking the Barriers of Drug Permeation via the Skin. *Trop. J. Pharm. Res.* 2007, *6*, 633–644.
32. Kalia, Y.N.; Naik, A.; Garrison, J.; Guy, R.H. Iontophoretic drug delivery. *Adv. Drug Deliv. Rev.* 2004, *56*, 619–658.
33. Mitragotri, S. Devices for overcoming biological barriers: The use of physical forces to disrupt the barriers. *Adv. Drug Deliv. Rev.* 2013, *65*, 100–103.
34. Touitou, E. Drug delivery across the skin. *Expert Opin. Biol. Ther.* 2002, *2*, 723–733.
35. Marwah, H.; Garg, T.; Goyal, A.K.; Rath, G. Permeation enhancer strategies in transdermal drug delivery. *Drug Deliv.* 2016, *23*, 564–578.
36. Patel, M.N.; Bharadia, P.D.; Patel, M.M. Skin Penetration Enhancement Techniques – Physical Approaches. *Int. J. Pharm. Appl. Sci.* 2010, *1*, 62–72.
37. Barry, B.W. Novel mechanisms and devices to enable successful transdermal drug delivery. *Eur. J. Pharm. Sci.* 2001, *14*, 101–114.
38. Denet, A.R.; Vanbever, R.; Préat, V. Skin electroporation for transdermal and topical delivery. *Adv. Drug Deliv. Rev.* 2004, *56*, 659–674.
39. Benson, H.A.E.; Grice, J.E.; Mohammed, Y.; Namjoshi, S.; Roberts, M.S. Topical and Transdermal Drug Delivery: From Simple Potions to Smart Technologies. *Curr. Drug Deliv.* 2019, *16*, 444–460.
40. Ogura, M.; Paliwal, S.; Mitragotri, S. Low-frequency sonophoresis: Current status and future prospects. *Adv. Drug Deliv. Rev.* 2008, *60*, 1218–1223.
41. Prausnitz, M.R. Microneedles for transdermal drug delivery. *Adv. Drug Deliv. Rev.* 2004, *56*, 581–587.
42. Tuan-Mahmood, T.M.; McCrudden, M.T.C.; Torrisi, B.M.; McAlister, E.; Garland, M.J.; Singh, T.R.R.; Donnelly, R.F. Microneedles for intradermal and transdermal drug delivery.

Eur. J. Pharm. Sci. 2013, *50*, 623–637.

43. Larrañeta, E.; Lutton, R.E.M.; Woolfson, A.D.; Donnelly, R.F. Microneedle arrays as transdermal and intradermal drug delivery systems: Materials science, manufacture and commercial development. *Mater. Sci. Eng. R Reports* 2016, *104*, 1–32.
44. Gerstel, M.S.; Place, V.A. Drug delivery device - US 3964482 A. *U. S. Pat.* 1976, *482*.
45. Henry, S.; McAllister, D. V.; Allen, M.G.; Prausnitz, M.R. Microfabricated microneedles: A novel approach to transdermal drug delivery. *J. Pharm. Sci.* 1998, *87*, 922–925.
46. Van Der Maaden, K.; Jiskoot, W.; Bouwstra, J. Microneedle technologies for (trans)dermal drug and vaccine delivery. *J. Control. Release* 2012, *161*, 645–655.
47. Yang, J.; Liu, X.; Fu, Y.; Song, Y. Recent advances of microneedles for biomedical applications: drug delivery and beyond. *Acta Pharm. Sin. B* 2019, *9*, 469–483.
48. Kumar, R.B. Needle-Free Injection System. *Pharma Inoovation J.* 2012, *1*, 57–72.
49. Kale, T.R.; Momin, M. Needle free injection technology - An overview. *Inov. Pharm.* 2014, *5*.
50. Logomasini, Mark; Stout, Richard; Marcinkoski, R. Jet Injection Devices for the Needle-free Administration of Compounds, Vaccines, and Other Agents. *Int. J. Pharm. Compd.* 2013, *17*, 270–280.
51. Mitragotri, S. Current status and future prospects of needle-free liquid jet injectors. *Nat. Rev.* 2006, *5*, 543–548.
52. Mohizin, A.; Kim, J.K. Current engineering and clinical aspects of needle-free injectors: A review. *J. Mech. Sci. Technol.* 2018, *32*, 5737–5747.
53. Roberts, M.S.; Mohammed, Y.; Pastore, M.N.; Namjoshi, S.; Yousef, S.; Alinaghi, A.; Haridass, I.N.; Abd, E.; Leite-Silva, V.R.; Benson, H.A.E.; et al. Topical and cutaneous delivery using nanosystems. *J. Control. Release* 2017, *247*, 86–105.
54. Lai, F.; Caddeo, C.; Manca, M.L.; Manconi, M.; Sinico, C.; Fadda, A.M. What's new in the field of phospholipid vesicular nanocarriers for skin drug delivery. *Int. J. Pharm.* 2020, *583*, 119398.
55. Sala, M.; Diab, R.; Elaissari, A.; Fessi, H. Lipid nanocarriers as skin drug delivery systems: Properties, mechanisms of skin interactions and medical applications. *Int. J. Pharm.* 2018, *535*, 1–17.
56. Iqbal, B.; Ali, J.; Baboota, S. Recent advances and development in epidermal and dermal drug deposition enhancement technology. *Int. J. Dermatol.* 2018, *57*, 646–660.

57. Manconi, M.; Mura, S.; Sinico, C.; Fadda, A.M.; Vila, A.O.; Molina, F. Development and characterization of liposomes containing glycols as carriers for diclofenac. *Colloids Surfaces A Physicochem. Eng. Asp.* 2009, *342*, 53–58.
58. Manconi, M.; Caddeo, C.; Sinico, C.; Valenti, D.; Mostallino, M.C.; Biggio, G.; Fadda, A.M. Ex vivo skin delivery of diclofenac by transcutol containing liposomes and suggested mechanism of vesicle-skin interaction. *Eur. J. Pharm. Biopharm.* 2011, *78*, 27–35.
59. Souto, E.B.; Baldim, I.; Oliveira, W.P.; Rao, R.; Yadav, N.; Gama, F.M.; Mahant, S. SLN and NLC for topical, dermal, and transdermal drug delivery. *Expert Opin. Drug Deliv.* 2020, *17*, 357–377.
60. Mishra, V.; Bansal, K.K.; Verma, A.; Yadav, N.; Thakur, S.; Sudhakar, K.; Rosenholm, J.M. Solid lipid nanoparticles: Emerging colloidal nano drug delivery systems. *Pharmaceutics* 2018, *10*, 1–21.
61. Qushawy, M.; Nasr, A. Solid lipid nanoparticles (SLNs) as nano drug delivery carriers: Preparation, characterization and application. *Int. J. Appl. Pharm.* 2020, *12*, 1–9.
62. Goyal, R.; Macri, L.K.; Kaplan, H.M.; Kohn, J. Nanoparticles and nanofibers for topical drug delivery. *J. Control. Release* 2016, *240*, 77–92.
63. Pardeshi, C.; Rajput, P.; Belgamwar, V.; Tekade, A.; Patil, G.; Chaudhary, K.; Sonje, A. Solid lipid based nanocarriers: An overview. *Acta Pharm.* 2012, *62*, 433–472.
64. Iqbal, M.A.; Md, S.; Sahni, J.K.; Baboota, S.; Dang, S.; Ali, J. Nanostructured lipid carriers system: Recent advances in drug delivery. *J. Drug Target.* 2012, *20*, 813–830.
65. Garcês, A.; Amaral, M.H.; Sousa Lobo, J.M.; Silva, A.C. Formulations based on solid lipid nanoparticles (SLN) and nanostructured lipid carriers (NLC) for cutaneous use: A review. *Eur. J. Pharm. Sci.* 2018, *112*, 159–167.
66. Loutfy, M.A.; Hassan, M.A. Methoxsalen. 1980, 0–12.
67. Sinico, C.; Valenti, D.; Manconi, M.; Lai, F.; Fadda, A.M. Cutaneous delivery of 8-methoxypsoralen from liposomal and niosomal carriers. *J. Drug Deliv. Sci. Technol.* 2006, *16*, 115–120.
68. Madigan, L.M.; Lim, H.W. *Psoralen-Ultraviolet Light A Therapy*; Elsevier, 2016; ISBN 9780323447980.
69. Lapolla, W.; Yentzer, B.A.; Bagel, J.; Halvorson, C.R.; Feldman, S.R. A review of phototherapy protocols for psoriasis treatment. *J. Am. Acad. Dermatol.* 2011, *64*, 936–949.

70. Kassem, A.A.; Abd El-Alim, S.H.; Asfour, M.H. Enhancement of 8-methoxypsoralen topical delivery via nanosized niosomal vesicles: Formulation development, in vitro and in vivo evaluation of skin deposition. *Int. J. Pharm.* 2017, *517*, 256–268.
71. Borowska, K.; Wołowiec, S.; Głowniak, K.; Sieniawska, E.; Radej, S. Transdermal delivery of 8-methoxypsoralene mediated by polyamidoamine dendrimer G2.5 and G3.5 - In vitro and in vivo study. *Int. J. Pharm.* 2012, *436*, 764–770.
72. Doppalapudi, S.; Jain, A.; Chopra, D.K.; Khan, W. Psoralen loaded liposomal nanocarriers for improved skin penetration and efficacy of topical PUVA in psoriasis. *Eur. J. Pharm. Sci.* 2017, *96*, 515–529.
73. Lai, F.; Sinico, C.; Valenti, D.; Manca, M.L.; Fadda, A.M. Nanoemulsions as Vehicle for Topical 8-Methoxypsoralen Delivery. *J. Biomed. Nanotechnol.* 2008, *4*, 1–5.
74. Oliveira, C.A.; Gouvêa, M.M.; Antunes, G.R. Nanoemulsion containing 8-methoxypsoralen for topical treatment of dermatoses: development, characterization and ex vivo permeation in porcine skin. *Int. J. Pharm.* 2018.
75. Nogueira Barradas, T.; Perdiz Senna, J.; Araujo Cardoso, S.; Nicoli, S.; Padula, C.; Santi, P.; Rossi, F.; de Holanda e Silva, K.G.; Elias Mansur, C.R. Hydrogel-thickened nanoemulsions based on essential oils for topical delivery of psoralen : Permeation and stability studies. *Eur. J. Pharm. Biopharm.* 2017, *116*, 38–50.
76. Baroli, B.; López-Quintela, M.A.; Delgado-Charro, M.B.; Fadda, A.M.; Blanco-Méndez, J. Microemulsions for topical delivery of 8-methoxsalen. *J. Control. Release* 2000, *69*, 209–218.
77. Wu, J.Y.; Li, Y.J.; Liu, T.T.; Ou, G.; Hu, X. Bin; Tang, T.T.; Wang, J.M.; Liu, X.Y.; Xiang, D.X. Microemulsions vs chitosan derivative-coated microemulsions for dermal delivery of 8-methoxypsoralen. *Int. J. Nanomedicine* 2019, *14*, 2327–2340.
78. Mahira, S.; Kommineni, N.; Doppalapudi, S.; Khan, W. Edge activated ultradeformable liposomes of psoralen and its derivatives: Development and comparative evaluation for vitiligo therapy. *J. Drug Deliv. Sci. Technol.* 2019, *52*, 83–95.
79. Zhang, Y.T.; Shen, L.N.; Wu, Z.H.; Zhao, J.H.; Feng, N.P. Comparison of ethosomes and liposomes for skin delivery of psoralen for psoriasis therapy. *Int. J. Pharm.* 2014, *471*, 449–452.
80. Fang, J.Y.; Fang, C.L.; Liu, C.H.; Su, Y.H. Lipid nanoparticles as vehicles for topical psoralen delivery: Solid lipid nanoparticles (SLN) versus nanostructured lipid carriers (NLC). *Eur. J.*

Pharm. Biopharm. 2008, *70*, 633–640.

81. Osborne, D.W.; Musakhanian, J. Skin Penetration and Permeation Properties of Transcutol®—Neat or Diluted Mixtures. *AAPS PharmSciTech* 2018, *19*, 3512–3533.
82. Pireddu, R.; Sinico, C.; Ennas, G.; Schlich, M.; Valenti, D.; Murgia, S.; Marongiu, F.; Fadda, A.M.; Lai, F. The effect of diethylene glycol monoethyl ether on skin penetration ability of diclofenac acid nanosuspensions. *Colloids Surfaces B Biointerfaces* 2018, *162*, 8–15.
83. Pradhan, M.; Singh, D.; Singh, M.R. Development characterization and skin permeating potential of lipid based novel delivery system for topical treatment of psoriasis. *Chem. Phys. Lipids* 2015, *186*, 9–16.
84. Sonawane, Rahul; Harde, H. Solid lipid nanoparticles-loaded topical gel containing combination drugs: an approach to offset psoriasis. *Expert Opin. Drug Deliv.* 2014, *11*, 1833–1847.
85. Jain, A.K.; Jain, A.; Garg, N.K.; Agarwal, A.; Jain, A.; Jain, S.A.; Tyagi, R.K.; Jain, R.K.; Agrawal, H.; Agrawal, G.P. Adapalene loaded solid lipid nanoparticles gel: An effective approach for acne treatment. *Colloids Surfaces B Biointerfaces* 2014, *121*, 222–229.
86. Raza, K.; Singh, B.; Singal, P.; Wadhwa, S.; Katare, O.P. Systematically optimized biocompatible isotretinoin-loaded solid lipid nanoparticles (SLNs) for topical treatment of acne. *Colloids Surfaces B Biointerfaces* 2013, *105*, 67–74.
87. Kang JH, Chon J, Kim YI, Lee HJ, Oh DW, Lee HG, Han CS, Kim DW, P.C. Preparation and evaluation of tacrolimus-loaded thermosensitive solid lipid nanoparticles for improved dermal distribution. *Int. J. Nanomedicine* 2019, *14*, 5381–5396.
88. Bhupinder, K; Newton, M. Acyclovir Solid Lipid Nanoparticles for Skin Drug Delivery: Fabrication, Characterization and In vitro Study. *Recent Pat. Drug Deliv. Formul.* 2017, *11*, 132–146.
89. El-Housiny, S.; Eldeen, M.A.S.; El-Attar, Y.A.; Salem, H.A.; Attia, D.; Bendas, E.R.; El-Nabarawi, M.A. Fluconazole-loaded solid lipid nanoparticles topical gel for treatment of pityriasis versicolor: formulation and clinical study. *Drug Deliv.* 2018, *25*, 78–90.
90. Vaghasiya, H.; Kumar, A.; Sawant, K. Development of solid lipid nanoparticles based controlled release system for topical delivery of terbinafine hydrochloride. *Eur. J. Pharm. Sci.* 2013, *49*, 311–322.
91. Tupal, A.; Sabzichi, M.; Ramezani, F.; Kouhsoltani, M.; Hamishehkar, H. Dermal delivery of doxorubicin-loaded solid lipid nanoparticles for the treatment of skin cancer. *J.*

Microencapsul. 2016, *33*, 372–380.

92. Geetha, T.; Kapila, M.; Prakash, O.; Deol, P.K.; Kakkar, V.; Kaur, I.P. Sesamol-loaded solid lipid nanoparticles for treatment of skin cancer. *J. Drug Target.* 2015, *23*, 159–169.
93. Khallaf, R.A.; Salem, H.F.; Abdelbary, A. 5-Fluorouracil shell-enriched solid lipid nanoparticles (SLN) for effective skin carcinoma treatment. *Drug Deliv.* 2016, *23*, 3452–3460.
94. Dragicevic, N.; Maibach, H. Combined use of nanocarriers and physical methods for percutaneous penetration enhancement. *Adv. Drug Deliv. Rev.* 2018, *127*, 58–84.
95. Pradhan, M.; Alexander, A.; Rawat, M.; Singh, D. Understanding the prospective of nano-formulations towards the treatment of psoriasis. *Biomed. Pharmacother.* 2018, *107*, 447–463.
96. Pradhan, M.; Singh, D.; Murthy, S.N.; Singh, M.R. Design, characterization and skin permeating potential of Fluocinolone acetonide loaded nanostructured lipid carriers for topical treatment of psoriasis. *Steroids* 2015, *101*, 56–63.
97. Yousef, S.A.; Mohammed, Y.H.; Namjoshi, S.; Grice, J.E.; Benson, H.A.E.; Sakran, W.; Roberts, M.S. Mechanistic evaluation of enhanced curcumin delivery through human skin in vitro from optimised nanoemulsion formulations fabricated with different penetration enhancers. *Pharmaceutics* 2019, *11*.
98. Mura, S.; Manconi, M.; Fadda, A.M.; Sala, M.C.; Perricci, J.; Pini, E.; Sinico, C. Penetration enhancer-containing vesicles (PEVs) as carriers for cutaneous delivery of minoxidil: In vitro evaluation of drug permeation by infrared spectroscopy. *Pharm. Dev. Technol.* 2013, *18*, 1339–1345.
99. Manconi, M.; Sinico, C.; Caddeo, C.; Vila, A.O.; Valenti, D.; Fadda, A.M. Penetration enhancer containing vesicles as carriers for dermal delivery of tretinoin. *Int. J. Pharm.* 2011, *412*, 37–46.
100. Rosa, A.; Atzeri, A.; Nieddu, M.; Appendino, G. New insights into the antioxidant activity and cytotoxicity of arzanol and effect of methylation on its biological properties. *Chem. Phys. Lipids* 2017, *205*, 55–64.
101. Rosa, A.; Murgia, S.; Putzu, D.; Meli, V.; Falchi, A.M. Monoolein-based cubosomes affect lipid profile in HeLa cells. *Chem. Phys. Lipids* 2015, *191*, 96–105.
102. Rosa, A.; Caprioglio, D.; Isola, R.; Nieddu, M.; Appendino, G.; Falchi, A.M. Dietary zerumbone from shampoo ginger: new insights into its antioxidant and anticancer activity.

Food Funct. 2019, *10*, 1629–1642.

103. Tscharnuter, W. Photon Correlation Spectroscopy in Particle Sizing. In *Encyclopedia of Analytical Chemistry*; Brookhaven Instruments Corporation: Holtsville, NY, USA, 2006 ISBN 9780470027318.
104. Tomaszewska, E.; Soliwoda, K.; Kadziola, K.; Tkacz-Szczesna, B.; Celichowski, G.; Cichomski, M.; Szmaja, W.; Grobelny, J. Detection Limits of DLS and UV-Vis Spectroscopy in Characterization of Polydisperse Nanoparticles Colloids. *J. Nanomater.* 2013, *2013*.
105. Cilurzo, F.; Minghetti, P.; Sinico, C. Newborn pig skin as model membrane in in vitro drug permeation studies: a technical note. *AAPS PharmSciTech* 2007, *8*, E94.
106. Songkro, S.; Purwo, Y.; Becket, G.; Rades, T. Investigation of newborn pig skin as an in vitro animal model for transdermal drug delivery. *STP pharma Sci.* 2004, *13*, 133–139.
107. Shinde, G.; Kesarla, R.; Prajapati, N.; Rayasa, M. Formulation, development and characterization of nanostructured lipid carrier (NLC) loaded gel for psoriasis. *Der Pharm. Lett.* 2013, *5*, 13–25.
108. Garg, B.J.; Garg, N.K.; Beg, S.; Singh, B.; Katare, O.P. Nanosized ethosomes-based hydrogel formulations of methoxsalen for enhanced topical delivery against vitiligo: formulation optimization, in vitro evaluation and preclinical assessment. *J. Drug Target.* 2016, *24*, 233–246.
109. Behera, J.; Keservani, R.K.; Yadav, A.; Tripathi, M.; Chadoker, A. Methoxsalen loaded chitosan coated microemulsion for effective treatment of psoriasis. *Int. J. Drug Deliv.* 2010, *2*, 159–167.
110. Sah, A.; Jain, S.K.; Pandey, R.S. Microemulsion based hydrogel formulation of methoxsalen for the effective treatment of psoriasis. *Asian J. Pharm. Clin. Res.* 2011, *4*, 140–145.
111. Javadzadeh, Y.; Adibkia, K.; Hamishehkar, H. Transcutol® (Diethylene Glycol Monoethyl Ether): A Potential Penetration Enhancer. In *Percutaneous Penetration Enhancers Chemical Methods in Penetration Enhancement*; Dragicevic, N., Maibach, H.I., Eds.; Springer, Berlin, Heidelberg, 2015; pp. 195–205 ISBN 978-3-662-47038-1.
112. Falchi, A.M.; Rosa, A.; Atzeri, A.; Incani, A.; Lampis, S.; Meli, V.; Caltagirone, C.; Murgia, S. Effects of monoolein-based cubosome formulations on lipid droplets and mitochondria of HeLa cells. *Toxicol. Res. (Camb).* 2015, *4*, 1025–1036.
113. Yuan, H.; Miao, J.; Du, Y.-Z.; You, J.; Hu, F.-Q.; Zeng, S. Cellular uptake of solid lipid nanoparticles and cytotoxicity of encapsulated paclitaxel in A549 cancer cells. *Int. J.*

Pharm. 2008, *348*, 137–145.

114. Sinico, C.; Fadda, A.. Vesicular carriers for dermal drug delivery. *Expert Opin. Drug Deliv.* 2009, *6*, 813–825.
115. Abdel-Mottaleb, M.M.A.; Try, C.; Pellequer, Y.; Lamprecht, A. Nanomedicine strategies for targeting skin inflammation. *Nanomedicine* 2014, *9*, 1727–1743.
116. Cevc, G.; Blume, G. Lipid vesicles penetrate into intact skin owing to the transdermal osmotic gradients and hydration force. *Biochim. Biophys. Acta - Biomembr.* 1992, *1104*, 226–232.
117. Touitou, E.; Dayan, N.; Bergelson, L.; Godin, B.; Eliaz, M. Ethosomes — novel vesicular carriers for enhanced delivery: characterization and skin penetration properties. *J. Control. Release* 2000, *65*, 403–418.
118. Manconi, M.; Sinico, C.; Fadda, A.M. Penetration Enhancer-Containing Vesicles for Cutaneous Drug Delivery. In *Percutaneous Penetration Enhancers Chemical Methods in Penetration Enhancement: Nanocarriers*; Dragicevic, N., Maibach, H.I., Eds.; Springer Berlin Heidelberg: Berlin, Heidelberg, 2016; pp. 93–110 ISBN 978-3-662-47862-2.
119. Castangia, I.; Manca, M.L.; Matricardi, P.; Sinico, C.; Lampis, S.; Fernàndez-Busquets, X.; Fadda, A.M.; Manconi, M. Effect of diclofenac and glycol intercalation on structural assembly of phospholipid lamellar vesicles. *Int. J. Pharm.* 2013, *456*, 1–9.
120. Oliveira, C.A.; Gouvêa, M.M.; Antunes, G.R.; Freitas, Z.M.F. de; Marques, F.F. de C.; Ricci-Junior, E. Nanoemulsion containing 8-methoxypsoralen for topical treatment of dermatoses: Development, characterization and ex vivo permeation in porcine skin. *Int. J. Pharm.* 2018, *547*, 1–9.
121. Corrias, F.; Schlich, M.; Sinico, C.; Pireddu, R.; Valenti, D.; Fadda, A.M.; Marceddu, S.; Lai, F. Nile red nanosuspensions as investigative model to study the follicular targeting of drug nanocrystals. *Int. J. Pharm.* 2017, *524*, 1–8.
122. Schlich, M.; Lai, F.; Pireddu, R.; Pini, E.; Ailuno, G.; Fadda, A.M.; Valenti, D.; Sinico, C. Resveratrol proniosomes as a convenient nanoingredient for functional food. *Food Chem.* 2020, *310*, 125950.
123. Mura, S.; Manconi, M.; Sinico, C.; Valenti, D.; Fadda, A.M. Penetration enhancer-containing vesicles (PEVs) as carriers for cutaneous delivery of minoxidil. *Int. J. Pharm.* 2009, *380*, 72–79.
124. Mura, S.; Fadda, A.M.; Sinico, C.; Vila, A.O.; Valenti, D.; Manconi, M. Transcutol containing

vesicles for topical delivery of minoxidil. *J. Drug Target.* 2010, *19*, 189–196.

125. Zhang, Y.T.; Shen, L.I.N.A.; Wu, Z.H.; Zhao, J.I.H.; Feng, N.P. Evaluation of skin viability effect on ethosome and liposome-mediated psoralen delivery via cell uptake. *J. Pharm. Sci.* 2014, *103*, 3120–3126.
126. Camović, M.; Biščević, A.; Brčić, I.; Borčak, K.; Bušatlić, S.; Ćenanović, N.; Dedović, A.; Mulalić, A.; Osmanlić, M.; Sirbubalo, M.; Tucak, A.; Vranić, E. Coated 3D Printed PLA Microneedles as Transdermal Drug Delivery Systems. *IFMBE Proc. - C.* 2019, *73*, 735–742.
127. Economidou, S.N.; Pere, C.P.P.; Reid, A.; Uddin, M.J.; Windmill, J.F.C.; Lamprou, D.A.; Douroumis, D. 3D printed microneedle patches using stereolithography (SLA) for intradermal insulin delivery. *Mater. Sci. Eng. C* 2019, *102*, 743–755.
128. Pere, C.P.P.; Economidou, S.N.; Lall, G.; Ziraud, C.; Boateng, J.S.; Alexander, B.D.; Lamprou, D.A.; Douroumis, D. 3D printed microneedles for insulin skin delivery. *Int. J. Pharm.* 2018, *544*, 425–432.
129. Jamróz, W.; Szafraniec, J.; Kurek, M.; Jachowicz, R. 3D printing in pharmaceutical and medical applications. *Pharm. Res.* 2018, *35*, Article 176.
130. Economidou, S.N.; Lamprou, D.A.; Douroumis, D. 3D printing applications for transdermal drug delivery. *Int. J. Pharm.* 2018, *544*, 415–424.
131. Melchels, F.P.W.; Feijen, J.; Grijpma, D.W. A review on stereolithography and its applications in biomedical engineering. *Biomaterials* 2010, *31*, 6121–6130.
132. Fiedor, P.; Ortyl, J. A new approach to micromachining: High-precision and innovative additive manufacturing solutions based on photopolymerization technology. *Materials (Basel).* 2020, *13*, 1–25.
133. Xu, X.; Robles-Martinez, P.; Madla, C.M.; Joubert, F.; Goyanes, A.; Basit, A.W.; Gaisford, S. Stereolithography (SLA) 3D printing of an antihypertensive polyprintlet: Case study of an unexpected photopolymer-drug reaction. *Addit. Manuf.* 2020, *33*, 101071.
134. Robles-Martinez, P.; Xu, X.; Trenfield, S.J.; Awad, A.; Goyanes, A.; Telford, R.; Basit, A.W.; Gaisford, S. 3D printing of a multi-layered polypill containing six drugs using a novel stereolithographic method. *Pharmaceutics* 2019, *11*.
135. Martinez, P.R.; Goyanes, A.; Basit, A.W.; Gaisford, S. Fabrication of drug-loaded hydrogels with stereolithographic 3D printing. *Int. J. Pharm.* 2017, *532*, 313–317.
136. Wang, J.; Goyanes, A.; Gaisford, S.; Basit, A.W. Stereolithographic (SLA) 3D printing of oral modified-release dosage forms. *Int. J. Pharm.* 2016, *503*, 207–212.

137. Kadry, H.; Wadnap, S.; Xu, C.; Ahsan, F. Digital light processing (DLP)3D-printing technology and photoreactive polymers in fabrication of modified-release tablets. *Eur. J. Pharm. Sci.* 2019, *135*, 60–67.
138. Krkobabić, M.; Medarević, D.; Cvijić, S.; Grujić, B.; Ibrić, S. Hydrophilic excipients in digital light processing (DLP) printing of sustained release tablets: Impact on internal structure and drug dissolution rate. *Int. J. Pharm.* 2019, *572*, 118790.
139. Goyanes, A.; Det-Amornrat, U.; Wang, J.; Basit, A.W.; Gaisford, S. 3D scanning and 3D printing as innovative technologies for fabricating personalized topical drug delivery systems. *J. Control. Release* 2016, *234*, 41–48.
140. Uddin, M.J.; Scoutaris, N.; Economidou, S.N.; Giraud, C.; Chowdhry, B.Z.; Donnelly, R.F.; Douroumis, D. 3D printed microneedles for anticancer therapy of skin tumours. *Mater. Sci. Eng. C* 2020, *107*, 110248.
141. Yao, W.; Li, D.; Zhao, Y.; Zhan, Z.; Jin, G.; Liang, H.; Yang, R. 3D Printed multi-functional hydrogel microneedles based on high-precision digital light processing. *Micromachines* 2020, *11*.
142. Kundu, A.; Arnett, P.; Bagde, A.; Azim, N.; Kouagou, E.; Singh, M.; Rajaraman, S. DLP 3D Printed "Intelligent" Microneedle Array (iμNA) for Stimuli Responsive Release of Drugs and Its in Vitro and ex Vivo Characterization. *J. Microelectromechanical Syst.* 2020, *29*, 685–691.
143. Vora, L.K.; Courtenay, A.J.; Tekko, I.A.; Larrañeta, E.; Donnelly, R.F. Pullulan-based dissolving microneedle arrays for enhanced transdermal delivery of small and large biomolecules. *Int. J. Biol. Macromol.* 2020, *146*, 290–298.
144. Donnelly, R.F.; Majithiya, R.; Singh, T.R.R.; Morrow, D.I.J.; Garland, M.J.; Demir, Y.K.; Migalska, K.; Ryan, E.; Gillen, D.; Scott, C.J.; et al. Design, optimization and characterisation of polymeric microneedle arrays prepared by a novel laser-based micromoulding technique. *Pharm. Res.* 2011, *28*, 41–57.
145. Kapoor, Y.; Milewski, M.; Dick, L.; Zhang, J.; Bothe, J.R.; Gehrt, M.; Manser, K.; Nissley, B.; Petrescu, I.; Johnson, P.; et al. Coated microneedles for transdermal delivery of a potent pharmaceutical peptide. *Biomed. Microdevices* 2020, *22*, 1–10.
146. Larrañeta, E.; McCrudden, M.T.C.; Courtenay, A.J.; Donnelly, R.F. Microneedles: A New Frontier in Nanomedicine Delivery. *Pharm. Res.* 2016, *33*, 1055–1073.
147. Lhernould, M.S.; Deleers, M.; Delchambre, A. Hollow polymer microneedles array

resistance and insertion tests. *Int. J. Pharm.* 2015, *480*, 8–15.

148. Chen, Z.; Ren, L.; Li, J.; Yao, L.; Chen, Y.; Liu, B.; Jiang, L. Rapid fabrication of microneedles using magnetorheological drawing lithography. *Acta Biomater.* 2018, *65*, 283–291.
149. Dharadhar, S.; Majumdar, A.; Dhoble, S.; Patravale, V. Microneedles for transdermal drug delivery: a systematic review. *Drug Dev. Ind. Pharm.* 2019, *45*, 188–201.
150. Larrañeta, E.; Moore, J.; Vicente-Pérez, E.M.; González-Vázquez, P.; Lutton, R.; Woolfson, A.D.; Donnelly, R.F. A proposed model membrane and test method for microneedle insertion studies. *Int. J. Pharm.* 2014, *472*, 65–73.
151. Donnelly, R.F.; Moffatt, K.; Alkilani, A.Z.; Vicente-Pérez, E.M.; Barry, J.; McCrudden, M.T.C.; Woolfson, A.D. Hydrogel-forming microneedle arrays can be effectively inserted in skin by self-application: A pilot study centred on pharmacist intervention and a patient information leaflet. *Pharm. Res.* 2014, *31*, 1989–1999.